



The author(s) shown below used Federal funding provided by the U.S. Department of Justice to prepare the following resource:

Document Title: Nitrogen-Containing Materials for Mechanochemical Synthesis, Luminescence Analysis, and Heterogeneous Catalysis

Author(s): David J. Nash

Document Number: 306200

Date Received: March 2023

Award Number: 2015-R2-CX-0035

This resource has not been published by the U.S. Department of Justice. This resource is being made publicly available through the Office of Justice Programs' National Criminal Justice Reference Service.

Opinions or points of view expressed are those of the author(s) and do not necessarily reflect the official position or policies of the U.S. Department of Justice.

NITROGEN-CONTAINING MATERIALS FOR MECHANOCHEMICAL SYNTHESIS, LUMINESCENCE ANALYSIS, AND HETEROGENEOUS CATALYSIS

by

DAVID J. NASH

B.S. University of Central Florida, 2011

M.S. University of Central Florida, 2014

A dissertation submitted in partial fulfillment of the requirements
for the degree of Doctor of Philosophy
in the Department of Chemistry
in the College of Sciences
at the University of Central Florida
Orlando, Florida

Summer Term
2017

Major Professors: Lei Zhai and Richard Blair

©2017 David J. Nash

ABSTRACT

Various inorganic nitrogen-containing materials have been exploited for their different properties. Several nitride materials are commercially attractive due to their mechanical properties making them suitable for ceramic industries and wide bandgaps fitting for use as semiconductor and insulator materials, as well as optoelectronics. Nitride materials can exhibit versatility in applications such as the use of gallium nitride to make blue LEDs, nitrides of titanium and silicon being utilized as medical implants for their chemical inertness and hardness, and the heavy use of boron nitride as a solid lubricant in the cosmetic industry. Amines have been used as nitrogen-containing organic ligands in organometallic complexes that exhibit phenomenal photophysical properties. These complexes have been heavily studied for potential applications in optoelectronics and chemical sensing.

This dissertation will focus on two nitrogen-containing materials that have yet to be explored for the potential applications to be discussed. The first is *hexagonal*-boron nitride (*h*-BN), which was previously mentioned to have a substantial use in the cosmetic industry, giving products such as lipstick, foundation, and blush their slick feeling. Computational models have shown the possibility of altered electronic properties of defect sites in the *h*-BN sheets. These defect sites will be explored experimentally to determine any catalytic activity. Specifically, the hydrogenation reaction using *defect-laden hexagonal*-boron nitride will be investigated. Successful catalysis would add to the short list of non-metal catalyst, and provide an alternative catalyst that costs significantly less than the traditional metal catalysts commonly used in commercial industries.

The second of the two nitrogen-containing materials is a class of metal complexes based on organometallic clusters of copper(I) iodide. Copper(I) iodide clusters formed with amine ligands have been studied for around four decades and the photophysics behind their photoluminescent properties are well understood. Much of the work has been done for use as a potential emissive material in the optoelectronics field. They have also been studied for applications in the sensing of environmental compounds. Here, research will display its use as a novel sensor for narcotic substances.

This forensic application will be further explored to develop and eventually commercialize a complete field drug testing system for law enforcement and crime lab use, with the goal to equip law enforcement personnel with a presumptive drug testing method that is accurate, easy-to-use, safe, adaptable, and affordable. This system will consist of a narcotic drug-indicating test strip, a handheld fluorescence spectrometer manufactured in-house using relatively inexpensive parts, and a mobile app that will leverage photoemission data of the tested drug samples collected by multiple crime labs to provide the ability for sample-to-reference data matching. Law enforcement users would have the ability to rapidly identify an unknown substance by applying it to a test strip, testing it using the spectrometer, and capturing an image of the resulting photoemission and analyzing the spectral profile in search of a match with the support of a cloud database.

This is dedicated to my mom and dad, aunts and uncles, brothers and cousins, and my closest of friends for always supporting me, being my motivation and inspiration, and being proud of me no matter what. I also dedicate this to my good friends that have passed: Robbie Buddington, Dre Ross, and Andre Chambers. To their families, I hope you all can celebrate with me knowing that the life of your loved one has driven me to be the person I am today. Rockledge, represent!

ACKNOWLEDGMENTS

I would like to start off by acknowledging my research adviser, Dr. Richard Blair. I express my thanks to him for allowing me work in his lab as an undergrad that did not have a passion for chemistry. He put me on a forensic science project I eventually grew passionate about, which ultimately paid my way through graduate school. If it was not for him, I never would have considered getting a PhD in chemistry. I cannot express my gratitude enough for the guidance, mentorship, and friendship he has provided over the last 7 years (6 years in graduate school), which has helped me grow confident in my knowledge in the realm of science. I appreciate the sacrifices he has made for me to get this degree and the experience this journey has given me.

I would like to thank my faculty adviser, Dr. Lei Zhai, for his academic support over the years. Although he might think what he has done to help was only minor, I still express my gratitude for I consider his support a big part of my completion of this degree. I thank the rest of those that served on my committee: Dr. Michael Hampton, Dr. Jim Harper, and Dr. Matthew Rex. I would also like to thank Dr. Rex for his help with the many instruments I have had to use over the years for my research projects.

For financial support, I thank the National Institute of Justice (NIJ) for funding the majority of my graduate education and research projects for drug identification. The support and enthusiasm for our project from our program manager, Dr. Frances Scott was greatly appreciated. Thanks to the National Science Foundation (NSF) and the NSF I-Corps™ program and its faculty for funding our exploration to commercialize our drug identification technology. I also thank the NSF for funding the boron nitride catalysis

project. Of all the projects I had the opportunity to work on, I found this one the most interesting and it is good to know that the science we do in the Blair Group is worthwhile in the eyes of the NSF.

Thanks to the many coworkers and fellow students that have been a part of my journey through grad school. Starting with my fellow researchers in the lab: Dr. David Restrepo, Jacob Todd, Deepti Siddhanti, Fernand Torres-Davila, Dr. Zhilin Xie, Justin Piedad, and Carolin Griebel, and the many undergraduate researchers that have helped me on the projects I have worked on: Amanda Binnion, Katerina Chagoya, Rachel Penabade, Kevin Bertrand, Andilys Andino, Natalia Parra, Meagan Harwick, Kelley Devoe, Kristine Jubilag, Natalie Abad, Caroline Arteaga, Bradley Brown, Erin Driscoll, Paul Alvarez, Michael Navarro, Nicole Mrvos, Natasha Reyes, Ashley Falvey, and Brandon Edwards.

For collaborative efforts on the research projects included in this dissertation, I would like to thank the following groups and organizations: Dr. Talat Rahman's group in UCF Physics, Dr. Laurene Tetard's group in UCF Physics and NSTC, Dr. Jim Harper's group in UCF Chemistry, Dr. Farha's group at Northwestern University, Dr. Jay Vargas and his students at California State University-Los Angeles, the Orange County Sheriff-Coroner Department Crime Lab in California, Nancy Ludwigsen and the Sarasota County Sheriffs Office Crime Lab, and Lt. Matthew Myers with the Peachtree City Police Department in Georgia.

I would like to thank all of my great friends in the UCF Chemistry Department that have accepted me and made me feel like I belong in this fraternity of "chemistry nerds"

with them: Josh Knorr, Simon Tang, Victor Diaz, Jacob Powell, Dom Valenti, Caleb Dunlap, Nirvani Mujumdar, Andrew Towers, Dawn Mills, Nomi Sherwin, Angel Ramos, and Kurtington Lorenz. The friends I have made in this chapter of my life will always have a fond place in my memories, even as we inevitably grow apart to follow our own career paths.

I would especially like to thank my close friends and family who have been there with me through thick and thin during my time in grad school and have done a great job of keeping me sane: Tyree Yates, Seth Kaplan, and Rudy Tucker. Thank you to Katerina for always “being there for me” and thanks to Deeps for being “my dawg”. Thanks to my Cypher Gang family for keeping me laughing during the busy, work-filled times over the last few years. Thanks to my parents, Merlinda and Victor for supporting my every decision and trusting me to make those decisions for myself. Thanks to my aunts and uncles, as well as Steve and Laurie, who have played their roles as second parents to me. Thank you to my brothers and cousins and their children for their support and being my inspiration to succeed.

TABLE OF CONTENTS

LIST OF FIGURES.....	xiii
LIST OF TABLES.....	xviii
CHAPTER 1: INTRODUCTION AND LITERATURE OVERVIEW.....	1
1.1 Mechanochemistry Overview	1
1.1.1 History of Mechanochemistry	2
1.1.2 Milling Equipment.....	4
1.1.3 Milling Conditions	10
1.1.4 Practicality for Reaction Scale-up	15
1.2 Mechanochemical Synthesis	16
1.2.1 Synthesis of Inorganic Compounds and Materials	16
1.2.2 Reactions in Organic Synthesis	17
1.3. Catalytic Hydrogenation	19
1.3.1 Heterogeneous Metal Catalysts for Hydrogenation	20
1.3.2 Homogeneous Catalysts for Hydrogenation.....	22
1.3.3 Frustrated Lewis Pairs (FLPs) and Other Metal-Free Catalysts for Hydrogenation.....	24
1.4 Methods for the Presumptive Identification of Illicit Substances.....	25
1.4.1 Traditional Methods for Presumptive Identification of Illicit Substances	26
1.4.2 Novel Methods for Presumptive Identification of Illicit Substances.....	28
1.5 References.....	30
CHAPTER 2: HETEROGENEOUS METAL-FREE HYDROGENATION OVER DEFECT-LADEN HEXAGONAL BORON NITRIDE.....	36
2.1 Introduction	36

2.2 Experimental	39
2.2.1 Synthesis of Defect-Laden Hexagonal-Boron Nitride (dh-BN).....	39
2.2.2 Hydrogenation	41
2.2.3 Analysis and Characterization of Defect-Laden Hexagonal-Boron Nitride (dh-BN).....	45
2.2.4 Computational Modeling of Mechanochemical Hydrogenation Over dh-BN..	51
2.3 Results and Discussion.....	54
2.3.1 Producing Defects	57
2.3.2 Bulk Scale Experiments	60
2.3.3 Metal-free Hydrogenation.....	62
2.3.4 Mechanically Equivalent Blank.....	63
2.3.5 Rigorously Metal-Free Implementation.....	64
2.3.6 Mechanical Factors Affecting Induction Periods and Reaction Rates	66
2.3.7 Surface Analyses, Bound Species, and Sites	67
2.3.8 Catalytically Active Defects and Reaction Mechanism	71
2.4 Conclusion	75
2.5 References.....	76
CHAPTER 3: PHOTOLUMINESCENT COPPER(I) IODIDE CLUSTER COMPOUNDS FOR THE NOVEL DETECTION AND IDENTIFICATION OF HETEROCYCLIC AMINES OF FORENSIC INTEREST	
3.1 Introduction	84
3.2 Experimental	88
3.2.1 Materials and Methods	88
3.2.2 Synthesis of Copper(I) Iodide Clusters	89

3.2.3 Limit of Detection (LOD) Studies	90
3.2.4 Testing Illicit Substances	91
3.2.5 Photoluminescence Analysis.....	91
3.3 RESULTS AND DISCUSSION.....	92
3.3.1 Copper(I) Iodide	92
3.3.2 Piperidine, Piperazine, and Piperazine Analogues.....	93
3.3.3 DABCO and Hexamine	97
3.3.4 Substances of Forensic Interest.....	97
3.3.5 Other substances (Indoles, xanthines, amphetamines, and sterically-hindered amines.....	102
3.3.6 Limit of detection (LOD)	103
3.3.7 Spectral Peak Analysis.....	104
3.4 Conclusion	105
3.5 References.....	106
CHAPTER 4: INTEGRATING BASIC RESEARCH WITH APP-BASED ANALYSIS ...	111
4.1 Project Scope.....	111
4.2 Customer Discovery and Market Validation	116
4.2.1 Market Research.....	116
4.2.2 Customer Discovery and Validation through NSF I-Corps™	117
4.2.3 Competing Technology in Commercial Market.....	120
4.2.4 Business Model Canvas: Product-Market Fit	123
4.3 Background on Drug Identification Technology Based on Photoluminescent Drug Indicators	130
4.4 Mobile App Development.....	131

4.4.1 Application Maps.....	132
4.5 References.....	136

LIST OF FIGURES

Figure 1. Diagram of compressive forces vs. shear forces via ball milling. The red arrows represent each the direction of impact for each ball bearing.	2
Figure 2. SPEX mixer mill, also commonly known as a shaker mill.	6
Figure 3. Planetary mill.....	7
Figure 4. Roller mill, also commonly known as a pebble mill. This mill was customized to allow for gas input and external heating.	8
Figure 5. Union Process attrition mill.....	9
Figure 6. Housing for the custom roller mill, which is equipped with a heating element to allow for external heating of the reaction vessel.	12
Figure 7. Ceramic reaction vessels and milling media used for metal-free reactions....	14
Figure 8. Mechanism of catalytic hydrogenation on metal surface.....	21
Figure 9. Mechanism of catalytic hydrogenation via oxidative addition using Wilkinson's catalyst.	22
Figure 10. Representation of hydrogen activation using frustrated Lewis pair.	25
Figure 11. A typical NIK [®] kit, one of the brands of color kits used by law enforcement agencies to presumptively identify drugs in the field.....	28
Figure 12. Hydrogenation of (E)-1,2-diphenylethene [6] under excess hydrogen at 170°C with different catalyst loadings. Five grams (27.7 mmol) of olefin was used. One gram of dh-BN activated for 48 hours under hydrogen (a) and unactivated h-BN coated milling media (b) both effectively hydrogenated the olefinic bond.....	38
Figure 13. The reaction vessel and reactor has controls for pressure, temperature, and mechanical force (a). A close-up of the steel reaction vessel shows the temperature and gas control (b). Hydrogen is introduced through the solenoid at the left. Heat is applied by a NiChrome element (top center). Temperature is monitored by two thermocouples with the larger one on the left also serving as the control thermocouple for the heating element. A drive wheel driven by a pulley or a chain driven sprocket (not pictured) rotates the reaction vessel. In order to perform rigorously metal-free reactions, an alumina reactor with titanium flanges was implemented (c). The titanium flanges have been anodized to reduce hydrogen interaction.	41

Figure 14. Alkenes are chemisorbed and physisorbed onto dh-BN while alkanes are merely physisorbed. Propene uptake on dh-BN was used to estimate the number of potential active sites on the catalyst surface. The potential active sites represent 27% of the adsorption sites. The curves presented are uptake over 5 g of dh-BN and have been offset by the unadsorbed moles of gas. 46

Figure 15. At elevated temperature dehydrogenation reaction produce carbon deposits on the catalyst. After use, the dh-BN exhibits a color change from white to pale yellow and tan (a). The intensity of the color increases with increasing reaction temperature. These deposits are highly fluorescent (b) indicative of coking. Thermogravimetric analysis (c) shows the trend of increased coking levels with increased process temperatures. X-ray photoelectron spectra of the carbon 1s region of h-BN as received (black), after inducing defects (red), and after use as a hydrogenation catalyst for the hydrogenation of (E)-cinnamic acid [7] (blue) confirmed carbon incorporation (d)..... 48

Figure 16. Steel and alumina reactors were simulated using DEM. The cross sections of these reactors (a) show the geometry differences. Three reaction vessels were investigated: steel (a, left), high alumina sloped sides (a, center), and a high alumina with straight sides (a, right). Lower forces were generated in the cylindrical reactor (b and c). No appreciable hydrogenation was observed in that reactor. Although the sloped reactors produce forces with similar magnitudes (b and c), the integral of the compressive forces produced over a 10 second time period (d) shows that less force if being applied over time. Lower total forces resulted in longer induction periods. 52

Figure 17. The olefinic bond chemisorbs onto four defect sites in dh-BN. Eight defect structures in BN were studied (left). These are (from top left to bottom right): 180° rotation of a BN bond (B/N), 90° rotation of a BN bond {Stone-Wales defect} (SW), nitrogen substitution for boron (N_B), boron substitution for nitrogen (B_N), carbon substitution for nitrogen (C_N), carbon substitution for boron (C_B), boron vacancy (V_B), and a nitrogen vacancy (V_N). Gray, green, and pink balls represent nitrogen, boron, and carbon atoms, respectively. The light-gray backgrounds indicate the defected areas. Charge-density redistribution and top view (right) after the adsorption of C₂H₄ (a) and C₃H₆ (b) on B_N, SW, V_B, and V_N defects in a BN substrate. Isosurfaces are drawn at 0.01 e/Bohr³. The blue and red isosurfaces represent, respectively, the charge-deficit and -accumulation regions. (i.e. charge flows from blue to red regions). Gray and green balls represent nitrogen and boron atoms, respectively. The light-gray backgrounds indicate the defected areas.... 56

Figure 18. Binding structure of hydrogen on h-BN with VB (a), VN (b), SW (c), and BN (d) defects. Blue, green, and magenta balls represent nitrogen, boron, and hydrogen atoms, respectively. 56

- Figure 19. Transmission electron microscopy images of as received h-BN (A and B) and dh-BN (C and D). The as received material is large flakes (A) with well-ordered staking of the BN sheets (B). The dh-BN is much smaller and thinner flakes (C) with much less order in the c direction. Evidence of delamination and curling of the BN sheet can be seen in C. 59
- Figure 20. The as received h-BN is highly crystalline with an intense 002 diffraction peak. After activation and hydrogenation of dh-BN, the 002 peak is diminished due to disordering in the c-direction. In plane ordering is still present as evident by the increased intensity of peaks due to diffraction off of planes with h and k components. 59
- Figure 21. The 002 diffraction peak is broadened with an asymmetry toward lower angles. This indicates a fraction of the material has large intersheet spacing. This may be due to adsorbed molecules or minor distortions in each BN sheet disrupting the stacking sequence. 60
- Figure 22. Hydrogenation of propene [1] with an excess of hydrogen at 220°C. Two grams of catalyst and 37.9 mmol of propene [1] were used. The reaction using dh-BN activated in a large batch had slower kinetics (black trace) than that using dh-BN activated in a smaller batch (gray trace). 62
- Figure 23. Starting with pristine BN (Initial), induction periods reduce and hydrogenation rates increase with each recycle. Continued propene [1] hydrogenation was observed after 3 recycles of the catalyst. Activation continued through the first two uses and by the 2nd and 3rd recycle the catalytic rate reached its maximum. 62
- Figure 24. ¹³C solid state NMR of dh-BN exposed to high and low partial pressures of propene. The peaks around 25 ppm are due to the methyl carbon on propene and shows 4 distinct binding modes. The peaks at 62 and 83 ppm are likely due to partial oxidation of the bound propene molecule. The spectra were obtained using a cross polarization technique. 68
- Figure 25. DSC of h- and dh-BN before and after exposure to 310.3 kPa of propene. The exotherm observed in the propene adsorbed dh-BN (solid red trace) corresponds to 181.4 kJ/mol. 70
- Figure 26. Temperature programmed desorption of ethene on dh-BN. The desorption profile is similar to that from defect-laden surfaces. 71
- Figure 27. Electronic density cross-sections plotted along the vertical plane, passing through the center of the two carbon atoms of gas-phase (A) ethene (C₂H₄) and (B) ethane (C₂H₆) , and of (C) C₂H₄/dh-BN for the defects BN, SW, VN and VB. Contours are drawn in a linear scale (9 contours from 0 to 0.27 e/bohr³). It can be seen that the electronic density of ethene on dh-BN exhibit similar structure as that

of C ₃ H ₆ , indicating reduction of the bond order of the C-C bond in the adsorbed ethene.	73
Figure 28. The largest barrier in the minimum energy pathway of propene hydrogenation over VN is 1.53 eV (148 kJ/mol). Zero potential energy corresponds to propene and hydrogen in the gas phase without any interaction with h-BN. Thick horizontal bars represent intermediate states. The barrier (in eV) for each elementary reaction step is calculated using the Climbing Image Nudged Elastic Band method and shown by the number (eV) between the states. * denote adsorbed species. The inserts are structure (a) of co-adsorbed of propene and hydrogen (C ₃ H ₆ * + 2H*) and (b) the intermediate state C ₃ H ₇ *.	74
Figure 29. Energies of the intermediate species formed during the hydrogenation of ethene interacting with hydrogen bound to a VB. The highest barrier is 3.67 eV or 354 kJ/mol.	75
Figure 30. Structure of the cubane form of Cu ₄ X ₄ L ₄ cluster.	87
Figure 31. Chemical structures of various substances of forensic interest, as well as some of their analogues. Many of them contain a piperidine ring (green circle) or piperazine ring (blue circle) in their structure.	92
Figure 32. Normalized PL spectrum of CuI at 255 nm excitation, after recrystallization from a saturated acetonitrile solution.	93
Figure 33. Normalized PL spectra of a) piperidine, CuI-piperidine cluster, and 4:1 CuI-piperidine cluster (the 4:1 CuI cluster spectra were used as a reference for comparison with the CuI-piperidine) and b) Piperazine, CuI-Piperazine cluster, and 4:1 CuI-piperazine cluster.	94
Figure 34. Normalized PL spectra of a) MBZP, CuI-MBZP cluster, and 4:1 CuI-MBZP cluster, b) TBZP, CuI-TBZP cluster, and 4:1 CuI-TBZP cluster, c) 4TFMPP, CuI-4TFMPP cluster, and 4:1 CuI-4TFMPP cluster, and d) 3TFMPP, CuI-3TFMPP cluster, and 4:1 CuI-3TFMPP cluster.	96
Figure 35. Normalized PL spectra of a) DABCO, CuI-DABCO cluster, and 4:1 CuI-DABCO cluster and b) hexamine, CuI-hexamine cluster, and 4:1 CuI-hexamine cluster.	97
Figure 36. Normalized PL spectra of a) quinine and CuI-quinine cluster, b) caffeine and CuI-caffeine cluster, and c) DM and CuI-DM cluster.	98
Figure 37. Normalized PL spectra of BZP and CuI-BZP.	99

Figure 38. Normalized PL spectra for CuI clusters with cocaine-HCl (black) and PCP (red).....	100
Figure 39. Normalized PL spectra of morphine and CuI-morphine.	100
Figure 40. Normalized PL spectra of (a) NPP and CuI-NPP and (b) 4MB-fentanyl and CuI-4MB-fentanyl.	101
Figure 41. An initial market evaluation of the law enforcement customer segments. ..	119
Figure 42. A 2-step NARK II® color test kit to test for synthetic cannabinoids. The test pouch on the right has been opened, showing a glass capsule filled with the test chemical reagent.	121
Figure 43. The Thermo Fisher Scientific TruNarc™ being used to identify a rock of crack cocaine in a plastic bag.	122
Figure 44. A prototype version of the handheld fluorescence spectrometer.....	131
Figure 45. The Home screen of the mobile app.	132
Figure 46. The Information screen after a positive match.	133
Figure 47. Application app for “Street mode”.....	134
Figure 48. Application map for “Lab Mode”	135

LIST OF TABLES

Table 1. Types of mills and information on resulting impacts of ball bearings for each type.	5
Table 2. Binding Energy for ethene and propene on h-BN, hydrogen on BN (both calculated in this work), ethene on platinum group metals, hydrogen on Pt(100), hydrogen on Pd(100), and hydrogen on Ni(100). No temperature or pressure effects were included in these calculations.....	57
Table 3. Hydrogenation yields, TOFs, and single use TONs of various substrates over defect-laden h-BN and other catalytic systems with a mill speed of 66 RPM unless otherwise specified. All information was derived from steel reactor data.....	64
Table 4. Close contacts with CH ₃ hydrogens in structures modeled and olefin bond length. SW1 and SW2 both consist of two 5-member rings and two 7-member rings. SW1 is distorted away from the substrate and SW2 is distorted toward the substrate.....	69
Table 5. Major spectral peak location and FWHM of CuI clusters with various amines tested obtained by Gaussian peak fitting and the limit of detection (LOD), showing the ability for the method to detect various amines at low concentrations.	104
Table 6. Categories of recommended analytical techniques used for drug analysis. ...	113

CHAPTER 1: INTRODUCTION AND LITERATURE OVERVIEW

1.1 Mechanochemistry Overview

Mechanochemistry is the process of using mechanical energy to induce chemical reactions. Traditionally, this has been done by grinding chemicals together with a mortar and pestle. With the advancement of technology, the application of ball milling to provide mechanical grinding has allowed the blossoming field to progress into a new horizon. A process that has commonly been used for industrial scale particle reduction and material mixing, ball milling has gained traction as a chemical reaction technique in recent times. Since the 2000s, mechanochemistry has made its way into the fields of organic synthesis, inorganic synthesis, materials synthesis, co-crystal formation, and catalysis.

The chemistry behind a mechanochemical reaction lies in the impacts of the ball bearings. At impact with other media in the reaction, the reaction material breaks down and the surface energy increases enough for a reaction to achieve its activation energy barrier and yield products. The kinetic energy of those impacts can be measured by the force, equal to the mass and acceleration of the ball bearings during the reaction. The forces within the process can be separated into two main types, compressive force and shear force. Compressive forces result from head on collisions between ball bearings or the ball bearings and the reaction vessel inner surface. Shear forces result from ball bearings sliding against each other or the reaction vessel inner surface in a grinding manner. Each type may be exclusive or prevalent in different ball milling techniques,

which can be advantageous when the goal of an experiment involves particle reduction (compressive force) or delamination of layered materials (shear force).

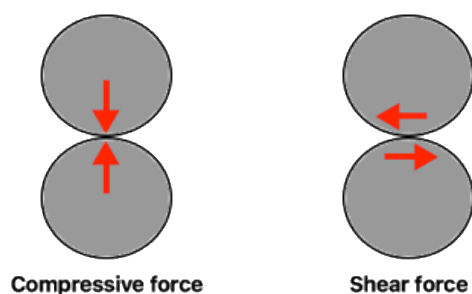


Figure 1. Diagram of compressive forces vs. shear forces via ball milling. The red arrows represent the direction of impact for each ball bearing.

1.1.1 History of Mechanochemistry

The use of mechanochemistry can be traced back to prehistoric times, in which humans made use of the mortar and pestle to prepare food by grinding materials down into smaller pieces. The unintended chemical reactions that are assumed to have occurred were not scientifically realized at the time. The first reported use of mechanochemistry was around 315 B.C. when cinnabar, a mineral containing mercury(II) sulfide, was ground with a copper mortar and pestle to produce mercury. It was not until the 19th century that the technique was reported again, when Faraday published his work on the reduction of silver chloride to silver metal by grinding it with other metals using a mortar and pestle.¹⁻³ In the 1880's, Belgian chemist Walthère Spring published papers on

the compression and its influence on phase changes and chemical reactions. Peers disputed his work, citing the lack of knowledge on the role of atmospheric moisture in the chemical reactions.² In the late 19th century, the “father of mechanochemistry”, Matthew Carey Lea made advances in the field with his work. Known for his pioneering work on the chemistry of photography investigating the effects of static pressure on silver materials to develop images, he observed that the mechanical grinding of silver halides and mercuric chloride, compounds that did not decompose when heated, resulted in the formation of subhalides. This led him to suggest that these reactions were possibly induced through mechanical action rather than heat, further laying the foundations of mechanochemistry.^{2, 4} In 1919, Friedrich Wilhelm Ostwald, who won a Nobel Prize for his work in catalysis, chemical equilibria, and reaction vessels, first coined the term “mechanochemistry” when he stated “Mechanochemistry is a branch of chemistry which is concerned with chemical and physico-chemical changes of all states of aggregation due to the influence of mechanical energy.”^{2, 5} From 1914-1918, L.H. Parker made strides by building the first mechanochemical reactor. The apparatus was essentially a mortar and pestle installed in a desiccator, which would allow for some control of the reaction environment. Parker used his reactor to conduct experiments of solid state reactions, observing a successful metathesis reaction between sodium carbonate and barium sulfate, a repeat of experiments done by Spring in the 1880’s.⁶ The 1920’s brought along the first mechanochemical reactions using organic molecules. Waentig published multiple papers regarding the effects of milling on the solubility of cellulose.⁷

The use of a mortar and pestle is not sufficient to obtain consistent results between experiments. Achieving certain particle sizes and applying a known amount of energy when grinding would be too difficult via this route. The development and advances in milling technology led to an increase in traction for research in mechanochemistry. Although early mills were developed for their use in industrial processing, they were utilized by some researchers to investigate new applications. In the mid- to late-20th century, the use of mechanical grinding made its way into mechanical alloying and inorganic synthesis.² It was not until the early 2000's the practicality of ball milling was extended to organic synthesis and the formation of organic co-crystals.

1.1.2 Milling Equipment

The components of a ball milling reaction typically consist of a reaction vessel, the milling media (ball bearings), and the reaction material. The reaction vessel usually has a gasket to prevent leakage of small particles and allow for a gas-tight environment. Ball milling processes can be categorized into two classifications based on the force of the impacts involved in the process: high-energy and low-energy. A variety of mills are available and can be chosen for specific reactions scales and applications. For example, all mills can be used for size reduction while one may be better-suited for delamination than another. Table 1 shows the common types of mills and the kinds of impacts involved. Provided below is a general description of each of the mills, with some details of the specific mills used in this work.

Table 1. Types of mills and information on resulting impacts of ball bearings for each type.

Mill	Strength of impacts	Type of stress from impacts
Shaker mill	High-energy (3053 N)	Mainly compressive
Planetary mill	Variable	Major shear, some compressive
Pebble or roller mill	Low-energy (329 N)	Major shear, minor compressive
Attrition mill	Variable (3881 N)	Shear and compressive
Hybrid	-	-

1.1.2.1 Shaker Mill

The shaker mill has become common equipment for laboratory-scale mechanochemistry research. SPEX® and RETSCH® are two companies that offer products in this market. The shaker mill is similar to a paint shaker, in which multiple paint colors are added into a paint can and mechanically shaken to obtain a homogeneous mixture, or new color. The mill is considered a high-energy process, so it shakes at a faster speed than a paint shaker. Various sizes of reaction vials can be purchased to mill 0.2 grams to 10 grams of reaction material. Setting up a reaction involves a few main components of the reaction vessel: vial, cap, gasket or O-ring, and ball bearings. The reaction material is charged to the reaction vessel before closing it with the cap. A gasket or O-ring between the cap and vial allow for a controlled reaction atmosphere and prevents the loss of reaction material as the particle size is reduced during milling. Once prepared, the vial is clamped into the vial slot of the mill. When milling, the clamps move back and forth in a figure eight movement at approximately 1200 RPM. SPEX® offers the

8000M and 8000D models which have one and two vial slots, respectively. A factory stock mill typically has a start button and a stop/pause button. When milling has started, the duration of the milling is dictated by a timer set by the user. A disadvantage of the shaker mill is the lack of ability to increase reaction scales higher than 10 grams. This method is not feasible for industrial processes.



Figure 2. SPEX mixer mill, also commonly known as a shaker mill.

1.1.2.2 Planetary Mill

A planetary mill is also a common choice for performing mechanochemical reactions. It consists of a larger reaction vessel that allows for reaction scales up to 100 kg. The vessel is charged with ball bearings and the reaction material, then covered by a lid with a gasket in between. The vessel clamps into a slot, and sits upright on a rotating platform, that sits on a larger rotating platform that rotates in the opposite direction of the

other. This rotation dynamic leads to the ball bearings sliding and grinding against each other and the inner walls to apply mostly shear forces to the reaction material.⁸ Like the shaker mill, the duration of milling is controlled by a timer set by the user. A setting that can be changed to control certain milling parameters, such as the impact forces of the ball bearings, is the rotation speed. Typical planetary mills can be set to speeds up to 700 RPM. A disadvantage of the planetary mill is its limit of scaling up to industrial-sized reactions.



Figure 3. Planetary mill.

1.1.2.3 Roller Mill

The roller mill, also known as the pebble mill, is typically used for laboratory-scale and industrial-scale processes for mixing and size reduction. The advantage of this type

of mill is that it is more easily scalable than the shaker mill and planetary mill. It consists of a cylindrical reaction vessel that sits on its side and rolls on a horizontal axis. The vessel is charged with ball bearings and the reaction material before rolling. The milling media tumbles like clothes in a dryer, causing the ball bearings to provide shear force as they grind against each other and the inner walls with the reaction material in between. As the ball bearings creep up the side of vessel, gravity eventually acts on them and causes them to fall on top of the others, providing relatively higher energy compressive forces. The rolling speed of the mill can be varied to control the force of impacts of the ball bearings, although at a high enough speed centripetal forces will prevent the ball bearings from tumbling. A laboratory-scale roller mill was custom-built with a gas inlet and outlet to allow for the introduction of gas phase reactants into the system and an external heating element to conduct experiments at moderately high temperatures.

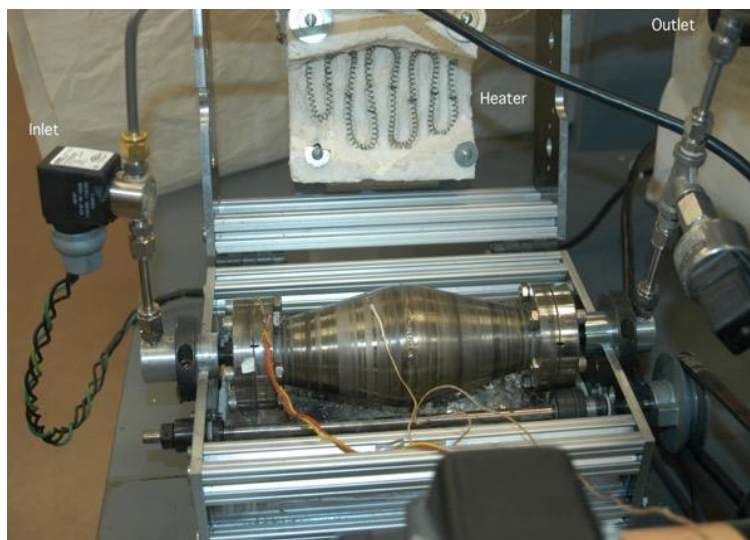


Figure 4. Roller mill, also commonly known as a pebble mill. This mill was customized to allow for gas input and external heating.

1.1.2.4 Attrition Mill

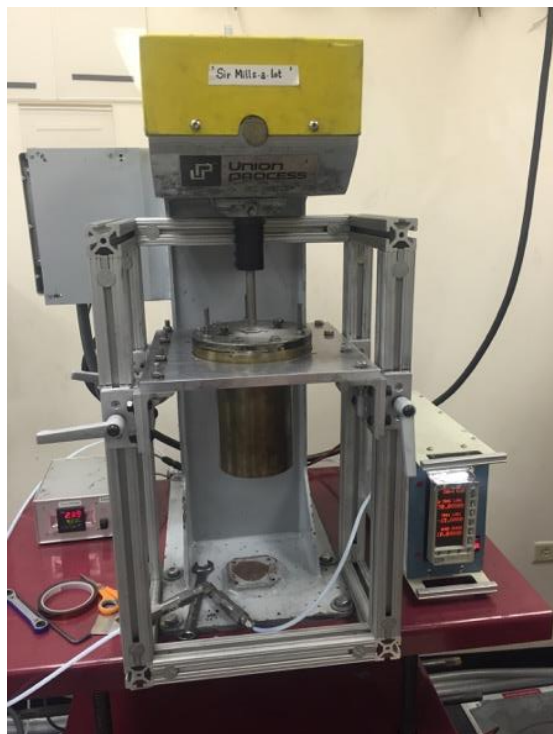


Figure 5. Union Process attrition mill.

The attrition mill is another type of mill that can be designed for either laboratory-scale or industrial-scale processes. Its components consist of a reaction vessel, lid, ball bearings, and stirring tree. The dynamics of attrition milling can be compared to a kitchen stand mixer, in which the beater attachment is directly connected to the motor that allows the beater to stir ingredients in a mixing bowl. On an attrition mill, the stirring tree is the beater attachment, the reaction vessel is the bowl, and the milling media and reaction material are the ingredients. Since the motor directly controls the stirring of the ball bearings, the mechanical energy provided by the motor correlates with the energy input

of the reaction. Union Process® offers mills that can stir at variable speeds between 1 RPM and 700 RPM. Experiments are conducted with a large amount of ball bearing that deliver both high-energy shear forces and impact forces when stirring at high velocities. A lid for the reaction vessel was modified with a gasket and gas inlet and outlet to allow for the input of gas to the milling process. A cooling jacket or heating jacket can be equipped to conduct temperature-controlled experiments.

1.1.3 Milling Conditions

With the application of ball milling to mechanochemical reactions, the ability to control the reaction environment is beneficial to learning more about the fundamentals of mechanochemistry. Some of the results of pioneering experiments conducted with simple grinding techniques, such as using a mortar and pestle, were challenged based on the unknown role atmospheric conditions played on the products that were formed. This led to L.H. Parker developing his mechanochemical reactor, which minimized the atmospheric effects on the reaction system. Technological advances in the 20th century have afforded new ways to control reaction conditions during ball milling.

1.1.3.1 Controlling the Atmosphere

The introduction of oxygen or moisture into mechanochemical reactions can be detrimental to reaction yields. Reactions that involve the use of pyrophoric metals or other reactants that violently interact with air benefit greatly from a controlled atmosphere.

Shaker mill vials and laboratory-scale roller mill reaction vessels are small enough to conveniently fit into a glove box. The use of a glove box allows for the preparation of reactions under an inert environment. Before bringing the reaction vessel out of the glove box to set up in its respective milling apparatus, it is sealed with the help of O-rings to retain the inert environment inside the vessel. Modifications to the roller mill and attrition mill could allow for the input of other gases from pressurized gas cylinders, such as carbon dioxide, nitrogen, propene, etc. This has been useful for mechanochemical methods for sugar production from biomass, in the high temperatures caused by friction in a high-speed attrition mill reaction would cause the resulting sugars to caramelize in the presence of atmospheric oxygen. Conducting the reaction under carbon dioxide would permit the toleration of higher temperatures without caramelization in said reaction.

1.1.3.2 Controlling the Temperature

Temperature changes could come from various sources during the milling process. Attrition mill reactions could reach temperatures of over 150 degrees Celsius when milling at high speeds due to the friction between the many ball bearing while stirring. In a shaker mill, the arms connected to the vial slots swing at 1200 RPM. The mechanical work generates heat inside the mill. The reaction itself must be considered when determining possible factors for an increase in temperature. Highly exothermic reactions may yield undesired products in some cases. On the other hand, certain reactions may need an input of additional energy by way of heat to improve the reaction rate and yield.

Regardless of the case, controlling the temperature during the milling process can be beneficial to the overall reaction.

For restricting high temperatures, the following options are provided. SPEX® offers a freezer mill to perform low temperature milling, equipped with a liquid nitrogen tub to cool the reaction vial during the milling process. Options for other types of mills require custom modifications to the apparatus. The attrition mill reaction vessel can be equipped with a cooling jacket that flows coolant through it.



Figure 6. Housing for the custom roller mill, which is equipped with a heating element to allow for external heating of the reaction vessel.

For higher milling temperatures, the apparatus of a mill can be equipped with a heating element to heat the exterior of the reaction vessel. This is practical for mills in

which the reaction vessel is exposed (e.g., roller mill and attrition mill), as opposed to one enclosed in steel housing (e.g., shaker mill and planetary mill).

1.1.3.3 Vials and Milling Media for Catalysis

Shaker mill vials and ball bearings made of various materials are commercially available. The most commonly used vials and media are made of stainless steel. Other commercially available vials include those that are made of plastic, agate, tungsten carbide, alumina, and zirconia. Depending on what reaction material needs to be milled, it may be necessary to choose a vial made of harder material. For example, milling silicon requires the use of a vial and media made of material with greater hardness, such as tungsten carbide. Using a stainless steel vial to mill silicon would damage the vial and milling media. Advances in mechanochemistry and its extension to organic synthesis led to an interesting discovery. In 2009, James Mack's work exhibited that Sonagashira Coupling reactions, conventionally achieved using a platinum catalyst and copper(I) co-catalyst, could result in high yields if a copper vial and milling media are used in place of copper(I) iodide as the co-catalyst.⁹

1.1.3.4 Metal-free reactions

For a proof of concept of a specific project, reaction conditions eliminating the presence of metal was necessary. The hydrogenation of olefins is catalyzed by the presence of late transition metals, such as iron or nickel. Investigations into metal-free

catalysis of the hydrogenation reaction would require the use of reaction vessels made of materials that will not inadvertently catalyze the reaction. Therefore, commonly used stainless steel reaction vessels and ball bearings are not suitable for metal-free reactions. For example, hexagonal boron nitride exhibits catalytic activity when defects are introduced to the boron nitride sheets by way of ball milling.¹⁰ This mechanical process of catalyst activation can be done using a shaker mill method. Using a stainless steel shaker mill reaction vial would result in iron and nickel contamination of the boron nitride powder, which must be avoided. Ceramic shaker mill vials and ball bearings made of zirconia or alumina can be used in place of the stainless steel vials to assure the boron nitride powder is metal-free. Once the catalyst is activated, it is used to react hydrogen and an olefin in a zirconia roller mill with zirconia milling media.

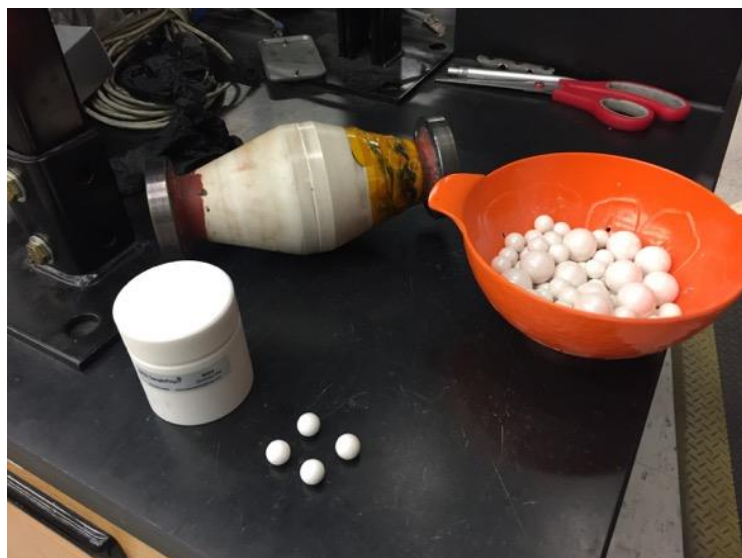


Figure 7. Ceramic reaction vessels and milling media used for metal-free reactions.

1.1.4 Practicality for Reaction Scale-Up

The various milling methods of mechanochemistry provide a practical means to scale a reaction from laboratory-sized to industrial-sized processes. Traditional wet chemistry reactions require efficient stirring and heating of the reaction solution, which may be difficult to scale up due to the necessary optimization of the heat transfer and mixing dynamics in a larger reaction. Optimization of mechanochemical reactions can be realized more easily with some possible factors to consider. For example, scaling up an attrition milling reaction will be used. Attrition milling delivers the easiest route to scale up to industrial-sized reactions because the technology is linearly scalable.¹¹ Increasing the reaction scale will require a larger reaction vessel and an increase of milling media. Attrition milling at high RPM creates enough friction to increase the systems temperature. For an industrial scale reaction, this temperature increase must be considered when optimizing a reaction done by an attrition milling method. Efficient stirring of the milling media must also be studied. A larger reaction will utilize a motor and stirring tree that can mechanically move the increase in weight of ball bearings without damage to the tree. The key is to translate the impact energies of the milling media observed in a laboratory scale reaction to a larger reaction. Discrete element modeling (DEM) can be used to simulate the impact energies under specific milling conditions.⁸ This will also help simulate the dynamics in the movement of ball bearings while stirring. Although most mechanochemical methods do not require heat and use little to no solvent, the power to run the mill requires energy input. Overall, economic assessments of automated industrial

processes must be done to determine the cost efficiency of a mechanochemical process regarding factors such as energy usage and decrease in solvent use and disposal relative to a traditional wet chemistry process.

1.2 Mechanochemical Synthesis

Ball milling has been a mainstay of techniques in the material processing industry since the invention of mechanical ball mills. Traditionally used for homogeneous mixing or size reduction, its applications have been expanded into broad areas of chemistry over the last half century. Some of those areas are metal alloying¹²⁻¹⁶, inorganic synthesis¹⁶⁻¹⁹, material synthesis^{11, 20-24}, organic synthesis^{16, 25-27}, catalysis^{9, 16, 19, 27-29}, and drug formulation^{16, 18, 30}.

1.2.1 Synthesis of Inorganic Compounds and Materials

Mechanochemical investigations started with simple reactions between inorganic substrates. In the 1890s, Matthew Carey Lea investigated the effects of mechanical grinding on silver halides and mercuric chloride, observing the decomposition of the compounds when grinding them in a mortar and pestle.^{2, 4} From 1914-1918, L.H. Parker developed the first mechanochemical reactor.⁶ This invention allowed him to perform solid-solid metathesis reactions between inorganic salts. The current state of mechanochemistry has roots that coincide with the invention of the SPEX 8000 mixer mill in 1957. The SPEX 8000 became a standard instrument for groups that investigated

mechanochemical reactions. In the 1960s, various research groups began to focus on mechanochemical methods for both metal alloying and inorganic processing techniques. Eventually, the two sub-branches merged to form a community that shared their knowledge from their work in mechanochemistry.² In these early years, mechanochemistry was used as a new route to process alloys and metal oxides. Today, it is applied to the synthesis of ceramic materials²⁰, processing graphene-based materials¹¹, synthesizing metal organic frameworks (MOFs)^{16, 18, 30}, forming pharmaceutical co-crystals^{16, 18, 30}, in addition to many other processes.

1.2.2 Reactions in Organic Synthesis

Mechanical grinding on organic substrates was first investigated in the 1920s, in Waentig's studies on the effects of grinding on cellulose solubility.⁷ From then, there was a gap that saw a lack of notable efforts to extend applications of mechanochemistry to organic chemistry. It was not until the 2000s, that research journals experienced an influx of literature on mechanochemical routes for organic reactions via ball milling. This increase in traction has proved the practicality for using ball milling in organic synthesis. Mechanochemistry is accustomed to ties to industrial processes, and it is no different in its extension to organic synthesis. The use of mechanochemical methods for synthesis has afforded green routes for industrial reactions, an attractive factor to prove their feasibility. One of the most significant advantages is that little to no solvent is required for a reaction.¹⁶ Current methods for organic synthesis require excess amounts of solvent to provide a medium to facilitate the reactions, in which most of the solvent is disposed as

waste after completion. For industrial scale reactions, the ability to decrease or eliminate the use of solvents would be considerably cost-effective.

Work on reactions within the realm of organic chemistry has been published showing successful translations into mechanochemical processes. Among the organic reactions that have been done via mechanochemical routes are nucleophilic substitution reactions between benzyl halides and nucleophilic group 1 halide salts²⁶, the reduction of aldehydes, ketones, and esters to their corresponding alcohols using sodium borohydride or lithium aluminum hydride³¹, the formation of α,β -unsaturated esters³², the Nobel Prize-earning Wittig reaction^{27, 33}, and the Nobel Prize-earning Diels-Alder reaction³⁴. Mechanochemistry has also started to become established in organic catalysis. The hydrolysis of cellulose has been popular for its potential bioethanol production process. Traditional methods involve the use of sulfuric acid solutions or the use of enzymes to convert cellulose to glucose, both methods having their disadvantages. A mechanochemical method that utilizes kaolin as a solid acid catalyst can convert cellulose to simple sugars without the use of solvent in the reaction step.^{11, 29} This method has led to other mechanochemical cellulose to sugar routes.³⁵ Base-catalyzed reactions such as the Tishchenko reaction³⁶ and Morita-Baylis-Hillman reaction^{27, 37} have been realized. Mechanochemical metal-catalyzed reactions have also been seen in literature. Work has been published on the Nobel Prize-earning Suzuki coupling, which is the palladium-catalyzed cross coupling of an aryl halide and organoboron species.²⁷⁻²⁸ Another coupling reaction, Sonogashira coupling, was done through ball milling methods.²⁷ This is the cross coupling of an aryl halide and terminal alkyne with the help of a palladium catalyst and

copper co-catalyst. Copper(I) iodide is typically used as the co-catalyst, but literature shows that ball milling in a copper reaction vial eliminates the use of copper(I) iodide to successfully yield the product.⁹

1.3. Catalytic Hydrogenation

The catalytic addition of hydrogen to unsaturated carbon bonds has served as an important process in various industries. The petrochemical industry utilizes it when alkenes from the cracking process need to be converted to alkanes. In the pharmaceutical industry, the synthesis of some active compounds may require the reduction of pi-bonds in steps leading to the final product. Polyunsaturated fatty acids are hydrogenated to make food products like peanut butter, margarine, and vegetable oil-based shortening. It has proved to be one of the more significant discoveries in science that has been widely commercialized to benefit large-scale industrial processes, crediting Paul Sabatier the 1912 Nobel Prize in chemistry. Hydrogenation is carried out by adding a hydrogen molecule, H_2 , to an unsaturated substrate (i.e. alkene) in the presence of a catalyst that provides a reaction path of lower energy in contrast to an uncatalyzed reaction. Group 10 metals have traditionally been used as hydrogenation catalysts, allowing for the use of lower temperatures to achieve bond reduction on an industrial scale. The types of catalysts can be separated into two general categories: heterogeneous catalysts and homogeneous catalysts. The former, conventionally used for large-scale commercial applications, consists of those catalysts that can be separated from the reaction mixture following the completion of the reaction. Homogeneous catalysts are those that dissolve

in the reaction mixture and result in a single phase at the end of the reaction, making them difficult to recover and reuse.

1.3.1 Heterogeneous Metal Catalysts for Hydrogenation

Since Paul Sabatier's discovery of their catalytic activity towards the hydrogenation reaction, platinum and palladium have been the industrial choice of catalysts for reducing unsaturated bonds. In 1912, Sabatier was awarded the Co-Nobel Prize award, along with Victor Grignard (who won it for the discovery of Grignard's Reagent), for his work on the innovative process that would improve the hydrogenation reaction. Before the use of catalysts, hydrogenation was only possible at high temperatures. In the presence of well-known catalysts, alkanes can be produced from their preceding alkenes at near-ambient temperatures. Although ambient temperature hydrogenation is achievable, large scale industrial processes employ elevated temperature conditions to improve catalytic efficiency and justify the use of the expensive precious metal catalysts as economically feasible. Sabatier's work on gas-phase hydrocarbons was an extension of the pioneering work done in the 1890s by James Boyce, who discovered that the presence of nickel could aid in the hydrogenation of cottonseed oil.³⁸⁻³⁹ This use of heterogeneous catalytic hydrogenation on cottonseed oil was further developed to be applied to vegetable oils by Wilhelm Normann.⁴⁰ By using trace nickel, he hydrogenated polyunsaturated fatty acids of vegetable oils in what was known as a "fat hardening" process. His work initiated the utilization of catalytic hydrogenation in the food industry, which is one of the most significant industries that uses hydrogenation.⁴¹

Hydrogenation proceeds on the catalytic metal surface by a series of steps (See Figure 8). The first step is the physisorption of substrates, alkene and hydrogen molecules, on the catalyst surface via Van der Waals forces. The next step is the chemisorption of the alkene and hydrogen molecules onto the catalyst surface, forming chemical bonds between the substrates and the catalyst surface. Through this bonding, the alkene is in equilibrium between pi-bonded and sigma-bonded species, with respect to the initial alkene carbons. The carbons of the sigma-bonded species are chemically bonded to the catalyst surface. The hydrogen molecule is cleaved and single hydrogen atoms are chemically bonded to the surface of the catalyst. The following step involves the chemisorbed carbon reacting with one of the hydrogens to form a new carbon-hydrogen bond, breaking the bond between that carbon and the catalyst surface to yield a semi-hydrogenated intermediate. The final step, desorption of the substrates, occurs when the other chemisorbed carbon reacts with a second hydrogen atom, leading to the addition of the hydrogen to the semi-hydrogenated intermediate to form a new carbon-hydrogen bond on the second carbon atom and break the bond between that carbon and the surface of the catalyst.⁴²

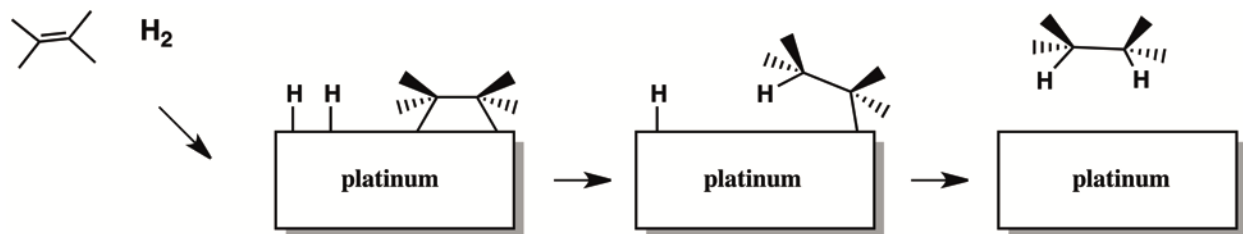


Figure 8. Mechanism of catalytic hydrogenation on metal surface.

1.3.2 Homogeneous Catalysts for Hydrogenation

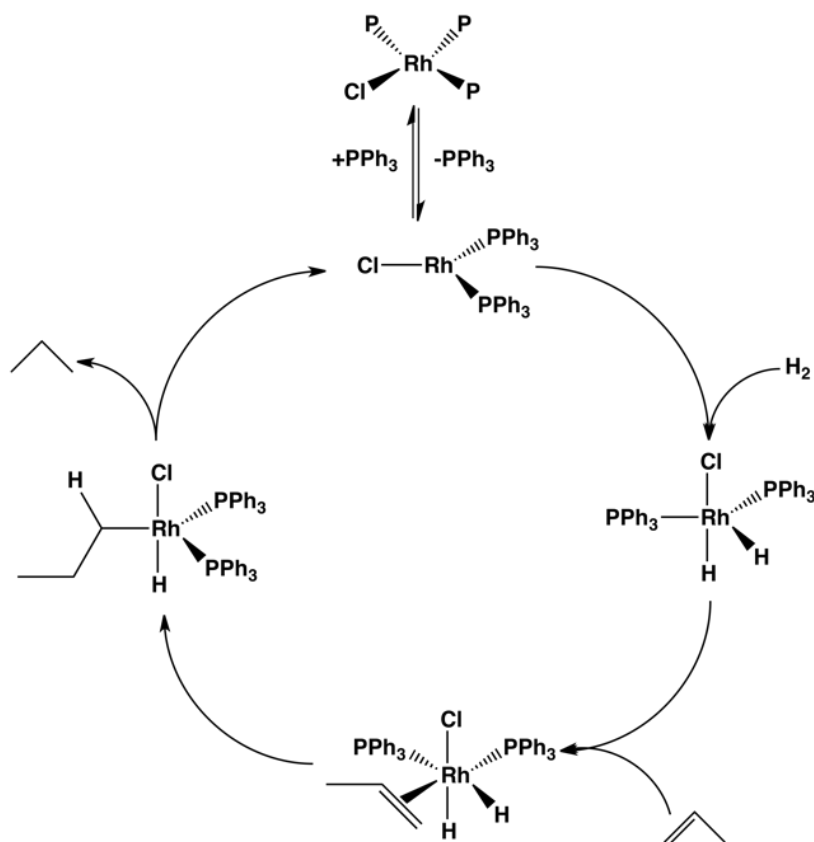


Figure 9. Mechanism of catalytic hydrogenation via oxidative addition using Wilkinson's catalyst.

Homogeneous catalysts for olefin hydrogenation traditionally employ organometallic complexes. Geoffrey Wilkinson's work on organometallic complexes of platinum group metals, which earned him the 1973 Nobel Prize in chemistry, includes his discovery of Wilkinson's catalyst.⁴³ This catalyst, chloridotris(triphenylphosphane)-rhodium(I), was the first non-ground state metal catalyst for olefin hydrogenation. This

opened the door for the discovery of other hydrogenation catalysts based on platinum group complexes, such as Schrock-Osborn catalyst⁴⁴ and Crabtree's catalyst⁴⁵.

The mechanism of olefin hydrogenation using these catalysts proceeds via three mechanisms that differ in their interaction with hydrogen: oxidative addition, heterolytic activation, and homolytic activation. For example, hydrogenation using Wilkinson's catalyst (Figure 9) starts with the dissociation of a triphenylphosphine ligand from the rhodium complex followed by the oxidative addition of hydrogen (in form of two hydrides individually coordinated to the metal) to the rhodium. Then the olefin complexes onto the rhodium. With the substrates coordinated to the rhodium, a hydride is transferred to the olefin. This is followed by the reductive elimination and transfer of the second hydride atom to the olefin, regenerating the catalyst in the process.⁴⁶ Olefin hydrogenation using dichlorotris(triphenylphosphine)ruthenium(II) starts with the complexation of a hydrogen molecule (in form of a dihydrogen ligand) to the ruthenium. An amine base is added to the reaction to abstract a proton from the hydrogen molecule to form an aminium ion, which takes away one of the chloride ligands to result in the trigonal bipyramidal RuHCl(PPh)_3 - heterolytically activating the hydrogen. From this step, the olefin inserts, forming an octahedral intermediate. The hydrogen is transferred to the olefin and reverts to a trigonal bipyramidal geometry, followed by a second heterolytic activation of hydrogen. This second hydrogen is transferred to the partially hydrogenated olefin to yield and eliminate the corresponding alkane from the metal complex.⁴⁷⁻⁴⁸ Hydrogenation by way of homolytic activation of hydrogen is rare. As seen in the Iguchi catalyst, it involves the formation of transition metal complexes stabilized by radicals. Two Co(CN)_5^{3-}

complexes homolytically cleave a hydrogen molecule to yield two $\text{COH}(\text{CN})_5^{3-}$. One hydrogen radical is transferred to an olefin, yielding an alkyl radical, followed by a second hydrogen radical transfer from the second $\text{COH}(\text{CN})_5^{3-}$. This last step affords the corresponding alkane and regenerates the catalyst.⁴⁹ The last decade has brought along novel catalysts for homogeneous hydrogenation that do not require transition metals and thus, proceed via different mechanisms.

1.3.3 Frustrated Lewis Pairs (FLPs) and Other Metal-Free Catalysts for Hydrogenation

The first metal-free catalyst for hydrogenation, known as frustrated Lewis pairs (FLPs), was discovered by Stephan in the mid-2000s.⁵⁰⁻⁵⁷ Observations were made of hydrogen activation on a compound containing a phosphine with bulky electron-donating groups and a borane with bulky electron-withdrawing groups.⁵⁷ This led to the discovery of the activation of other small molecules and the hydrogenation of an olefin.⁵⁵ The mechanism involves the use of a mixture of a bulky nucleophilic species and a bulky electrophilic species in the presence of hydrogen and the olefin. The more nucleophilic and electrophilic the pair of species, the more active they are. A bulky Lewis base such as tri-*tert*-butylphosphine and a bulky Lewis acid like tris(pentafluorophenyl)borane (seen in Figure 10) would not be able to form a Lewis adduct due to the steric constraints of the bulky functional groups. A mixture of such FLPs is able to heterolytically cleave a hydrogen molecule, with a proton transferring to the phosphorous atom and the remaining hydride transferring to the boron atom to form a phosphonium borate salt. The subsequent hydrogenation of an olefin is thermodynamically favored, wherein a proton

transfer occurs from the phosphorous atom to the olefin followed by a hydride transfer from the boron atom to the semi-hydrogenated olefin species.⁵⁵

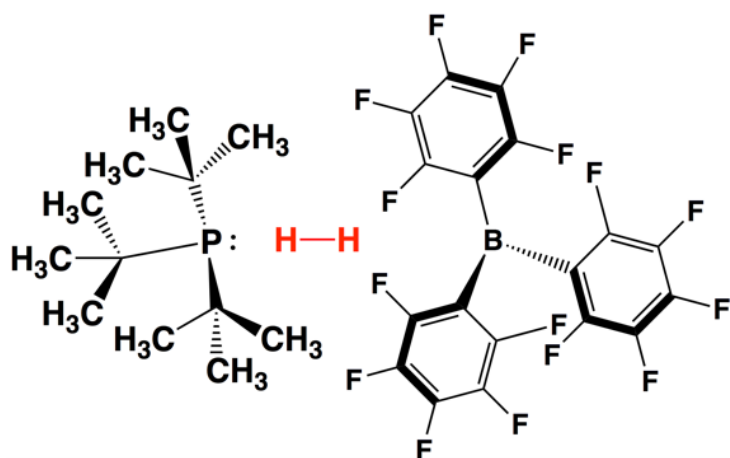


Figure 10. Representation of hydrogen activation using frustrated Lewis pair.

1.4 Methods for the Presumptive Identification of Illicit Substances

The accurate identification of an illicit substance is vital in the fields of criminalistics and law enforcement. The lack of accuracy in the identification process could yield false positives or false negatives. This process can be broken up into two types of methods: presumptive tests and confirmatory tests. Law enforcement personnel are commonly equipped with only presumptive tests in the field while crime lab analysts typically have the luxury of access to both types.

1.4.1 Traditional Methods for Presumptive Identification of Illicit Substances

Presumptive tests are typically used as the first line of testing to detect the possible presence of an illicit substance in a suspected sample. The most popular presumptive test used are known as chemical spot tests, which change a specific color in the presence of drugs. For example, the Scott test (also known as the cobalt(II) thiocyanate test) will turn blue in the presence of cocaine.⁵⁸ Police use a variety of different chemical spot tests, commercially available as NARK II® kits and NIK® kits, to detect illicit drugs and provide probable cause for an arrest. These presumptive tests are not widely used as evidence in court. Crime lab analysts are responsible for providing solid evidence by confirming that the identity of the substance matches with that of the arresting officer's presumptive test results. Confirmatory testing methods are those that provide information on the chemical structure of the sample. Those commonly used in crime labs are gas chromatography-mass spectrometry, infrared spectroscopy, and Raman spectroscopy. In the confirmatory identification of an unknown, analysts may deploy the variety of chemical spot tests as a quick screening process to verify the presumptive identity before they move forward to the more time-consuming confirmatory methods.

Although convenient as a testing method, the chemical spot test method has many flaws. News outlets around the US have told stories of people that were arrested due to false positives. OTC Cold medicines⁵⁹, OTC pain relievers⁵⁹, salt⁵⁹, quinine⁵⁹, and sugar⁵⁹ will cause some of these tests to yield a false positive for illicit substances. The Scott test is known to turn blue not only in the presence of cocaine, but also diphenhydramine, or Benadryl.⁵⁸ The chemicals in the spot tests react with certain functional groups of the target analyte, forming a new compound indicated by a color change or formation of precipitate. Many different drugs can be categorized into classes by their chemical structures (i.e. amphetamines, opioids, barbituates, etc.) in which those in the same class share similar functional groups. The lack of selectivity for a chemical spot test may also result in false positives (presence of an illicit substance) when testing non-illicit drugs.⁵⁸,⁶⁰ Another flaw is the ability to keep up with designer drugs that are being introduced regularly. It is common for law enforcement to encounter substances and pills they cannot presumptively identify, due to the absence of a test that can detect the new drug. These new drugs must be studied to develop new presumptive methods to identify them, a process that requires time and effort. By the time a method is developed and deployed for field use, it is possible that there would be a new popular drug appearing in the underground markets that cannot be presumptively detected. Also, drugs on a controlled substance list are banned based on their chemical structure. Simply changing a functional group on the chemical structure of a banned substance could give rise to a new drug that is not controlled, and therefore, technically legal.



Figure 11. A typical NIK® kit, one of the brands of color kits used by law enforcement agencies to presumptively identify drugs in the field.

1.4.2 Novel Methods for Presumptive Identification of Illicit Substances

The failings of traditional presumptive drug testing methods bring about the need for a better method, especially for use in the field by law enforcement personnel. The number of false positives and inability to keep up with the constant introduction of new synthetic drugs are significant disadvantages that must be addressed.

Raman spectroscopy has been one of the many confirmatory techniques large crime labs may use to test evidence. Recently, portable Raman spectroscopy-based systems have been deployed for presumptive field use. The most popular of devices is the Thermo Scientific® TruNarc™ Handheld Analyzers. Different versions of the device are marketed to law enforcement that are in narcotics divisions and bomb squad divisions.

These handheld devices have a LCD touchscreen and work with an offline database of tens of thousands of Raman spectral profiles for various compounds. With the TruNarc™ the user can determine the identity of an unknown substance within seconds by placing the optical sensor near the sample to scan. The scanning can be done through a plastic bag or a glass vial, allowing the tester to avoid touching the sample in most cases. The non-contact sampling is also an advantage when considering hazard concerns in handling drugs such as fentanyl, which is readily absorbed through the skin and can harm the tester if handled without taking proper safety precautions. One major disadvantage of the TruNarc™ is its price point. Most agencies do not have the budget to afford one so they are left with using the flawed chemical spot tests. Although superior as a testing method, wide law enforcement adoption of the portable devices like the TruNarc™ is not feasible unless it becomes more affordable.

Aptamer-based techniques have made their way into forensic applications. Aptamers are oligonucleotides or peptides that can selectively bind to a target substrate. Custom-made aptamers have been developed for various applications, notably for new sensor technologies. As sensors, the aptamers are intended to yield a signal when they bind to a target molecule. In the field of forensic science, aptamers that can detect cocaine have been developed. One type will yield a voltage signal and another type will emit light in the presence of cocaine.⁶¹⁻⁶³ The disadvantage in using aptamer technology is that each sensor is highly selective. Since different substances would require a different sensor, new aptamers must be developed for the wide variety of substances. The

development of each aptamer can be a long and expensive process, but they are easily mass produced once developed.

1.5 References

1. Takacs, L., The Mechanochemical Reduction of AgCl with metals: Revisiting an Experiment of M. Faraday. *Journal of Thermal Analysis and Calorimetry* 2007, 90 (1), 81-84.
2. Takacs, L., The historical development of mechanochemistry. *Chem. Soc. Rev.* 2013, 42, 7649-7659.
3. Faraday, M., On the Decomposition of Chloride of Silver, by Hydrogen, and by Zinc. *Quarterly Journal of Science, Literature, and the Arts* 1820, 8, 374-376.
4. Takacs, L., M. Carey Lea, the first mechanochemist. *Journal of Materials Science* 2004, 39 (16), 4987-4993.
5. Ostwald, W., *Handbuch der Allgemeinen Chemie, Band 1*. Akademische Verlagsgesellschaft mbH: Leipzig, 1919; Vol. 70.
6. Parker, L. H., CXLII.-Reactions by Trituration. *J. Chem. Soc. Trans.* 1914, 105, 1504-1516.
7. Baláž, P., *Mechanochemistry in Nanoscience and Minerals Engineering*. Springer-Berlin Heidelberg: Berlin, 2008.
8. Burmeister, C. F.; Kwade, A., Process engineering with planetarty ball mills. *Chem. Soc. Rev.* 2013, 42, 7660.
9. Fulmer, D. A.; Shearouse, W. C.; Medonza, S. T.; Mack, J., Solvent-Free Sonogashira Coupling Reaction via High Speed Ball Milling. *Green Chem.* 2009, 11, 1821-1825.
10. Nash, D. J.; Restrepo, D. T.; Parra, N. S.; Giesler, K. E.; Penabade, R. A.; Aminpour, M.; Le, D.; Li, Z.; Farha, O. K.; Harper, J. K.; Rahman, T. S.; Blair, R. G., Heterogeneous Metal-Free Hydrogenation over Defect Laden Hexagonal Boron Nitride. *ACS Omega* 2016, 1, 1343-1354.
11. Blair, R. G.; Chagoya, K.; Biltek, S.; SJackson, S.; Sinclair, A.; Taraboletti, A.; Restrepo, D. T., The scalability in the mechanochemical syntheses of edge

- functionalized graphen materials and biomass-derived chemicals. *Faraday Discuss.* 2014, 170, 223-233.
12. Suryanarayana, C., Mechanical Alloying and Milling. *Progress in Materials Science* 2001, 46 (1-2), 1-184.
 13. Suryanarayana, C.; Ivanov, E.; Boldyrev, V. V., The Science and Technology of Mechanical Alloying. *Materials Science and Engineering: A* 2001, 304-306, 151-158.
 14. Suryanarayana, C., *Mechanical Alloying and Milling*. CRC Press: New York, 2004.
 15. Lü, L.; Lai, M. O., *Mechanical Alloying*. Springer Science & Business Media: New York, 2013.
 16. James, S. L.; Adamns, C. J.; Bolm, C.; Braga, D.; Collier, P.; Friščič, T.; Grepioni, F.; Harris, K. D. M.; Hyett, G.; Jones, W.; Krebs, A.; Mack, J.; Maini, L.; Orpen, A. G.; Parkin, I. P.; Shearouse, W. C.; Steed, J. W.; Waddell, D. C., Mechanochemistry: opportunities for new and cleaner synthesis. *Chem. Soc. Rev.* 2012, 41, 413-447.
 17. Garay, A. L.; Pichon, A.; James, S. L., Solvent-Free Synthesis of Metal Complexes. *Chem. Soc. Rev.* 2007, 36 (7), 846-855.
 18. Friščič, T.; Halasz, I.; Štrukil, V.; Eckert-Maksić; Dinnebier, R. E., Clean and Efficient Synthesis Using Mechanochemistry: Coordination Polymers, Metal-Organic Frameworks and Metallodrugs. *Croat. Chem. Acta* 2012, 85 (3), 367-378.
 19. Ralphs, K.; Hardacre, C.; James, S. L., Application of heterogeneous catalysts prepared by mechanochemical synthesis. *Chemical Society Reviews* 2013, 42 (18), 7701-7718.
 20. Šepelák, V.; Düvel, A.; Wilkening, M.; BEcker, K.-D.; Heitjans, P., Mechanochemical reactions and syntheses of oxides. *Chem. Soc. Rev.* 2013, 42, 7507-7520.
 21. Jeon, I.-Y.; Choi, H.-J.; Jung, S.-M.; Seo, J.-M.; Kim, M.-J.; Dai, L.; Baek, J.-B., Large-Scale Production of Edge-Selectively Functionalized Graphene Nanoplatelets via Ball Milling and Their Use as MEtal-Free Electrocatalysts for Oxygen Reduction Reaction. *J. Am. Chem. Soc.* 2013, 135 (4), 1386-1393.
 22. Bux, S. K.; Yeung, M. T.; Toberer, E. S.; Snyder, G. J.; Kaner, R. B.; Fleurial, J.-P., Mechanochemical synthesis and thermoelectric properties of high quality magnesium silicide. *J. Mater. Chem.* 2011, 21 (33), 12259-12266.

23. Baláž, P.; Achimovičova, M.; Baláž, M.; Billik, P.; Cherkezova-Zheleva, Z.; Criado, J. M.; Delogu, F.; Dutková, E.; Gaffet, E.; Gotor, F. J.; Kumar, R.; Mitov, I.; Rojac, T.; Senna, M.; Streletskii, A.; Wieczorek-Ciurowa, K., Hallmarks of mechanochemistry: from nanoparticles to technology. *Chem. Soc. Rev.* 2013, **42**, 7571-7637.
24. Zhu, S.-E.; Li, F.; Wang, G.-W., Mechanochemistry of fullerenes and related materials. *Chem. Soc. Rev.* 2013, **42**, 7535-7570.
25. Stolle, A.; Szuppa, T.; Leonhardt, S. E.; Ondruschka, B., Ball Milling in Organic Synthesis: Solutions and Challenges. *Chem. Soc. Rev.* 2011, **40** (5), 2317-2329.
26. Vogel, P.; Figueira, S.; Muthukrishnan, S.; Mack, J., Environmentally Benign Nucleophilic Substitution Reactions. *Tetrahedron Letters* 2009, **50**, 55-56.
27. Wang, G.-W., Mechanochemical organic synthesis. *Chem. Soc. Rev.* 2013, **42**, 7668-7700.
28. Schneider, F.; Stolle, A.; Ondruschka, B.; Hopf, H., The Suzuki-Miyaura Reaction Under Mechanochemical Conditions. *Org. Process Res. Dev.* 2009, **13** (1), 44-48.
29. Hick, S. M.; Griebel, C.; Restrepo, D. T.; Truitt, J. H.; Buker, E. J.; Bylda, C.; Blair, R. G., Mechanocatalysis for biomass-derived chemicals and fuels. *Green Chem.* 2010, **12**, 468-474.
30. Friščič, T., New opportunities for materials synthesis using mechanochemistry. *J. Mater. Chem.* 2010, **20**, 7599-7605.
31. Mack, J.; Fulmer, D. A.; Stofel, S.; Santos, N., The first solvent-free method for the reduction of esters. *Green Chem.* 2007, **9** (10), 1041-1043.
32. Shearouse, W. C.; Korte, C. M.; Mack, J., A two-step ball milling method synthesized and purifies alpha, beta-unsaturated esters. *Green Chem.* 2011, **13** (3), 598-601.
33. Balema, V. P.; Wiench, J. W.; Pruski, M.; Pecharsky, V. K., Mechanically Induced Solid-State Generation of Phosphorous Ylides and the Solvent-Free Wittig Reaction. *J. Am. Chem. Soc.* 2002, **124** (22), 6244-6245.
34. McKissic, K. S.; Caruso, J. T.; Blair, R. G.; Mack, J., Comparison of shaking versus baking: further understanding the energetics of a mechanochemical reaction. *Green Chemistry* 2014, **16** (3), 1628-1632.

35. Kobayashi, H.; Kaiki, H.; Shrotri, A.; Techkawara, K.; Fukuoka, A., Hydrolysis of woody biomass by a biomass-derived reusable heterogeneous catalyst. *Chem. Sci.* 2016, 7 (692-696).
36. Waddell, D. C.; Mack, J., An environmentally benign solvent-free Tishchenko reaction. *Green Chem.* 2009, 11, 79-82.
37. Mack, J.; Shumba, M., Rate enhancement of the Morita-Baylis-Hillman reaction through mechanochemistry. *Green Chem.* 2007, 9 (4), 328-330.
38. Allardyce, C. S., *Fat Chemistry: The Science Behind Obesity*. Royal Society of Chemistry: Cambridge, 2012; p 329.
39. Boyce, J. Food product and manufacture thereof. 1924.
40. Bailey, A. E., Nickel Catalysts In Hydrogenation of Fats and Oils. *Industrial & Engineering Chemistry* 1952, 44 (5), 990-994.
41. Ranken, M. D., *Food Industries Manual*. 23rd ed.; Springer Science+Business Media: New York, 2012.
42. Červený, L., *Catalytic Hydrogenation*. Elsevier: New York, 1986; Vol. 27.
43. Osborn, J. A.; Jardine, F. H.; Young, J. F.; Wilkinson, G., The preparation and properties of tris(triphenylphosphine)halogenorhodium(I) and some reactions thereof including catalytic homogeneous hydrogenation of olefins and acetylenes and their derivatives. *J. Chem. Soc. A* 1966, 1711-1732.
44. Schrock, R. R.; Osborn, J. A., Catalytic Hydrogenation Using Cationic Rhodium Complexes. I. Evolution of the Catalytic System and the Hydrogenation of Olefins. *J. Am. Chem. Soc.* 1976, 98 (8), 2134-2143.
45. Crabtree, R. H., Iridium Compounds in Catalysis. *Acc. Chem. Res.* 1979, 12 (9), 331-337.
46. Halpern, J.; Okamoto, T.; Zakhariev, A., Mechanism of the chlorotris(triphenylphosphine) rhodium(I)-catalyzed hydrogenation of alkenes. The reaction of chlorodihydridotris(triphenyl-phosphine)rhodium(III) with cyclohexene. *Journal of Molecular Catalysis* 1976, 2, 65-68.
47. Hallman, P. S.; McGarvey, B. R.; Wilkinson, G., The Preparation and Reactions of Hydrido-chlorotris(triphenylphosphine)ruthenium(II) Including Homogeneous Catalytic Hydrogenation of Alk-1-enes. *J. Chem. Soc. A* 1968, 3143-3150.

48. Halpern, J.; James, B. R., Homogeneous Catalysis of D₂-H₂O Exchange by Ruthenium(III) Chloride: Evidence for the Heterolytic Splitting of Hydrogen. *Canadian Journal of Chemistry* 1966, *44* (6), 671-675.
49. Pregaglia, G.; Morelli, D.; Conti, F.; Gregorio, G.; Ugo, R., Catalysis by Cobalto-Cyano Complexes in Aqueous Solvents. *Discuss. Faraday Soc.* 1968, *46*, 110-121.
50. Stephan, D. W., Frustrated Lewis pairs: a new strategy to small molecule activation and hydrogenation catalysis. *Dalton Transactions* 2009, (17), 3129-3136.
51. Stephan, D. W., Frustrated Lewis Pairs. *Journal of the American Chemical Society* 2015, *137* (32), 10018-32.
52. Stephan, D. W., Frustrated Lewis Pairs: From Concept to Catalysis. *Accounts of Chemical Research* 2015, *48* (2), 306-316.
53. Stephan, D. W.; Erker, G., Frustrated Lewis pair chemistry: development and perspectives. *Angewandte Chemie International Edition in English* 2015, *54* (22), 6400-41.
54. Stephan, D. W.; Greenberg, S.; Graham, T. W.; Chase, P.; Hastie, J. J.; Geier, S. J.; Farrell, J. M.; Brown, C. C.; Heiden, Z. M.; Welch, G. C.; Ullrich, M., Metal-Free Catalytic Hydrogenation of Polar Substrates by Frustrated Lewis Pairs. *Inorganic Chemistry* 2011, *50* (24), 12338-12348.
55. Greb, L.; Oña-Burgos, P.; Schirmer, B.; Grimme, S.; Stephan, D. W.; Paradies, J., Metal-free Catalytic Olefin Hydrogenation: Low-Temperature H₂ Activation by Frustrated Lewis Pairs. *Angewandte Chemie International Edition* 2012, *51*, 10164-10168.
56. Welch, G. C.; Cabrera, L.; Chase, P. A.; Hollink, E.; Masuda, J. D.; Wei, P.; Stephan, D. W., Tuning Lewis acidity using the reactivity of "frustrated Lewis pairs": facile formation of phosphine-boranes and cationic phosphonium-boranes. *Dalton Transactions* 2007, (31), 3407-3414.
57. Welch, G. C.; San Juan, R. R.; Masuda, J. D.; Stephan, D. W., Reversible, Metal-Free Hydrogen Activation. *Science (Washington, DC, U. S.)* 2006, *314* (5802), 1124-1126.
58. Tsumura, Y.; Mitome, T.; Kimoto, S., False positives and false negatives with a cocaine-specific field test and modification of test proptocol to reduce false decision. *Forensic Science International* 2005, *155*, 158-164.

59. O'Neal, C. L.; Crouch, D. J.; Fatah, A. A., Detection of twelve chemical spot tests for the detection of drugs of abuse. *Forensic Science International* 2000, *109*, 189-201.
60. Kelly, J. F.; Addanki, K.; Bagasra, O., The Non-Specificity of the Duquenois-Levine Field Test for Marijuana. *The Open Forensic Science Journal* 2012, *5*, 4-8.
61. Stojanovic, M. N.; de Prada, P.; Landry, D. W., Aptamer-Based Folding Fluorescent Sensor for Cocaine. *J. Am. Chem. Soc.* 2001, *123* (21), 4928-4931.
62. Baker, B. R.; Lai, R. Y.; Wood, M. S.; Doctor, E. H.; Heeger, A. J.; Plaxco, K. W., An Electronic, Aptamer-Based Small-Molecule Sensor for the Rapid Label-Free Detection of Cocaine in Adulterated Samples and Biological Fluids. *J. Am. Chem. Soc.* 2006, *128* (10), 3138-3139.
63. Shen, B.; Li, J.; Cheng, W.; Yan, Y.; Tang, R.; Li, Y.; Ju, H.; Ding, S., Electrochemical aptasensor for highly sensitive determination of cocaine using a supramolecular aptamer and rolling circle amplification. *Microchimica Acta* 2014, *182* (1), 361-367.

CHAPTER 2: HETEROGENEOUS METAL-FREE HYDROGENATION OVER DEFECT-LADEN HEXAGONAL BORON NITRIDE

This work was previously published as “Heterogeneous Metal-Free Hydrogenation Over Defect-Laden Boron Nitride” by David J. Nash, David T. Restrepo, Natalia S. Parra, Kyle E. Giesler, Rachel A. Penabade, Maral Aminpour, Duy Le, Zhanyong Li, Omar K. Farha, James K. Harper, Talat S. Rahman, and Richard G. Blair in *ACS Omega*, Volume 1, 2016, pp. 1343-1354 © 2016 American Chemical Society. Reproduced by permission of American Chemical Society.

2.1 Introduction

Originally discovered in 1897 by Sabatier, who received a Nobel prize for this work in 1912, catalytic hydrogenation is widely used in industry and is heavily utilized in the synthesis of many pharmaceutical and agricultural chemicals.¹ Although the conversion of olefins to alkanes is thermodynamically favored under appropriate conditions, such reactions are so sluggish that a catalyst is required to facilitate hydrogenation. It was first observed that traces of nickel could mediate the addition of H₂ to olefins² and later that palladium, platinum, rhodium, and other precious metals exhibited similar catalytic activity, owing to the overlap between the metal d-orbitals and the hydrogen molecular orbitals.

Two disadvantages in the use of these metals are cost and leaching of metals into the product. Utilizing nickel-based catalysts, particularly in the hydrogenation of fats, has

largely circumvented the problem of cost. However, nickel is readily poisoned by sulfur-containing compounds when natural fats or decomposition products can introduce sulfides into the catalytic system.³ Additionally, unacceptable levels of nickel can leach into the final product with nickel levels of 0.1 to 1.5 ppm known to be present in hydrogenated oils.⁴⁻⁶ These and other factors have stimulated research efforts to develop benign, nonmetallic hydrogenation catalysts. Homogeneous nonmetallic catalysis has been developed for a wide range of reactions.⁷ However, metal-free hydrogenations using molecular hydrogen were not realized until 2006 when Stephan and co-workers developed the first non-transition-metal system capable of releasing and absorbing molecular hydrogen.⁸ Soon after, the term “frustrated Lewis pair” or FLP was coined to describe these systems.⁹ An explosion of research activity followed.¹⁰⁻¹² The key feature of an FLP-catalyzed reaction is the formation of a Lewis acid and base that cannot form a conventional adduct, either from steric or electronic frustration. Early work showed that these FLPs could bind olefins and alkynes.^{9, 13} By utilizing the interaction with hydrogen and other molecules, FLPs have been shown to successfully catalyze the hydrogenation of imines, enamines, aldehydes^{2, 14-15}, olefins,¹⁶ and alkynes to alkenes.¹⁷ More recently, carbon dioxide has been reduced over a solid indium oxide-based FLP.¹⁸

Heterogeneous catalytic hydrogenation, which is preferred for large-scale industrial processes due to ease of catalyst separation and applicability to continuous flow reactions,¹⁹ has only been recently reported for metal-free systems with low conversion rates.²⁰ Based on our experience with mechanochemical processes and the fact that it has been shown that defects in *h*-BN (*dh*-BN) can reduce the hydrogen bond

order¹⁹, we investigated the hydrogenation of a series of olefins over *dh*-BN. Defects were introduced into *h*-BN and mobilized by performing the hydrogenation reactions using a reactor based on a ball mill (Figure 13). To our delight, hydrogenation of a variety of substrates was successful under milder conditions than those used for nickel catalysts, with better olefin hydrogenation turnover frequencies (TOF) than the best FLP catalysts with very low catalyst loadings (Figure 12).

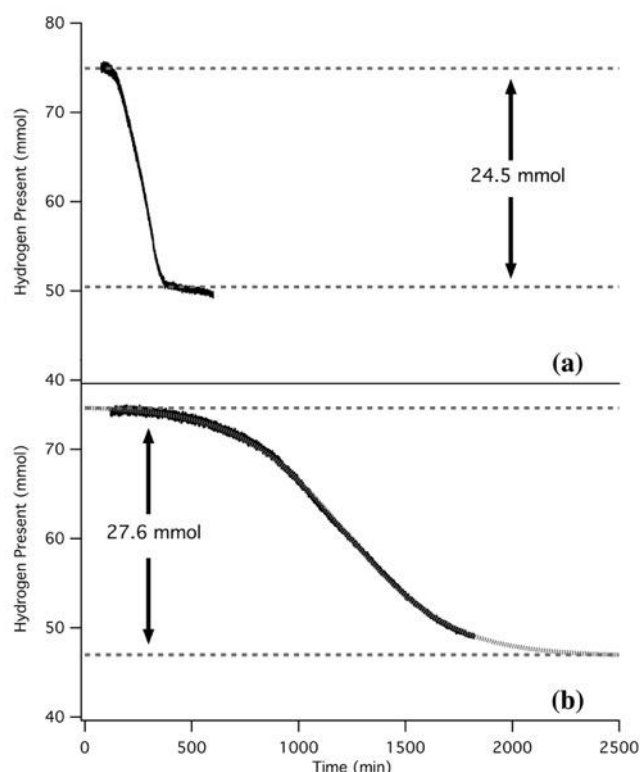


Figure 12. Hydrogenation of (E)-1,2-diphenylethene [6] under excess hydrogen at 170°C with different catalyst loadings. Five grams (27.7 mmol) of olefin was used. One gram of *dh*-BN activated for 48 hours under hydrogen (a) and unactivated *h*-BN coated milling media (b) both effectively hydrogenated the olefinic bond.

2.2 Experimental

2.2.1 Synthesis of *Defect-Laden Hexagonal*-Boron Nitride (*dh*-BN)

Defect-laden *h*-BN was prepared using three methods. For all methods, pristine *h*-BN (Grade PCTF5, Saint-Gobain Ceramic Materials) was first dried at 180°C under dynamic vacuum for 12 hours and transferred to an argon-filled glovebox.

2.2.1.1 Method 1

Approximately 2 grams of *h*-BN were mixed with 0.200 g of lithium (99.9%, Alfa Aesar) and reacted via high-energy ball-milling in an 8000M and/or 8000D SPEX CertiPrep mixer/mills. Milling vials were constructed from 440C stainless steel with an approximate volume of 65 ml. Buna-N quad O-rings were used to maintain a seal during milling. Kinetic energy was supplied for 30 minutes with one 12.7 mm stainless steel ball weighing approximately 8.0 g. After 30 minutes, two additional 12.7 mm stainless steel balls were added and the reaction was milled for an additional 7.5 hours. The resulting lithiated solid was subsequently hydrolyzed using excess H₂O to remove Li₃N, producing vacancies in the *h*-BN sheets. The morphology of this defect-laden *h*-BN was examined via scanning electron microscopy (SEM) performed on a Tescan Vega SBH operating at 30 kV.

2.2.1.2 Method 2

Twenty grams of dry *h*-BN was loaded into a custom pebble mill in an argon-filled glovebox. The milling container was constructed of 304 stainless steel. Spherical milling media (440C) were added in the following quantities and sizes: (12) 19.1 mm balls, (27) 12.7 mm balls, and (50) 6.35 mm balls. The mill was run at 60 rpm for 96 hours under 929 kPa of UHP hydrogen. The milling container was transferred to an argon-filled glovebox and the prepared catalyst powder was removed and stored until needed.

2.2.1.3 Method 3

Five grams of dry *h*-BN was loaded into a 65 ml zirconia milling vial. Silicone O-rings and a custom clamping mechanism were used to maintain a seal during milling. Kinetic energy was supplied for 30 minutes with four 12.7 mm zirconia balls weighing approximately 5.97 g. The material was removed with plastic tools and at no point in its preparation was it exposed to metal. The resulting defect-laden solid was used for catalysis without further processing. The morphology of this material is shown in the TEM images in Figure 19. It was found that activation by milling alone was just as effective as using lithium. Higher energy activation (Method 3) resulted in shorter induction periods (Figure 22). All hydrogenation data presented in this manuscript is from mechanically activated BN.

2.2.2 Hydrogenation

2.2.2.1 Reaction Vessel

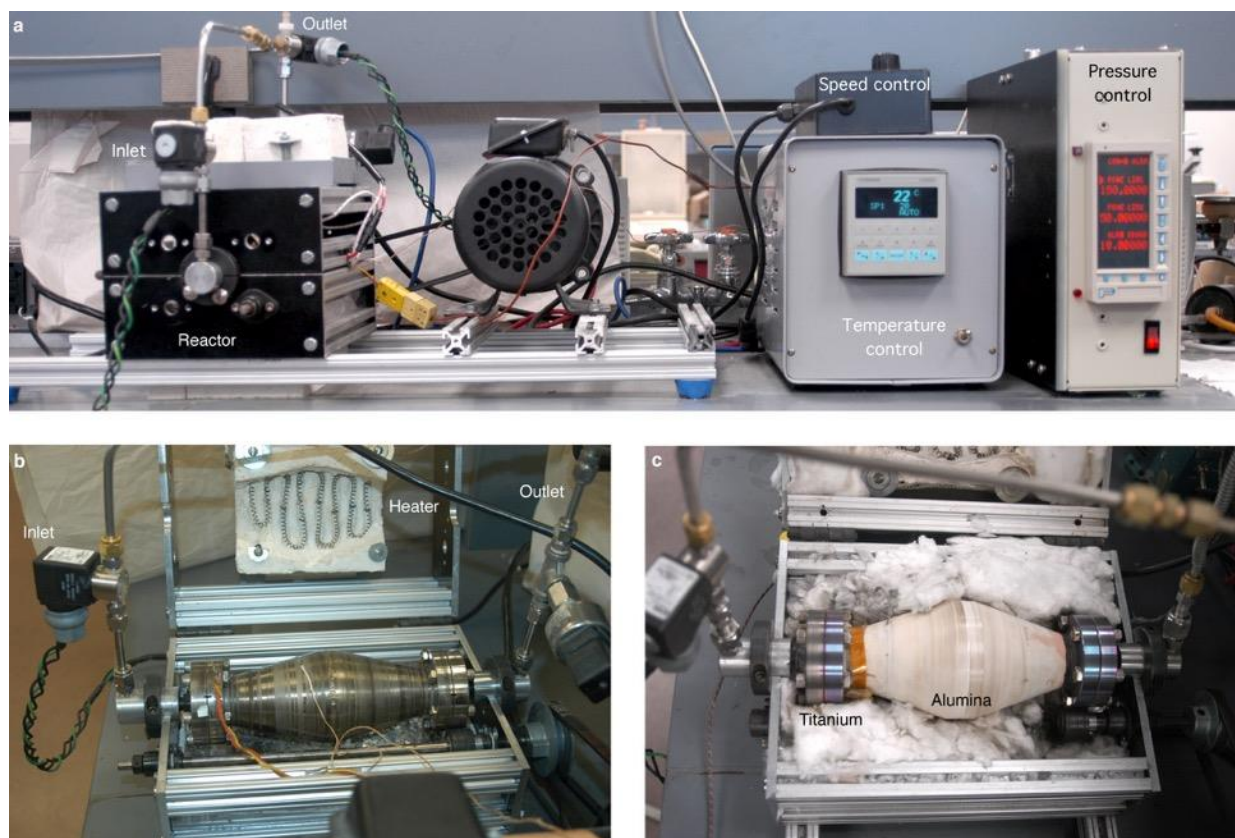


Figure 13. The reaction vessel and reactor has controls for pressure, temperature, and mechanical force (a). A close-up of the steel reaction vessel shows the temperature and gas control (b). Hydrogen is introduced through the solenoid at the left. Heat is applied by a NiChrome element (top center). Temperature is monitored by two thermocouples with the larger one on the left also serving as the control thermocouple for the heating element. A drive wheel driven by a pulley or a chain driven sprocket (not pictured) rotates the reaction vessel. In order to perform rigorously metal-free reactions, an alumina reactor with titanium flanges was implemented (c). The titanium flanges have been anodized to reduce hydrogen interaction.

Hydrogenation was performed in a custom pebble mill with gas-tight milling containers constructed of 304 stainless steel and high alumina (Figure 13). The reaction

vessel is shaped as a double truncated cone to ensure adequate tumbling of the milling media.

2.2.2.1.1 Steel

Two 2.75" Conflat flanges (A&N Corporation CF275 flanges with 1.5" bore, 275-162) were welded onto two 1.5"x3" conical reducers (A&N Corporation 300X150-WCR) welded large end to end to produce the reaction vessel in Figure 13. Deublin rotary feedthroughs (1005-020-019, 1005 Series, RH and 1005-020-039 , 1005 Series, LH) retrofit with Kalrez® O-rings and Krytox™ lubricant (GPL 105) were used to maintain gas tight conditions during operation. The feedthroughs were sealed to two 2.75" Conflat flanges with 10-32 tapped through holes (A&N Corporation CF275 blank flanges 275-000). The seal between the feedthrough and the flange was maintained with a copper gasket. Stainless steel frits (6-32 threaded) (Applied Porous Materials) were fitted to the tapped entry and exit feedthroughs to eliminate the accumulation of dust in the sealing surfaces of the feedthroughs. The flange seals were maintained with either two silicone or Kalrez® O-rings (ASA -223) depending on the substrate being used at the time. Spherical milling media (440C, $d=7.67 \text{ g/cm}^3$) was added in the following quantities and sizes: (12) 19.1 mm balls, (53) 12.7 mm balls, and (86) 6.35 mm balls.

2.2.2.1.2 Alumina

Two alumina reactor designs were implemented. A small ceramic lined reactor with

straight sides was constructed by boring holes in the bottom and lid of a high alumina crucible (CoorsTek, 99.8%, Part #65540). The crucible was used to line a steel reactor with parallel walls and Conflat flanges. High-temperature room temperature vulcanizing sealant (RTV, tin-cured) was used to seal the crucible lid onto the body. The steel frits were replaced with glass filters. Spherical milling media (yttria-stabilized zirconia, $d=6 \text{ g/cm}^3$, Inframat® Advanced Materials™ LLC) was added in the following quantities and sizes: (5) 19.1 mm balls, (15) 12.7 mm balls, and (50) 6.35 mm balls. A duplicate of the steel reactor, with 6mm walls, was manufactured in high alumina (99.8%) by CoorsTek, Inc. Titanium flanges with the same dimensions as the steel flanges, save that the Conflat knife edge was replaced with an O-ring groove, were machined. Titanium was chosen to match the coefficient of thermal expansion of the alumina body and reduce the risk of incorporation of catalytically active metals. The titanium flanges were anodized to reduce the possibility of hydrogen embrittlement. Flanges were sealed to the alumina body using Cotronics Duralco™ 4700 two-part epoxy. A 1 mm thick PTFE shield was placed between the frit body and the flange to eliminate media interaction with the flange material. The steel frit was covered with a piece of tin-cured silicone tube (I.D.=6.35 mm) to prevent media from interacting with the steel of the frit. Spherical milling media (yttria-stabilized zirconia, $d=6 \text{ g/cm}^3$, Inframat® Advanced Materials™ LLC) was added in the following quantities and sizes: (12) 20 mm balls, (53) 12.7 mm balls, and (86) 6.35 mm balls. Before any hydrogenation, the media and reactor interior were washed with concentrated nitric acid and rinsed three times with ultrapure water.

2.2.2.2 Control

Temperature was controlled with an Omega CN3000 process controller and a K-type thermocouple spring mounted to the inlet flange. A wound NiChrome heating element embedded in shaped firebrick applied heat. Pressure was monitored with a NOSHOK pressure transducer and controlled with a MicroMod 53MC5000 loop controller. The mill's rotational speed was controlled with a 1/3 hp variable speed DC motor coupled to the reactor with a steel drive chain.

2.2.2.3 Reactions

Hydrogenation reactions were carried out at temperatures up to 220°C, pressures between 446 and 1135 kPa, and rotary speeds of 66 rpm and 114 rpm. Hydrogenations were performed with 5 grams of substrate and trace to 7.5 g of defect-laden *h*-BN. Trace quantities of *dh*-BN were introduced into the reactor by suspending 1 g of *dh*-BN in 200 mL of dry acetone and pouring over the milling media. The wet media was then dried at 100 °C. The substrates investigated were: propene [1] (Worthington Industries, 95%), allyl bromide (Fisher Scientific, 99%), allyl butyl ether (Sigma-Aldrich, 90%), phenylethene (Acros Organics, 99%), cyclohexene [2] (Fisher Scientific), octadec-1-ene [3] (Acros Organics 90%), d-limonene (Florida Chemical, technical grade), 1,1-diphenylethene [4] (Sigma-Aldrich, 97%), (Z)-1,2-diphenylethene [5] (Alfa-Aesar 97%), (E)-1,2-diphenylethene [6] (Sigma-Aldrich, 96%), (E)-cinnamic acid [7] (Eastman, Practical Grade), (9Z)-Octadec-9-enoic acid [8] (Fisher Scientific, Lab Grade),

benzylideneacetophenone [9] (Acros Organics, 97%), and eugenol [10](clove bud oil, Nature's Alchemy, 80-90%).

2.2.2.4 Mechanically Similar Blanks

Dry graphite and dry graphitic carbon nitride (C_3N_4) were used as blanks with mechanical properties similar to BN. Graphitic carbon nitride was prepared by heating 10 grams of dicyandiamide (Alfa Aesar 99%) for 1 hour in air at 500 °C. Two grams of each compound were loaded into the reactor in an argon-filled glovebox. Hydrogenation activity was examined by milling 20 grams of (E)-cinnamic acid [7] with 2 grams of processed graphite at 170°C, pressures between 446 and 1135 kPa, and rotary speeds of 66 rpm. Hydrogenation of propene with graphitic carbon nitride was investigated by milling 2 grams of *g*- C_3N_4 under 425 kPa of an equimolar mixture of hydrogen and propene at 20 °C.

2.2.3 Analysis and Characterization of *Defect-Laden Hexagonal*-Boron Nitride (*dh*-BN)

2.2.3.1 Active Sites

Active sites were measured by loading the steel reactor with 5 grams of *dh*-BN and pressurizing with 345 kPa of propane, propene, hydrogen, or argon. Surface adsorption produced a measureable pressure loss. No pressure loss was observed for argon and minimal for hydrogen. Propane (which is expected to physisorb) and propene (which is

expected to chemisorb as well as physisorb) both showed pressure loss with more loss observed using propene (Figure 14).

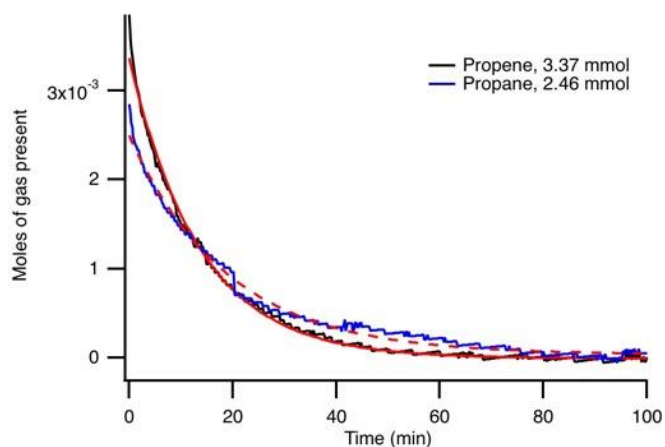


Figure 14. Alkenes are chemisorbed and physisorbed onto dh-BN while alkanes are merely physisorbed. Propene uptake on dh-BN was used to estimate the number of potential active sites on the catalyst surface. The potential active sites represent 27% of the adsorption sites. The curves presented are uptake over 5 g of dh-BN and have been offset by the unadsorbed moles of gas.

2.2.3.2 Surface Area

BET surface area testing was performed with a Micromeritics Tristar II 3020 instrument at 77 K. Before measurement, each sample was evacuated on a Smart Vac Prep for 5 hours at 50°C. Surface areas for pristine, defect-laden, and propene adsorbed defect-laden BN were measured.

2.2.3.3. Temperature Programmed Desorption (TPD)

The TPD experiment was carried out with an Altamira AMI-200 instrument using ethene as an adsorbed gas.

2.2.3.4 Solid State NMR

All solid state NMR spectra were acquired on a 500 MHz Agilent narrow bore spectrometer operating at 125.68 MHz. A 1.6 mm Agilent T3 probe was employed using a spinning speed of 12.0 kHz. A ^1H pulse width of 1.0 μs was utilized followed by a conventional (i.e. constant amplitude) cross polarization step with a time of 3 ms. SPINAL ^1H decoupling at a frequency of 499.78 MHz was employed using a 165° pulse of 1.84 μs . Both spectra were acquired using spectral widths of 29.8 kHz, acquisition times 17.2 ms and recycle times of 15 s to avoid sample heating. The digital resolution acquired for each spectrum was of 58.1 Hz/point.

2.2.3.5 Coking

After use in hydrogenation, the *dh*-BN exhibited colors from white to brown (Figure 15a). The color deepened at elevated reaction temperatures with little observed color change for propene hydrogenations performed at room temperature. This color change was due to the incorporation of carbon compounds. This coking was highly fluorescent

(Figure 15b). Thermogravimetric analysis was performed on a TA Instruments model 2050 TGA. The results for coked and pristine materials are shown in Figure 15c.

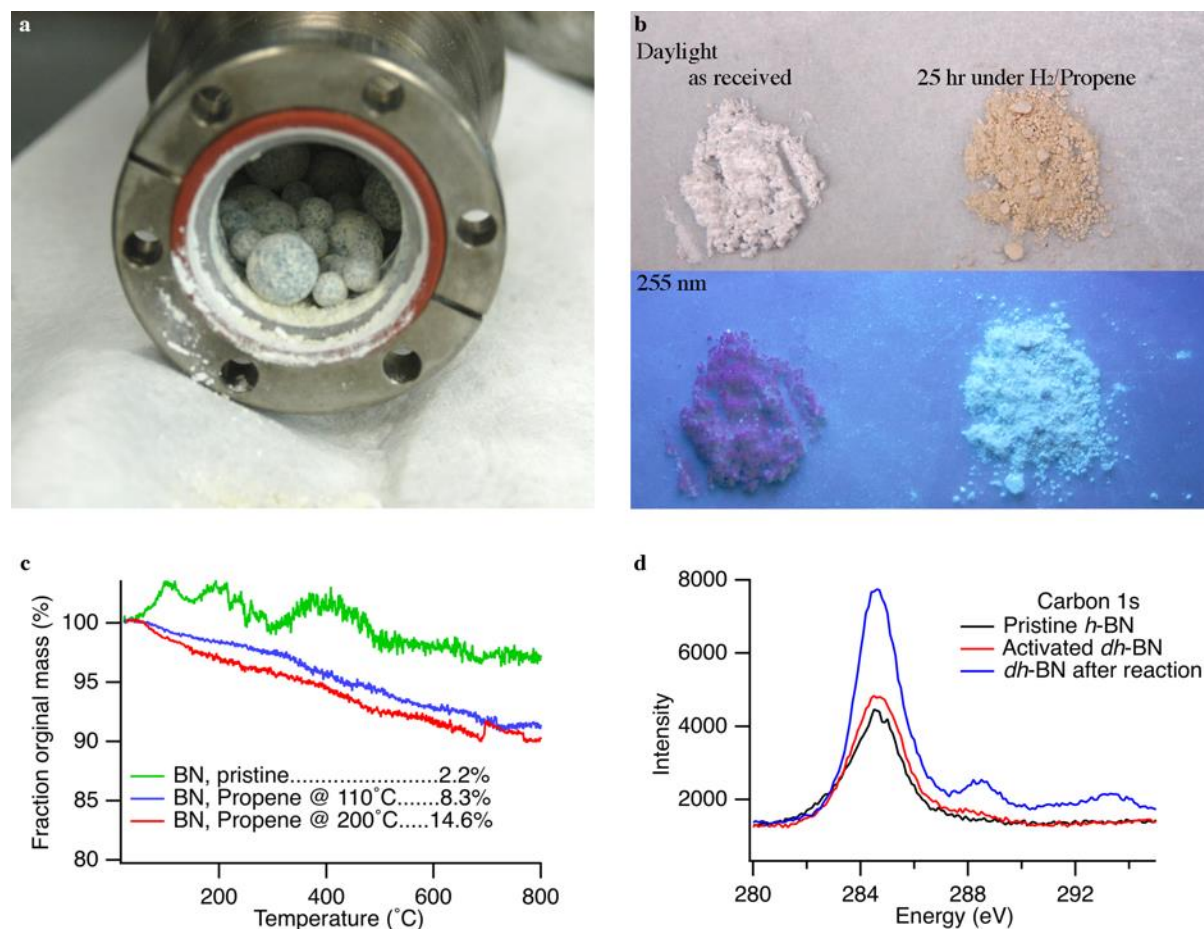


Figure 15. At elevated temperature dehydrogenation reaction produce carbon deposits on the catalyst. After use, the *dh*-BN exhibits a color change from white to pale yellow and tan (a). The intensity of the color increases with increasing reaction temperature. These deposits are highly fluorescent (b) indicative of coking. Thermogravimetric analysis (c) shows the trend of increased coking levels with increased process temperatures. X-ray photoelectron spectra of the carbon 1s region of *h*-BN as received (black), after inducing defects (red), and after use as a hydrogenation catalyst for the hydrogenation of (E)-cinnamic acid [7] (blue) confirmed carbon incorporation (d).

2.2.3.6 Gas Chromatography with Mass Sensitive Detection

GC-MS analysis was performed on an Agilent 6850 GC with an Agilent 19091-433E HP-5MS column (5% phenyl methyl siloxane, 30 m x 250 μ m x 0.25 μ m nom.) coupled with a 5975C VL mass selective detector. Samples were pulled from the reactor, dissolved in dichloromethane and filtered through a Whatman 0.2 μ m PTFE syringe filter before injection. Quantitation of the (E)-cinnamic acid [7] hydrogenation products was performed by using external standard solutions of (E)-cinnamic acid [7] (Eastman, Practical Grade) and hydrocinnamic acid (Acros Organics, 99%) in dichloromethane.

Gas samples from propene [1] hydrogenation experiments were obtained by venting the reactor into a 50 ml serum vial crimp sealed with a PTFE lined septum. Gas was introduced via a 22 gauge needle attached to the vent line and an additional 22 gauge exit needle that was properly vented. Quantitation of propene/propane ratios was performed using external standards consisting of mixtures of propene and propane.

2.2.3.7 ICP-AES

Inductively coupled plasma atomic emission analysis was performed by Saint-Gobain Advanced Ceramics. Samples of boron nitride before and after activation were digested in an oxygen bomb and analyzed for iron and nickel.

2.2.3.8 XPS

X-ray photoelectron spectra were recorded on a Physical Electronics 5400 photoelectron spectrometer with a magnesium source. The spectra of the carbon 1s region is presented in Figure 15d.

2.2.3.9 XRD

Powder X-ray diffraction (PXRD) was performed using a Rigaku Multiflex theta–theta powder X-ray diffractometer with a copper source ($\text{Cu K}\alpha = 1.5418 \text{ \AA}$). Diffractograms were collected from 5 to 80 degrees 2θ using 0.010-degree steps and 0.3 seconds of dwell time. Size and strain were analyzed by applying the method of integral breadths⁷⁰ and constructing a Williamson-Hall plot. Sheet parallel and perpendicular diffraction peaks were analyzed separately to obtain in-sheet size and strain and intersheet ordering.

2.2.3.10 Thermogravimetric Analysis (TGA) and Differential Scanning Calorimetry (DSC)

Pristine, defect laden BN, and propene adsorbed samples were studied with a TA Instruments 2950 TGA and 2920 DSC. Propene adsorbed samples were prepared by loading a 500 ml pressure cell with 2 grams of material in an argon filled glove box. The pressure cell was then removed and filled with 310.3 kPa of propene. The sample was allowed to equilibrate for 3 days and then removed from the cell and stored in an argon-

filled glove box. TGA samples were stored in argon filled vials and loaded into the sample pan in the air. TGA runs were performed under flowing air. DSC samples were loaded into unsealed aluminum pans under argon and loaded into the DSC cell in air. All defect-laden samples were found to retain their propene even after extended storage at 1 atm.

2.2.4 Computational Modeling of Mechanochemical Hydrogenation Over *dh*-BN

2.2.4.1 Discrete element modeling

Discrete element models of the milling process were generated using EDEM (DEM Solutions Ltd.). The geometry and composition of the reaction vessel was investigated using discrete element modeling. Three reaction vessels were investigated: steel (Figure 16a, left), high alumina sloped sides (Figure 16a, center), and a high alumina with straight sides (Figure 16a, right).

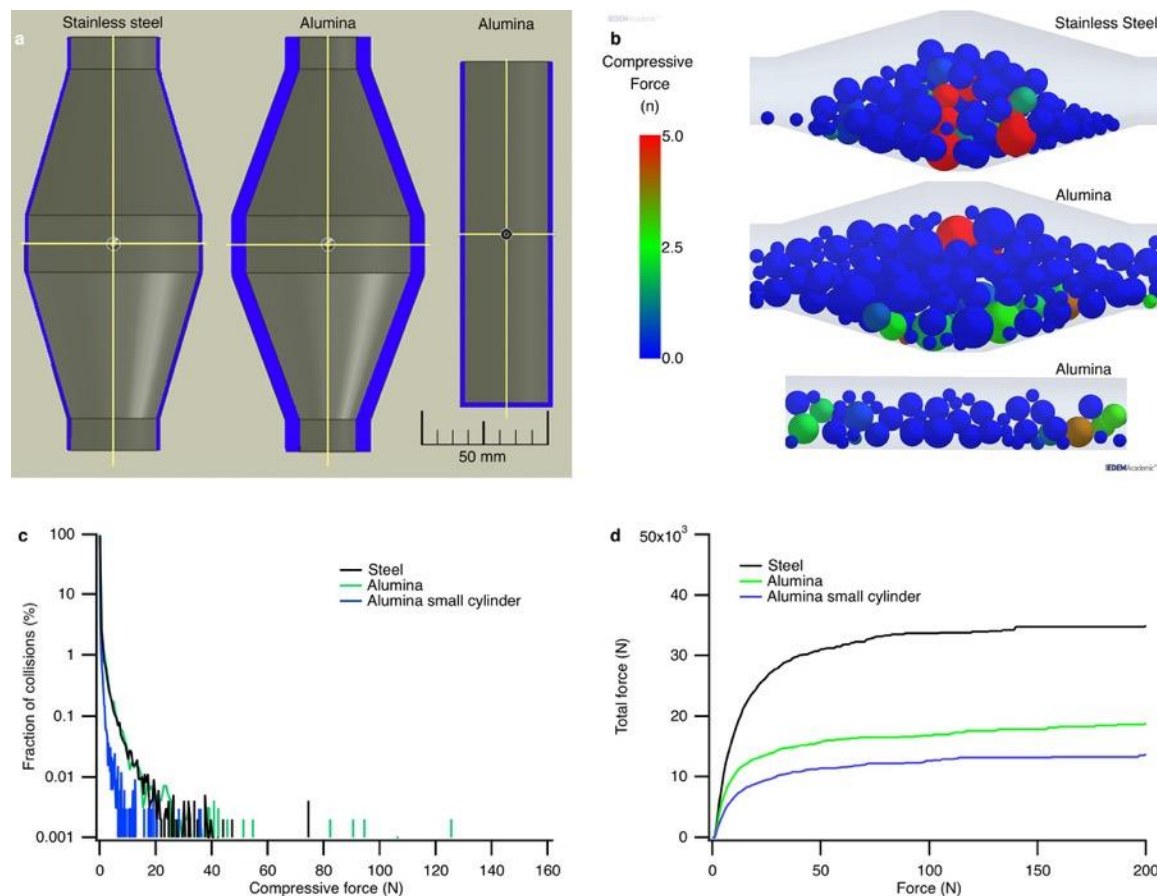


Figure 16. Steel and alumina reactors were simulated using DEM. The cross sections of these reactors (a) show the geometry differences. Three reaction vessels were investigated: steel (a, left), high alumina sloped sides (a, center), and a high alumina with straight sides (a, right). Lower forces were generated in the cylindrical reactor (b and c). No appreciable hydrogenation was observed in that reactor. Although the sloped reactors produce forces with similar magnitudes (b and c), the integral of the compressive forces produced over a 10 second time period (d) shows that less force is being applied over time. Lower total forces resulted in longer induction periods.

2.2.4.2 TOF

Turnover frequencies were estimated using the minimum of the derivative of each substrate's hydrogen uptake curve as the maximum rate of hydrogenation.

2.2.4.3 Computational details

Density functional theory (DFT) calculations were performed to evaluate the binding energies and electronic structure of the C₂H₄ molecule on defect-laden boron nitride single layers employing the formalism of the van der Waals density functional (vdW-DF)⁶¹⁻⁶² as implemented in the VASP code⁷¹⁻⁷⁴. In this formalism, the exchange-correlation energy is calculated as: $E_{XC} = E_{GGA}^X + E_{lc}^C + E_{nlc}^C$; where E_{GGA}^X is a semi-local exchange functional from the revised generalized-gradient approximation (GGA) in the form of the Perdew-Burke-Ernzerhof functional (revPBE)⁷⁵, E_{lc}^C is a local correlation energy described within the local density approximation, E_{nlc}^C is the nonlocal correlation energy as described by Dion et al.⁶¹. The efficient algorithm proposed by Román-Pérez and Soler⁷⁶ is responsible for making the computation feasible for systems such as ours which contain a large number of atoms in the calculational super cell. The projector augmented wave (PAW) scheme⁷⁷⁻⁷⁸ is utilized with the potentials taken from the potential-library provided with VASP. The electronic wave functions were expanded in a plane wave basis set with a cutoff of 500 eV. Given the size of the super cell, a single k-point (Gamma) was deemed adequate to sample the Brillouin zone of a (6x6) BN slab with 15 Å vacuum on top of it. The systems were optimized so that all force components acting on each atom are smaller than 0.01 eV/Å. The lattice parameters of *h*-BN were optimized to be 2.523 Å (in agreement with experimental value of 2.505 Å⁷⁹.) No temperature or pressure effects were included in our DFT calculations.

2.2.4.4 Binding Energies

The binding energy is calculated using the formula: $E_{BE} = E_{System} - (E_{Mol} + E_{BN})$; where E_{System} , E_{Mol} , and E_{BN} are the total energy of the molecule on the substrate, the molecule alone, and of the defective *h*-BN substrate, respectively.

2.3 Results and Discussion

Defects have been shown to be important features of active catalytic solids.²¹⁻²³ and are responsible for the increased activity observed in catalysts prepared mechanochemically²⁴ as well as catalysts under the application of mechanical force.²⁵ These results suggest that a defect-laden solid with regions of electron deficiency and excess will interact with olefins and molecular hydrogen to reduce their respective bond orders enough to facilitate hydrogenation. Prior work in hydrogen storage examined the role of defects in *h*-BN. DFT calculation shows a favorable binding energy for hydrogen on nitrogen vacancies (V_N), boron vacancies (V_B), boron-nitrogen swap (B/N), boron substitution for nitrogen (B_N), nitrogen substitution for boron (N_B), carbon substitution (B_C and N_C), silicon substitution (N_{Si} and B_{Si}) and Stone-Wales (SW) defects.¹⁹ We looked at a 2 five-member ring and 2 seven-member ring SW defect. This defect can cause the sheet to distort above (SW1) or below the original plane (SW2). SW2 had the most favorable interaction with the substrate. Chemisorption of hydrogen (up to 70% of the adsorbed hydrogen) is favored over these sites.^{19, 26} In fact, single sheets and nanotubes of BN can absorb up to 4.6 mass% hydrogen.²⁶⁻²⁷ If *h*-BN has a high affinity for hydrogen

then it may also have one for olefins. We omitted silicon substituted structured and examined the 8 remaining defects for affinity for olefin and hydrogen binding (Figures 17 and 18). We found that 4 of these defects exhibited an affinity for olefins. Binding-energy calculations (Table 2) confirm this assertion, with ethene, propene and hydrogen binding energies on par with those of metals that possess known hydrogenation activity (Pt, Pd, and Ni). Of these defects, B_N and V_N have a binding energy closest to metals with known hydrogenation activity. Olefin binding at SW defects is less favored (desorption may reduce availability of activated species) and hydrogen binding is disfavored. Binding at V_B sites is very favorable for both the olefin and hydrogen and reactivity will be limited. Solid-state NMR experiments on propene saturated *dh*-BN showed a low concentration of B_N sites and a much higher concentration of V_N sites. Additionally, there is evidence for V_N formation after ball milling and V_N are some of the most stable defects in *h*-BN.²⁸⁻

30

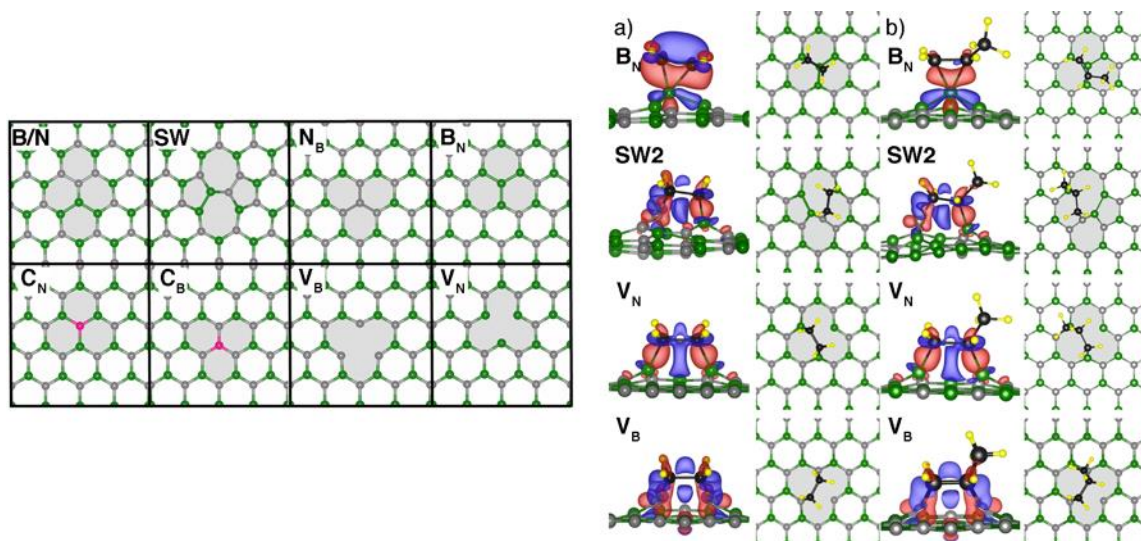


Figure 17. The olefinic bond chemisorbs onto four defect sites in dh-BN. Eight defect structures in BN were studied (left). These are (from top left to bottom right): 180° rotation of a BN bond (B/N), 90° rotation of a BN bond {Stone-Wales defect} (SW), nitrogen substitution for boron (N_B), boron substitution for nitrogen (B_N), carbon substitution for nitrogen (C_N), carbon substitution for boron (C_B), boron vacancy (V_B), and a nitrogen vacancy (V_N). Gray, green, and pink balls represent nitrogen, boron, and carbon atoms, respectively. The light-gray backgrounds indicate the defected areas. Charge-density redistribution and top view (right) after the adsorption of C_2H_4 (a) and C_3H_6 (b) on B_N , SW, V_B , and V_N defects in a BN substrate. Isosurfaces are drawn at 0.01 e/Bohr^3 . The blue and red isosurfaces represent, respectively, the charge-deficit and -accumulation regions. (i.e. charge flows from blue to red regions).

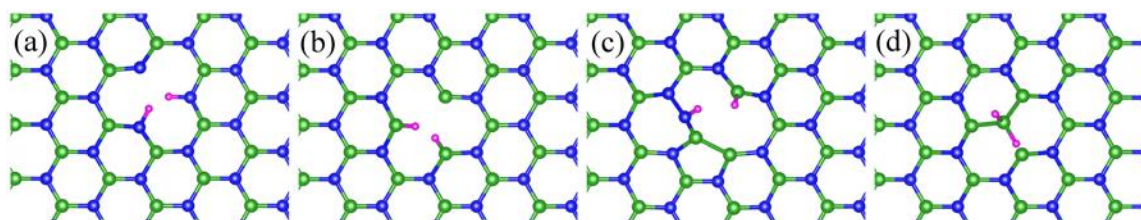


Figure 18. Binding structure of hydrogen on h-BN with V_B (a), V_N (b), SW (c), and BN (d) defects. Blue, green, and pink balls represent nitrogen, boron, and hydrogen atoms, respectively.

Table 2. Binding Energy for ethene and propene on *h*-BN, hydrogen on BN (both calculated in this work), ethene on platinum group metals³¹, hydrogen on Pt(100)³², hydrogen on Pd(100)³³, and hydrogen on Ni(100)³⁴. No temperature or pressure effects were included in these calculations.

	Binding Energy (eV)		
BN	Ethene	Propene	Hydrogen
V _B	-3.71	-3.69	-4.95
V _N	-1.90	-1.76	-1.43
SW2	-0.23	-0.35	0.62
B _N	-1.95	-2.05	-1.77
Pt 100			
di sigma	-2.32		-2.88
pi-top	-1.55		
Pd 100			
di sigma	-0.84		-2.92
pi-top	-0.33		
Ni 100			
di sigma	-1.76		-2.81
pi-top	-0.82		

2.3.1 Producing Defects

Pristine sheets of *h*-BN are exceptionally robust and chemically inert,^{26, 35-36} the application of mechanical force is required to induce delamination and introduce point

defects.³⁷ By designing a hydrogenation reactor around a pebble mill we have been able to study the catalytic activity of defect in *h*-BN. The continuous grinding motion within the mill prevents cluster formation, maximizes the number of few-layer sheets, and induces plastic deformation in the catalyst. In order to verify the presence of these sheets and defects, transmission electron microscopy was used to characterize the morphology of the *d*/*h*-BN catalyst (Figure 19b and c). Nanosheets are observed by TEM and appear to form tubular structures or nano-scrolls as seen in Figure 19c. Although point defects could not be imaged directly the material shows significant disruption of the structure (Figure 19a and b). Powder X-ray diffraction of pristine and defect-laden *h*-BN (Figures 20 and 21) shows disorder in the *c* direction consistent with delamination and retention of order in the sheet. Propene uptake experiments (Figure 14) indicate a defect level of 0.46 mol%. Integral breadth analysis using the 00*l* and *hk*0 peaks found that the average crystalline region in the sheet was 6.7 nm with 0.56% strain and the average crystallite size in the *c* direction was 18.3 nm (or 55 *h*-BN layers) with 0.23% strain. The higher in-sheet strain is indicative of defects and confirmed by the TEM images.

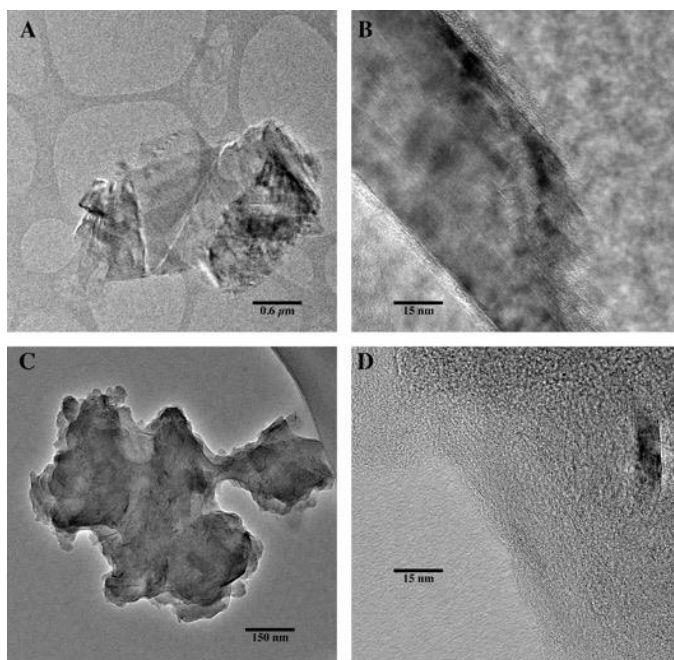


Figure 19. Transmission electron microscopy images of as received *h*-BN (A and B) and *dh*-BN (C and D). The as received material is large flakes (A) with well-ordered staking of the BN sheets (B). The *dh*-BN is much smaller and thinner flakes (C) with much less order in the *c* direction. Evidence of delamination and curling of the BN sheet can be seen in C.

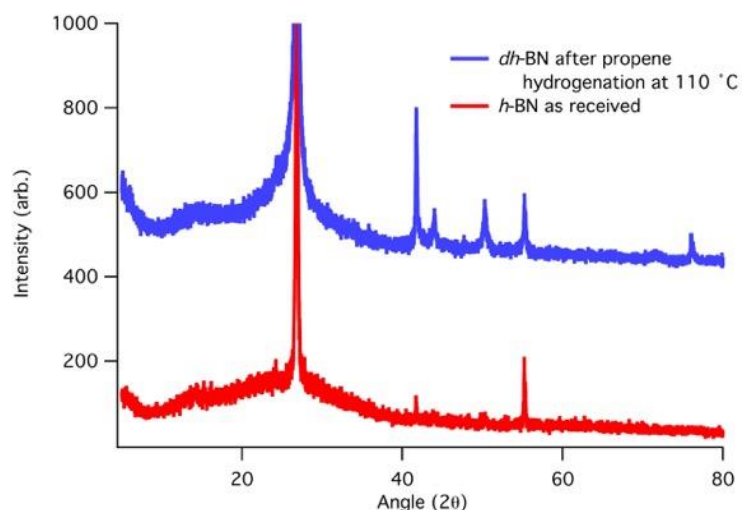


Figure 20. The as received *h*-BN is highly crystalline with an intense 002 diffraction peak. After activation and hydrogenation of *dh*-BN, the 002 peak is diminished due to disordering in the *c*-direction. In plane ordering is still present as evident by the increased intensity of peaks due to diffraction off of planes with *h* and *k* components.

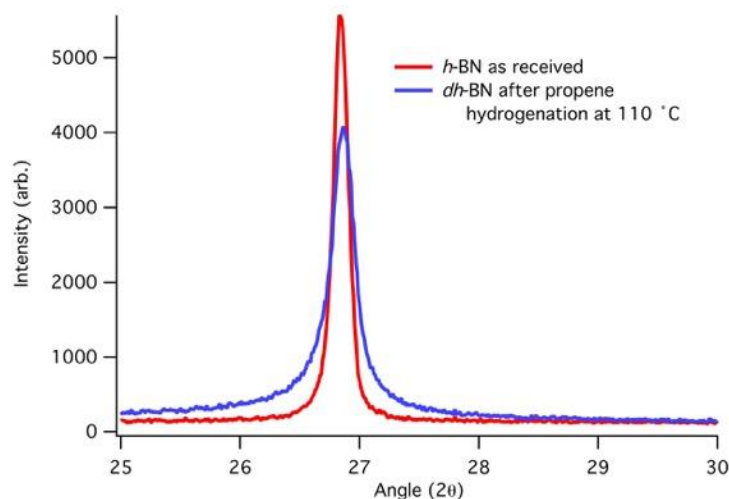


Figure 21. The 002 diffraction peak is broadened with an asymmetry toward lower angles. This indicates a fraction of the material has large intersheet spacing. This may be due to adsorbed molecules or minor distortions in each BN sheet disrupting the stacking sequence.

2.3.2 Bulk Scale Experiments

Nearly complete hydrogenation, of substrates without acidic functional groups, was achieved with reaction temperatures as low as 20 °C. This temperature is much lower than that used for industrial hydroprocessing (300 °C – 450 °C).³⁸ No aromatic carbons were hydrogenated, such as can occur over Raney nickel.³⁹ Benzylideneacetophenone was not reduced to an alcohol as with metal-based catalysts. Additionally, no C-H activation products were observed, as was reported over nanocrystals of *h*-BN.²⁷ Hydrogenation of phenylethene, a known product of the thermal decomposition of (E)-cinnamic acid [7], was observed in the by-products of the hydrogenation of (E)-cinnamic acid [7] at 170 °C.⁴⁰ For all substrates, except the two carboxylic acids, upper limits for the

turnover frequencies were determined from the steepest slope of the hydrogen uptake curve (Figure 22) and propene adsorption studies (Figure 14). For the carboxylic acids, TOFs were determined from the product yield and the total reaction time. Turnover numbers were calculated assuming deactivation after one reaction, although, we have been able to recycle the catalyst three times with minimal loss in catalytic efficiency (Figure 23). The results are presented in Table 3 as well as those for other catalytic systems. The TOFs over *dh*-BN are better than that achieved using FLPs for the same substrate. Although the internal sheet atoms of a single *h*-BN layer are relatively inert, defects and edges are potentially reactive. In the presence of hydrogen, the edges of the *dh*-BN sheets possess reactive species which reductively aminate carboxylic acids. Lower yields of hydrogenation products were realized from reactions with (E)-cinnamic acid [7] and (9Z)-Octadec-9-enoic acid [8] as a result of reaction of the carboxylic acid group with these edges. This is evidenced by the production of nitriles from these reagents (Table 3). Nitriles are produced by reaction of the carboxylic acid with edge nitrogens on the *dh*-BN sheet followed by dehydration. XPS analysis of the catalyst after hydrogenation confirmed the presence of carbon on the surface (Figure 15d) and TGA analysis of the catalyst after propene hydrogenation shows that coking is reduced at lower temperatures (Figure 15c).

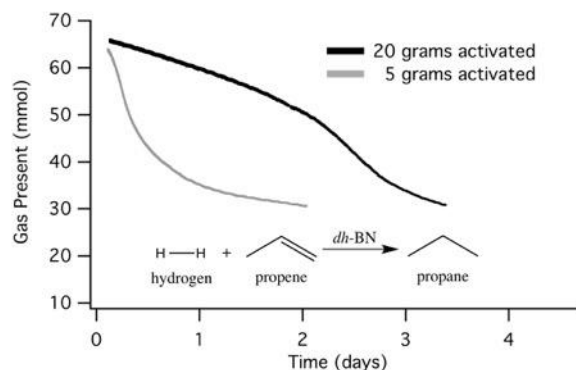


Figure 22. Hydrogenation of propene [1] with an excess of hydrogen at 220°C. Two grams of catalyst and 37.9 mmol of propene [1] were used. The reaction using dh-BN activated in a large batch had slower kinetics (black trace) than that using dh-BN activated in a smaller batch (gray trace).

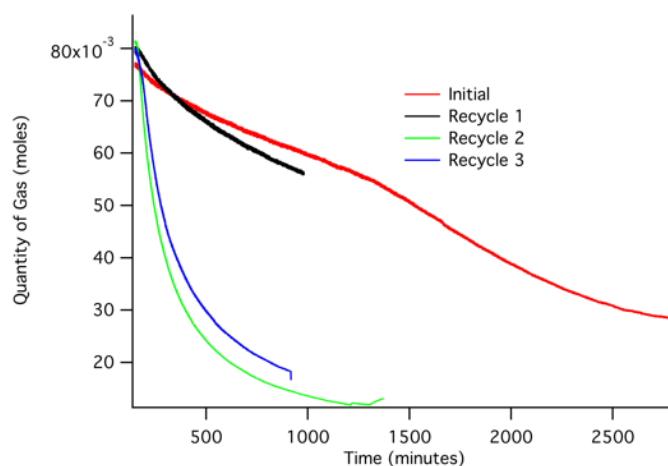


Figure 23. Starting with pristine BN (Initial), induction periods reduce and hydrogenation rates increase with each recycle. Continued propene [1] hydrogenation was observed after 3 recycles of the catalyst. Activation continued through the first two uses and by the 2nd and 3rd recycle the catalytic rate reached its maximum.

2.3.3 Metal-free Hydrogenation

Small amounts of metal impurities can lead to the observation of anomalous catalytic activity⁴¹ and hydrogenation over stainless steel has recently been observed.⁴²

Mechanical processing can introduce metals into the material through wear of the media and vessel. The two main components of the steel used are iron and nickel. Both of these metals can be active toward hydrogenation. Nickel is a known hydrogenation catalyst and iron acts as a catalyst when in the nanoparticle form.⁴³⁻⁴⁴ In a previous study using graphite, iron was not incorporated into the product even after extended milling times.⁴⁵ Inductively coupled plasma atomic emission analysis of the boron nitride before and after activation indicated that little metal incorporation occurred. The starting material is marketed for cosmetic use and has no detectable iron or nickel. After activation, the material had 7 ppm iron and 10 ppm nickel.

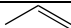
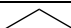
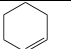
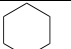


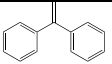
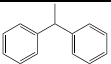
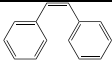
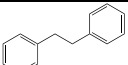
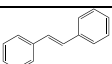
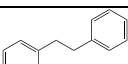
2.3.4 Mechanically Equivalent Blank

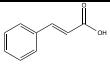
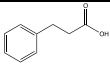
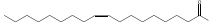
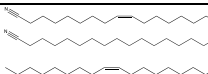
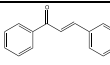
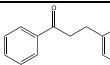
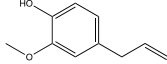
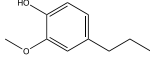
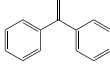
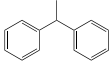
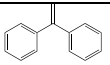
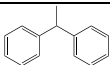
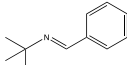
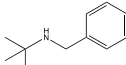
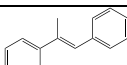
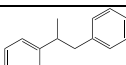
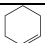
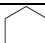
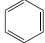
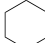
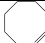
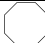
The effect of this small amount of metal contamination was examined by substituting graphite and graphitic C₃N₄ for boron nitride. Both have mechanical properties similar to boron nitride and will exhibit wear behavior. Although graphite is a suitable support for iron and nickel catalysts it lacks the electronic structure needed for hydrogen and alkene binding. Graphitic C₃N₄ is closer chemically to *h*-BN. Both were processed under hydrogen in the same manner as the boron nitride and then used in a (E)-cinnamic acid [7] hydrogenation reactions at 170 °C and propene [1] hydrogenations at 20 °C. No hydrogen uptake or hydrogenation products were observed.

2.3.5 Rigorously Metal-Free Implementation

To further eliminate the possibility of metal-mediated hydrogenation, a metal-free (alumina) reactor was constructed (Figure 13c). Additionally, propene was chosen as a substrate as it would be free from metal impurities that may be found in liquid or solid substrates. Initially, propene [1] was hydrogenated with 90% efficiency after a much longer induction period.

Table 3. Hydrogenation yields, TOFs, and single use TONs of various substrates over defect-laden *h*-BN and other catalytic systems with a mill speed of 66 RPM unless otherwise specified. All information was derived from steel reactor data.

[Reference Number] / Compound	Reactant	Product(s)	Rxn Temp (°C)	TOF (s ⁻¹)/ TON	Yield/Comment
[1] Propene			20 200	1.25 x 10 ⁻³ /16.10 4.15 x 10 ⁻³ /90.69	100%; 114 RPM 100%
[2] Cyclohexene			20	2.88 x 10 ⁻⁴ /15.88	100%; 114 RPM
[3] octadec-1-ene			150 220	6.51 x 10 ⁻⁵ /3.92 1.86 x 10 ⁻⁴ /11.19	35% at 150 °C 100% at 220 °C ^a
[4] 1,1-diphenylethene			170	1.17 x 10 ⁻³ /21.07	97%
[5] (Z)-1,2-diphenylethene			170	1.41 x 10 ⁻³ /14.49	100%
[6] (E)-1,2-diphenylethene			135	1.09 x 10 ⁻³ /5.00 1.15 x 10 ⁻³ /13.47	99% 99%

[7] (E)- cinnamic acid			170	$1.19 \times 10^{-4}/10.28$	55.1% hydrocinnamic acid after catalyst recycle
[8] (9Z)- Octadec-9- enoic acid			170	$5.79 \times 10^{-5}/5.00$	58% oleyl nitrile, 33% stearyl nitrile, 10%
[9] benzylidene-			240	$1.56 \times 10^{-4}/13.56$	90%
[10] eugenol			240		65%
1,1- diphenylethane			Room Temp	$5.73 \times 10^{-5}/4.95$	99% 20 mol% (C ₆ F ₅) ₃ B•(C ₆ F ₅)P h ₂ P ¹⁶
1,1- diphenylethane			Room Temp	$1.21 \times 10^{-4}/17.4$	87% 5 mol% (C ₆ F ₅) ₃ B•
(E)-N- benzylidene-2- methylpropan- 2-amine			Room Temp	$2.61 \times 10^{-1}/470$	47% 0.1 mol% [((MeCNCl) ₂ C)B C ₈ H ₁₄]
1-methyl-1,2- diphenylethane			23	$5.22 \times 10^{-3}/18.79$	Fe-dinitrogen complex ⁴⁷
cyclohexene			20	3.2×10^{-1} to 6.6×10^{-1}	Ni on various supports ⁴⁸
benzene			50- 170	4×10^{-3} to 1.6×10^{-1}	Ni on various supports ³⁸
Cyclooctene			80	$6 \times 10^{-5}/38$	graphene ²⁰

^a After addition of 5 mass% fumed silica.

2.3.6 Mechanical Factors Affecting Induction Periods and Reaction Rates

Discrete element models of the reactors used in this study indicated that the compressive forces achieved in both the steel and alumina reactors were comparable. However, the total amount of compressive force delivered over a 10 second time period was significantly less for the alumina reactor (Figure 16d). Without activation, a significant induction period (over 16 hours, Figure 23) was observed. The initial activation step that produces *dh*-BN was performed with 20 grams of material. At such high loading the impacts of the media are dampened. By activating a smaller amount (5 grams) of boron nitride the induction period was eliminated and stoichiometric yields were obtained (Figure 2).

Defects, which are stable up to 900°C,⁴⁹ can be produced during hydrogenation or in a pretreatment step. However, they must be mobile in order for the bound hydrogen and olefin to interact. Defects are mobile under plastic deformation,⁵⁰ which occurs when the yield strength of a material is exceeded. The motion of defects in *h*-BN nanotubes has been observed under applied load⁵¹ as well as modeled in *h*-BN sheets⁵² and the forces generated during milling can be sufficient to exceed the compressive yield strength of *h*-BN (41.3 MPa). However, the generation of high forces during milling requires the efficient transfer of mechanical force to the *dh*-BN. Therefore, the rheological properties, of the reaction mixture during hydrogenation, are an important factor. There must be media (ball)-media impacts or media-wall impacts in order for force to be transferred to the reaction. This occurs as frictional forces allow the media to climb up the wall of the rotating reactor. At a certain point gravity wins out and the media tumbles. Liquids, such as

octadec-1-ene [3], lower the impact forces by reducing the friction and eliminating tumbling. They are effectively lubricants. If tumbling is reduced or eliminated, impact forces are reduced and the amount of plastic deformation experienced by the *dh*-BN catalyst is limited. Consequently, lower hydrogenation yields were obtained when pure octadec-1-ene [3] was utilized. DEM models showed that the lowered coefficients of restitution, static friction, and rolling friction produced by lubrication significantly reduced the number of high force impacts. By adding 5 mass% fumed silica the lubricity of the mixture was greatly reduced and hydrogenation proceeded rapidly.

2.3.7 Surface Analyses, Bound Species, and Sites

Two separate samples were prepared and ^{13}C isotropic spectra were acquired for each. The first sample was exposed to propene under a pressure of 310 kPa for 4 days while a second sample was exposed to small quantities of propene present in our Ar-filled glovebox (partial pressure <100 Pa or 4.5 ppt). Both samples show some uptake of propene, as best observed by the presence of methyl signals from 5–30 ppm (Figure 24). The surface area of the parent BN was 5 m²/g. After activation by milling in a zirconia vial, the surface area increased to 340 m²/g and decreased to 270 m²/g upon exposure to propene. This suggests that propene tightly binds to a fraction of the adsorption sites or 0.70% mass% of the catalyst.

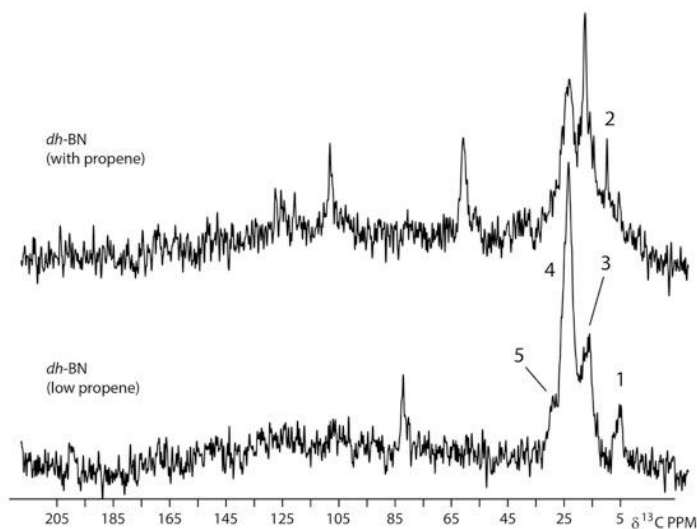


Figure 24. ^{13}C solid state NMR of *dh*-BN exposed to high and low partial pressures of propene. The peaks around 25 ppm are due to the methyl carbon on propene and shows 4 distinct binding modes. The peaks at 62 and 83 ppm are likely due to partial oxidation of the bound propene molecule. The spectra were obtained using a cross polarization technique.

The presence of five distinct CH_3 resonances in each sample indicates that multiple environments are available to propene. This is consistent with the presence of at least 5 structurally unique defect sites. A tentative assignment of each site can be made based on prior work establishing that methyl groups at lower frequencies represent those most sterically imposed upon by neighboring sites.⁵³⁻⁵⁵ A summary of $\text{C-H}\cdots\text{X}$ steric interactions ($\text{X} = \text{N}$ or B) for each structural model is given in Table 4. Site **1** represented by the signal near 7 ppm is only occupied at low surface coverages and, based on ^{13}C shift, is expected to display the most significant steric interactions with neighboring atoms. This resonance is thus assigned to structural model B_N with 4 $\text{C-H}\cdots\text{X}$ interactions < 3.0 Å. In contrast, the narrow resonance near 10 ppm (2) is exclusively occupied in the sample exposed to high pressure. Structural model V_B is consistent with this resonance

as it has 3 C–H...X with the shortest interaction distance. The two sites with signals at 17 and 25 ppm (resonances 3 and 4, respectively) are found in both samples and are therefore occupied regardless of the preparation condition. Site 3 is consistent with V_N , while site 4 is tentatively assign to model SW2 with 2 C–H...X contacts < 3.0 Å. It is notable that the resonance near 17 ppm is also more strongly represented in the pressurized sample. Site 5 near 30 ppm is the least sterically involved with neighboring sites and is thus assigned to structural model SW1 with 1 C–H...X interaction < 3.0 Å.

Table 4. Close contacts with CH₃ hydrogens in structures modeled and olefin bond length. SW1 and SW2 both consist of two 5-member rings and two 7-member rings. SW1 is distorted away from the substrate and SW2 is distorted toward the substrate.

Model	Close contacts ^a	Distance (Å)	Olefin Bond Length (Å)
Alkane C-C	<i>none</i>	<i>none</i>	1.54
Alkene C=C	<i>none</i>	<i>none</i>	1.34
SW1	C–H _a ...B11	2.89	1.340
BN	C–H _a ...N74	2.90	1.456
	C–H _a ...B7	2.86	
	C–H _b ...B37	2.91	
	C–H _b ...B2	2.95	
SW2	C–H _a ...B35	2.86	1.537
	C–H _b ...B2	2.81	
V_N	C–H _a ...B35	2.84	1.566
	C–H _a ...N64	2.88	
	C–H _b ...B35	2.77	
V_B	C–H _a ...N69	2.72	1.568
	C–H _b ...N69	2.79	
	C–H _b ...B34	2.80	

^aNumbering refers to model structures.

Overall, these ^{13}C NMR results suggest that there are at least 5 structurally distinct sites and that some are solely or preferentially occupied at higher pressures. We note that the olefinic carbons are also observed in the spectrum at 107 ppm (tentatively assigned as CH) and at 122–127 ppm (CH_2). These are less useful for analysis due to the low signal-to-noise ratio, but help to verify the presence of propene. Curiously, in both samples an additional resonance is observed at 62 ppm and 83 ppm in the high and low pressure samples, respectively. This is consistent with the formation of two distinct species containing a C–O bond, perhaps from oxidation of the double bond after the sample was briefly exposed to air when transferred to the NMR. This is consistent with DSC in air, which shows an exotherm at 62°C (Figure 25) whereas the TPD of material not exposed to air shows a desorption peak at 287°C (Figure 26).

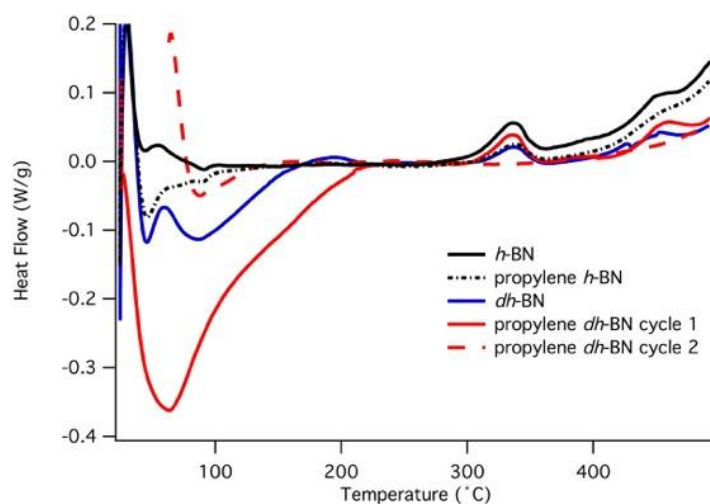


Figure 25. DSC of *h*- and *dh*-BN before and after exposure to 310.3 kPa of propene. The exotherm observed in the propene adsorbed *dh*-BN (solid red trace) corresponds to 181.4 kJ/mol.

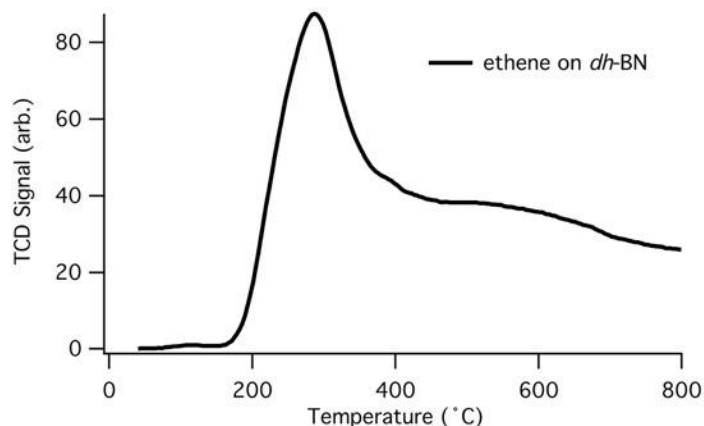


Figure 26. Temperature programmed desorption of ethene on *dh*-BN. The desorption profile is similar to that from defect-laden surfaces.⁵⁶⁻⁵⁷

2.3.8 Catalytically Active Defects and Reaction Mechanism

Hydrogenation over traditional metal catalysts proceeds through the Horiuti-Polanyi mechanism where the olefin adsorbs onto a hydrogenated catalyst surface, hydrogen migrates to the β carbon of the olefin, and the free alkane is reductively eliminated from the surface.⁵⁸ This is significantly different from the mechanism of olefin activation using an FLP. In an FLP system, hydrogenation proceeds via three steps, addition of molecular hydrogen to an FLP, olefin protonation to form a carbocation, and hydride transfer to the carbocation.⁵⁹ This also differs from hydrogenation observed over acid zeolites where the olefin first reacts with an acidic proton to form a transient carbonium ion.⁶⁰ In order to understand this process it is useful to evaluate the binding energies and electronic structure of the propene molecule on the boron nitride substrate. Ethene (C_2H_4), the simplest possible molecule with such a bond, and propene were investigated. First-principles electronic structure calculations of a C_2H_4 and C_3H_8 molecule on a single *h*-BN layer were employed by utilizing the Van der Waals density

functional (vdW-DF)⁶¹⁻⁶². It quickly became clear that these olefins do not chemisorb onto pristine *h*-BN sheets. This was also noted for hydrogen adsorption on *h*-BN sheets, which is at best weakly favored.¹⁹ Olefin chemisorption occurs at four of the eight defects investigated.

The effect these defects have on the carbon double bond can be elucidated by focusing on hybridization of the olefinic carbons interacting with the defect. A comparison of the charge density along a vertical plane passing through the two C atoms with those for gas phase C₂H₄ and C₂H₆ illustrates the substrate's effect (Figure 27). When ethene or propene chemisorb onto a B_N defect, its C atoms partially retain their original sp² hybridization (C=C), but when the molecule adsorbs on a SW, V_B, or V_N defect, its C atoms rehybridize to sp³ (C-C), facilitating hydrogenation and desorption of C₂H₆. The results also hold for the adsorption of propene on defect-laden BN. Coupled with the previously calculated binding modes of H₂ on *h*-BN¹⁹ defects, this data suggest that the hydrogenation mechanism is closer to the Horiuti-Polanyi mechanism for olefin hydrogenation over metals than that proposed for FLP catalyzed hydrogenation or acid-zeolite catalyzed hydrogenation. The significant difference between hydrogen bound to defects on a *h*-BN sheet and to a metal surface is that the resultant protons bound to the surface are confined to the region by the defect.

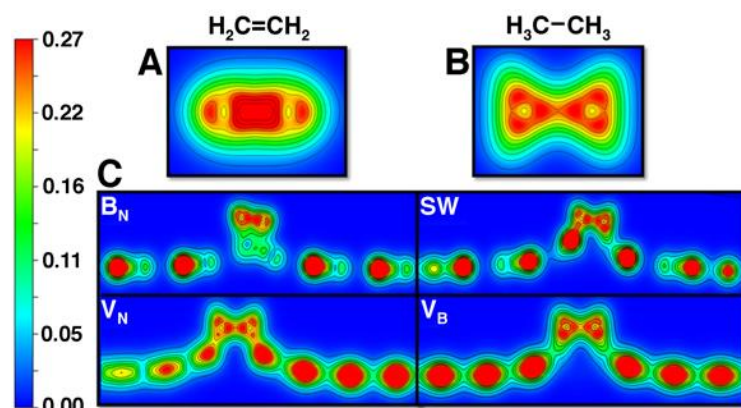


Figure 27. Electronic density cross-sections plotted along the vertical plane, passing through the center of the two carbon atoms of gas phase (A) ethene (C_2H_4) and (B) ethane (C_2H_6), and of (C) $\text{C}_2\text{H}_4/\text{dh-BN}$ for the defects B_N , SW, V_N and V_B . Contours are drawn in a linear scale (9 contours from 0 to 0.27 e/bohr^3). It can be seen that the electronic density of ethene on *dh*-BN exhibit similar structure as that of C_3H_6 , indicating reduction of the bond order of the C-C bond in the adsorbed ethene.

It is difficult to unambiguously identify the active site and hydrogenation mechanism. This is mainly due to the fact that there are many possible defects on the surface from the dynamic nature of the milling process. Based on the binding energies of propene, the calculated C=C bond lengths, SSNMR data, and on previous studies of the binding of hydrogen on defects in *h*-BN, it is most likely that hydrogenation occurs over V_N . The calculated binding energy of propene is on par with catalytic metals (Table 2). The C-C bond length of adsorbed propene (1.566 Å) is closer to the C-C bond length in propane (Table 4). The reaction pathway of propene hydrogenation on this defect is shown in Figure 28. The minimum energy path for such hydrogenation starts by the practically barrierless adsorption of propene (with a barrier of 5 meV), followed by the dissociative adsorption of H_2 with a barrier of 0.52 eV to form co-adsorption state ($\text{C}_3\text{H}_6^* + 2\text{H}^*$) with a co-adsorption binding energy of 2.22 eV. C_3H_6^* , then picks up an atomic

hydrogen (H^*) to form $\text{CH}_2\text{CH}_2\text{CH}_3^*$. This reaction has a barrier of 0.50 eV. C_3H_7^* will then react with the remaining H^* to form propane. This reaction faces a large barrier of 1.53 eV (148 kJ/mol). An alternative pathway for forming co-adsorption state is also calculated. In this pathway, the dissociative adsorption of H_2 occurs first, with a barrier of 1.01 eV, follow by the adsorption of propene with a barrier of 0.37 eV. Hydrogenation over a V_B faces a much larger barrier of 3.67 eV (Figure 29).

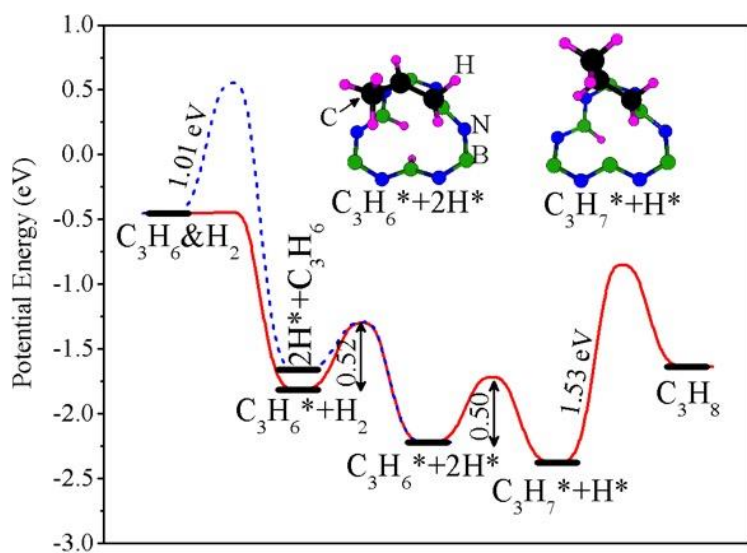


Figure 28. The largest barrier in the minimum energy pathway of propene hydrogenation over V_N is 1.53 eV (148 kJ/mol). Zero potential energy corresponds to propene and hydrogen in the gas phase without any interaction with h -BN. Thick horizontal bars represent intermediate states. The barrier (in eV) for each elementary reaction step is calculated using the Climbing Image Nudged Elastic Band method⁶³ and shown by the number (eV) between the states. * denote adsorbed species. The inserts are structures (a) of co-adsorbed propene and hydrogen ($\text{C}_3\text{H}_6^* + 2\text{H}^*$) and (b) the intermediate state C_3H_7^* .

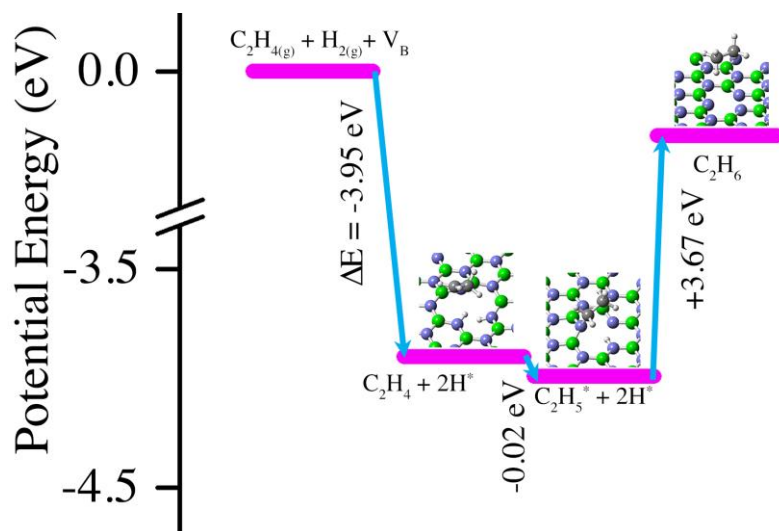


Figure 29. Energies of the intermediate species formed during the hydrogenation of ethene interacting with hydrogen bound to a V_B . The highest barrier is 3.67 eV or 354 kJ/mol.

It is worth noting that the calculated barriers are low enough for facile reactions at experimental condition (room temperature and the application of mechanical force). Reactions with activation energies between 95 and 134 kJ/mol have been driven mechanochemically⁶⁴⁻⁶⁸ and our computed maximum barrier is not far outside this range. Our calculated barrier lies between that for propene hydrogenation over zeolites (58-90 kJ/mol)⁶⁰ and the hydrogenation of propene over a silica-supported Zn(II) catalyst (191 kJ/mol).⁶⁹

2.4 Conclusion

A new metal-free heterogeneous hydrogenation catalyst has been realized through the introduction of defects into *h*-BN sheets. Stoichiometric yields were obtained

for both simple olefins (propene [1]) and complex olefins (benzylideneacetophenone [9]) with TOFs 1-2 orders of magnitude better than catalytic hydrogenation of the same olefin over metal-free FLP and graphene catalysts. Superior selectivity was observed, with minimal dehydrogenation and no cracking products produced at low temperatures. Through the application of a rigorously metal-free reactor, we confirmed that the observed hydrogenation is due to *dh*-BN and not introduced metal impurities. DFT calculations show that the olefinic bond in ethene and propene is weakened over four types of defect sites: boron substitution for nitrogen (B_N), nitrogen (V_N) vacancies, boron (V_B) vacancies, and Stone-Wales defects. The binding energy for olefins and hydrogen at the V_N defect is on par with those of metals currently used for catalytic hydrogenation. It is most likely that the majority of catalytic activity is due to V_N defects. The use of metal-free hydrogenation catalysts will reduce the risks associated with incorporation of metals into hydrogenation products.

2.5 References

1. Bullock, M. R., Front Matter. In *Catalysis without Precious Metals*, Bullock, M. R., Ed. Wiley-VCH Verlag GmbH & Co. KGaA: Weinheim, 2010; pp I-XVIII.
2. Stephan, D. W.; Greenberg, S.; Graham, T. W.; Chase, P.; Hastie, J. J.; Geier, S. J.; Farrell, J. M.; Brown, C. C.; Heiden, Z. M.; Welch, G. C.; Ullrich, M., Metal-Free Catalytic Hydrogenation of Polar Substrates by Frustrated Lewis Pairs. *Inorganic Chemistry* **2011**, 50 (24), 12338-12348.
3. Irandoust, S.; Edvardsson, J., Poisoning of nickel-based catalysts in fat hydrogenation. *Journal of the American Oil Chemists' Society* **1993**, 70 (11), 1149-1156.

4. Anwa, F.; T.G.Kazi; Saleem, R.; M.I.Bhanger, Rapid determination of some trace metals in several oils and fats. *Grasas y Aceites* **2004**, 55 (2), 160-168.
5. Cempel, M.; Nikel, G., Nickel: A review of its sources and environmental toxicology. *Polish Journal of Environmental Studies* **2006**, 15 (3), 375-382.
6. Select Committee on GRAS Substances *Nickel (elemental)*; SCOGS-Report Number: 97; U.S. Food and Drug Administration: Washington, D.C., 1979.
7. Bertelsen, S.; Jorgensen, K. A., Organocatalysis-after the gold rush. *Chemical Society Reviews* **2009**, 38 (8), 2178-2189.
8. Welch, G. C.; San Juan, R. R.; Masuda, J. D.; Stephan, D. W., Reversible, Metal-Free Hydrogen Activation. *Science (Washington, DC, U. S.)* **2006**, 314 (5802), 1124-1126.
9. McCahill, J. S. J.; Welch, G. C.; Stephan, D. W., Reactivity of "frustrated Lewis pairs": three-component reactions of phosphines, a borane, and olefins. *Angewandte Chemie International Edition in English* **2007**, 46 (26), 4968-71.
10. Stephan, D. W., Frustrated Lewis Pairs. *Journal of the American Chemical Society* **2015**, 137 (32), 10018-32.
11. Stephan, D. W., Frustrated Lewis Pairs: From Concept to Catalysis. *Accounts of Chemical Research* **2015**, 48 (2), 306-316.
12. Stephan, D. W.; Erker, G., Frustrated Lewis pair chemistry: development and perspectives. *Angewandte Chemie International Edition in English* **2015**, 54 (22), 6400-41.
13. Dureen, M. A.; Stephan, D. W., Terminal alkyne activation by frustrated and classical Lewis acid/phosphine pairs. *Journal of the American Chemical Society* **2009**, 131 (24), 8396-7.
14. Stephan, D. W., Frustrated Lewis pairs: a new strategy to small molecule activation and hydrogenation catalysis. *Dalton Transactions* **2009**, (17), 3129-3136.
15. Welch, G. C.; Cabrera, L.; Chase, P. A.; Hollink, E.; Masuda, J. D.; Wei, P.; Stephan, D. W., Tuning Lewis acidity using the reactivity of "frustrated Lewis pairs": facile formation of phosphine-boranes and cationic phosphonium-boranes. *Dalton Transactions* **2007**, (31), 3407-3414.
16. Greb, L.; Oña-Burgos, P.; Schirmer, B.; Grimme, S.; Stephan, D. W.; Paradies, J., Metal-free Catalytic Olefin Hydrogenation: Low-Temperature H₂ Activation by

- Frustrated Lewis Pairs. *Angewandte Chemie International Edition* **2012**, 51, 10164-10168.
17. Chernichenko, K.; Madarász, Á.; Pápai, I.; Nieger, M.; Leskelä, M.; Repo, T., A frustrated-Lewis-pair approach to catalytic reduction of alkynes to cis-alkenes. *Nature Chemistry* **2013**, 5 (8), 718-723.
 18. Ghuman, K. K.; Hoch, L. B.; Szymanski, P.; Loh, J. Y. Y.; Kherani, N. P.; El-Sayed, M. A.; Ozin, G. A.; Singh, C. V., Photoexcited Surface Frustrated Lewis Pairs for Heterogeneous Photocatalytic CO₂ Reduction. *Journal of the American Chemical Society* **2016**, 138 (4), 1206-1214.
 19. Shevlin, S. A.; Guo, Z. X., Hydrogen sorption in defective hexagonal BN sheets and BN nanotubes. *Physical Review B* **2007**, 76 (2), 024104.
 20. Primo, A.; Neatu, F.; Florea, M.; Parvulescu, V.; Garcia, H., Graphenes in the absence of metals as carbocatalysts for selective acetylene hydrogenation and alkene hydrogenation. *Nature Communications* **2014**, 5.
 21. Behrens, M.; Studt, F.; Kasatkin, I.; Köhl, S.; Hävecker, M.; Abild-Pedersen, F.; Zander, S.; Girgsdies, F.; Kurr, P.; Knief, B.-L.; Tovar, M.; Fischer, R. W.; Nørskov, J. K.; Schlögl, R., The Active Site of Methanol Synthesis over Cu/ZnO/Al₂O₃ Industrial Catalysts. *Science* **2012**, 336 (6083), 893-897.
 22. Polarz, S.; Strunk, J.; Ischenko, V.; van den Berg, M. W. E.; Hinrichsen, O.; Muhler, M.; Driess, M., On the role of oxygen defects in the catalytic performance of zinc oxide. *Angewandte Chemie, International Edition* **2006**, 45 (18), 2965-2969.
 23. Voorhoeve, R. J. H.; Remeika, J. P.; Trimble, L. E., Defect chemistry and catalysis in oxidation and reduction over perovskite-type oxides. *Annals of the New York Academy of Sciences* **1976**, 272 (Catal. Chem. Solid-State Inorg.), 3-21.
 24. Ralphs, K.; Hardacre, C.; James, S. L., Application of heterogeneous catalysts prepared by mechanochemical synthesis. *Chemical Society Reviews* **2013**, 42 (18), 7701-7718.
 25. Immohr, S.; Felderhoff, M.; Weidenthaler, C.; Schüth, F., An Orders-of-Magnitude Increase in the Rate of the Solid-Catalyzed CO Oxidation by *In Situ* Ball Milling. *Angewandte Chemie International Edition* **2013**, 125 (48), 12920-1293.
 26. Wu, J. C. S.; Cheng, T.-S.; Lai, C.-L., Boron nitride supported PtFe catalysts for selective hydrogenation of crotonaldehyde. *Applied Catalysis A: General* **2006**, 314 (2), 233-239.

27. Hao, X. P.; Cui, D. L.; Yu, X. Q.; Liu, Z. G.; Xu, X. G.; Wang, Q. L.; Jiang, M. H., The activation of benzene molecules by BN nanocrystals. *Materials Letters* **2002**, 57 (3), 703-707.
28. Lin, Y.; Williams, T. V.; Cao, W.; Elsayed-Ali, H. E.; Connell, J. W., Defect Functionalization of Hexagonal Boron Nitride Nanosheets. *J. Phys. Chem. C* **2010**, 114, 17434-17439.
29. Huang, J. Y.; Jia, X. B.; Yasuda, H.; Mori, H., Stacking disordering in hexagonal BN induced by shearing under ball milling. *Philosophical Magazine Letters* **1999**, 79 (5), 217-224.
30. Orellana, W.; Chacham, H., Stability of native defects in hexagonal and cubic boron nitride. *Physical Review B* **2001**, 63 (12), 125205.
31. Bernardo, C. G. P. M.; Gomes, J. A. N. F., The adsorption of ethylene on the (100) surfaces of platinum, palladium and nickel: a DFT study. *Journal of Molecular Structure (Theochem)* **2001**, 542, 263-271.
32. Novell-Leruth, G.; Valcárcel, A.; Clotet, A.; Ricart, J. M.; Pérez-Ramírez, J., DFT characterization of adsorbed NH_x species on Pt(100) and Pt(111) surfaces. *Journal of Physical Chemistry B* **2005**, 109, 18061-18069.
33. Tomanek, D.; Louie, S. G.; Chan, C.-T., *Ab Initio* calculation of coverage-dependent adsorption properties of H on Pd(001). *Physical Review Letters* **1986**, 57 (20), 2594-2597.
34. Wang, S.-G.; Cao, D.-B.; Li, Y.-W.; Wang, J.; Jiao, H., CH₄ dissociation on Ni surfaces: Density functional theory study. *Surface Science* **2006**, 600, 3226-3234.
35. Golberg, D.; Bando, Y.; Huang, Y.; Terao, T.; Mitome, M.; Tang, C.; Zhi, C., Boron Nitride Nanotubes and Nanosheets. *ACS Nano* **2010**, 4 (6), 2979-2993.
36. Wang, L.; Sun, C.; Xu, L.; Qian, Y., Convenient synthesis and applications of gram scale boron nitride nanosheets. *Catalysis Science & Technology* **2011**, 1 (7), 1119-1123.
37. Bettinger, H. F.; Dumitrica, T.; Scuseria, G. E.; Yakobson, B. I., Mechanically induced defects and strength of BN nanotubes. *Physical Review B* **2002**, 65, 041406.
38. Molina, R.; Poncelet, G., Hydrogenation of benzene over alumina-supported nickel catalysts prepared from Ni(II) acetylacetonate. *Journal of Catalysis* **2001**, 199 (2), 162-170.

39. Mastagli, P.; Metayer, M., Hydrogenation of cinnamic and p-hydroxycinnamic acids with Raney nickel. *Comptes rendus de l'Académie des Sciences* **1947**, 224, 1779-81.
40. Nomura, E.; Hosoda, A.; Mori, H.; Taniguchi, H., Decarboxylation of cinnamic acid derivatives by microwave heating. *Kenkyu Hokoku - Wakayama-ken Kogyo Gijutsu Senta* **2005**, 20.
41. Crabtree, R. H., Resolving Heterogeneity Problems and Impurity Artifacts in Operationally Homogeneous Transition Metal Catalysts. *Chemical Reviews* **2012**, 112, 1536-1554.
42. Zhao, F.; Ikushima, Y.; Arai, M., Hydrogenation of 2-butyne-1,4-diol to butane-1,4-diol in supercritical carbon dioxide. *Green Chemistry* **2003**, 5, 656-658.
43. Yoon, K. J.; Walker, P. L.; Mulay, L. N.; Vannice, M. A., Benzene hydrogenation over iron. 1. Specific activities and kinetic behavior over unsupported iron and iron dispersed on silicon dioxide, aluminum oxide, carbon, and doped carbon. *Industrial & Engineering Chemistry Product Research and Development* **1983**, 22 (4), 519-526.
44. Phu, P.-H.; Lefort, L.; Boogers, J. A. F.; Tristany, M.; Vries, J. G. d., Soluble iron nanoparticles as cheap and environmentally benign alkene and alkyne hydrogenation catalysts. *Chemical Communications* **2009**, (3747-3749), 3747.
45. Hick, S. M.; Griebel, C.; Blair, R. G., Mechanochemical Synthesis of Alkaline Earth Carbides and Intercalation Compounds. *Inorganic Chemistry* **2009**, 48 (5), 2333-2338.
46. Farrell, J. M.; Posaratnanathan, R. T.; Stephan, D. W., A family of N-heterocyclic carbene-stabilized borenium ions for metal-free imine hydrogenation catalysis. *Chemical Science* **2015**, 6 (3), 2010-2015.
47. Yu, R. P.; Darmon, J. M.; Hoyt, J. M.; Margulieux, G. W.; Turner, Z. R.; Chirik, P. J., High-Activity Iron Catalysts for the Hydrogenation of Hindered, Unfunctionalized Alkenes. *ACS Catalysis* **2012**, 2 (8), 1760-1764.
48. Boudart, M., Turnover Rates in Heterogeneous Catalysis. *Chemical Reviews* **1995**, 95 (3), 661-666.
49. Wang, P.; Orimo, S.; Matsushima, T.; Fujii, H.; Majer, G., Hydrogen in mechanically prepared nanostructured h-BN: a critical comparison with that in nanostructured graphite. *Applied Physics Letters* **2002**, 80 (2), 318-320.

50. Suenaga, K.; Wakabayashi, H.; Koshino, M.; Sato, Y.; Urita, K.; Iijima, S., Imaging active topological defects in carbon nanotubes. *Nature Nanotechnology* **2007**, 2 (6), 358-360.
51. Ghassemi, H. M.; Lee, C. H.; Yap, Y. K.; Yassar, R. S., In situ observation of reversible rippling in multi-walled boron nitride nanotubes. *Nanotechnology* **2011**, 22 (11), 115702/1-115702/6.
52. Zobelli, A.; Ewels, C. P.; Gloter, A.; Seifert, G., Vacancy migration in hexagonal boron nitride. *Physical Review B: Condensed Matter and Materials Physics* **2007**, 75 (9), 094104/1-094104/7.
53. Soderquist, A.; Facelli, J. C.; Horton, W. J.; Grant, D. M., Low-Temperature ^{13}C Magnetic Resonance. 9. Steric Effects for Methyl Chemical Shift Tensors in Methylcyclohexanes. *Journal of the American Chemical Society* **1995**, 117 (32), 8441-8446.
54. Harper, J. K.; McGeorge, G.; Grant, D. M., Solid-state ^{13}C chemical shift tensors in terpenes. Part I. Spectroscopic methods and chemical shift structure correlations in caryophyllene oxide. *Magnetic Resonance in Chemistry* **1998**, 36 (S1), S135-S144.
55. Harper, J. K.; McGeorge, G.; Grant, D. M., Solid-State ^{13}C Chemical Shift Tensors in Terpenes. 2. NMR Characterization of Distinct Molecules in the Asymmetric Unit and Steric Influences on Shift in Parthenolide. *Journal of the American Chemical Society* **1999**, 121 (27), 6488-6496.
56. Kim, Y. D.; Stultz, J.; Goodman, D. W., Identification of Defect Sites on MgO(100) Surfaces. *Langmuir* **2002**, 18 (10), 3999-4004.
57. van der Niet, M. J. T. C.; den Dunnen, A.; Juurlink, L. B. F.; Koper, M. T. M., A detailed TPD study of H_2O and pre-adsorbed O on the stepped Pt(553) surface. *Physical Chemistry Chemical Physics* **2011**, 13 (4), 1629-1638.
58. Mattson, B.; Foster, W.; Greimann, J.; Hoette, T.; Le, N.; Mirich, A.; Wankum, S.; Cabri, A.; Reichenbacher, C.; Schwanke, E., Heterogeneous Catalysis: The Horiuti–Polanyi Mechanism and Alkene Hydrogenation. *Journal of Chemical Education* **2013**, 90 (5), 613-619.
59. Greb, L.; Tussing, S.; Schirmer, B.; Ona-Burgos, P.; Kaupmees, K.; Lokov, M.; Leito, I.; Grimme, S.; Paradies, J., Electronic effects of triarylphosphines in metal-free hydrogen activation: a kinetic and computational study. *Chemical Science* **2013**, 4 (7), 2788-2796.

60. Gounder, R.; Iglesia, E., Catalytic hydrogenation of alkenes on acidic zeolites: Mechanistic connections to monomolecular alkane dehydrogenation reactions. *Journal of Catalysis* **2011**, 277 (1), 36-45.
61. Dion, M.; Rydberg, H.; Schröder, E.; Langreth, D. C.; Lundqvist, B. I., Van der Waals Density Functional for General Geometries. *Physical Review Letters* **2004**, 92 (24), 246401.
62. Thonhauser, T.; Cooper, V. R.; Li, S.; Puzder, A.; Hyldgaard, P.; Langreth, D. C., Van der Waals density functional: Self-consistent potential and the nature of the van der Waals bond. *Physical Review B* **2007**, 76 (12), 125112.
63. Henkelman, G.; Uberuaga, B. P.; Jónsson, H., A climbing image nudged elastic band method for finding saddle points and minimum energy paths. *The Journal of Chemical Physics* **2000**, 113 (22), 9901-9904.
64. McKissic, K. S.; Caruso, J. T.; Blair, R. G.; Mack, J., Comparison of shaking versus baking: further understanding the energetics of a mechanochemical reaction. *Green Chemistry* **2014**, 16 (3), 1628-1632.
65. Hick, S. M.; Griebel, C.; Restrepo, D. T.; Truitt, J. H.; Buker, E. J.; Bylda, C.; Blair, R. G., Mechanocatalysis for biomass-derived chemicals and fuels. *Green Chem.* **2010**, 12, 468-474.
66. Rodriguez, B.; Bruckmann, A.; Rantanen, T.; Bolm, C., Solvent-free carbon-carbon bond formations in ball mills. *Adv. Synth. Catal.* **2007**, 349 (14+15), 2213-2233.
67. Milosavljevic, I.; Suuberg, E. M., Cellulose Thermal Decomposition Kinetics: Global Mass Loss Kinetics. *Industrial & Engineering Chemistry Research* **1995**, 34 (4), 1081-1091.
68. Davydov, V. A.; Kashevarova, L. S.; Rakhmanina, A. V.; Senyavin, V. M.; Oleœnikov, N. N.; Agafonov, V. N., Determination of the Reaction Rate Constant and Activation Energy for Pressure-Induced 2 + 2 Cycloaddition of the C₆₀ Fullerene. *Physics of the Solid State* **2002**, 44 (3), 557-559.
69. Schweitzer, N. M.; Hu, B.; Das, U.; Kim, H.; Greeley, J.; Curtiss, L. A.; Stair, P. C.; Miller, J. T.; Hock, A. S., Propylene Hydrogenation and Propane Dehydrogenation by a Single-Site Zn²⁺ on Silica Catalyst. *ACS Catalysis* **2014**, 4 (4), 1091-1098.
70. Klug, H. P.; Alexander, L. E., Method of Integral Breadths. In *X-ray Diffraction Procedures for Polycrystalline and Amorphous Materials*, 2 ed.; John Wiley & Sons: New York, 1974; pp 661-665.

71. Kresse, G.; Furthmüller, J., Efficiency of *ab-initio* total energy calculations for metals and semiconductors using a plane-wave basis set. *Computational Materials Science* **1996**, 6 (1), 15-50.
72. Kresse, G.; Furthmüller, J., Efficient iterative schemes for *ab initio* total-energy calculations using a plane-wave basis set. *Physical Review B* **1996**, 54 (16), 11169-11186.
73. Kresse, G.; Hafner, J., *Ab initio* molecular dynamics for liquid metals. *Physical Review B* **1993**, 47 (1), 558-561.
74. Kresse, G.; Hafner, J., *Ab initio* molecular-dynamics simulation of the liquid-metal–amorphous-semiconductor transition in germanium. *Physical Review B* **1994**, 49 (20), 14251-14269.
75. Zhang, Y.; Yang, W., Comment on “Generalized Gradient Approximation Made Simple”. *Physical Review Letters* **1998**, 80 (4), 890-890.
76. Román-Pérez, G.; Soler, J. M., Efficient Implementation of a van der Waals Density Functional: Application to Double-Wall Carbon Nanotubes. *Physical Review Letters* **2009**, 103 (9), 096102.
77. Blöchl, P. E., Projector augmented-wave method. *Physical Review B* **1994**, 50 (24), 17953-17979.
78. Kresse, G.; Joubert, D., From ultrasoft pseudopotentials to the projector augmented-wave method. *Physical Review B* **1999**, 59 (3), 1758-1775.
79. Paszkowicz, W.; Pelka, J. B.; Knapp, M.; Szyszko, T.; Podsiadlo, S., Lattice parameters and anisotropic thermal expansion of hexagonal boron nitride in the 10–297.5 K temperature range. *Applied Physics A: Materials Science & Processing* **2002**, 75 (3), 431-435.

CHAPTER 3: PHOTOLUMINESCENT COPPER(I) IODIDE CLUSTER COMPOUNDS FOR THE NOVEL DETECTION AND IDENTIFICATION OF HETEROCYCLIC AMINES OF FORENSIC INTEREST

3.1 Introduction

The ability to conclusively identify an unknown compound that may be an illicit drug or other substance of abuse is crucial in the criminalistics and law enforcement fields. Current methods of identification include GC-MS, LC-MS, thin-layer chromatography, infrared spectroscopy, Raman spectroscopy, microcrystal tests, and chemical spot tests.¹ Mass spectrometry methods are most commonly used as a confirmatory identification method in the crime lab, and only rarely as an on-site presumptive test. Portable GC-MS devices tend to be too expensive and too large to put into the hands of every field agent or police officer. These instruments, in the sense of compactness, are portable relative to their laboratory desktop counterparts, but are still so large that they need to be transported by vehicle. Raman spectroscopy and infrared spectroscopy are other identification techniques usually used in the crime lab. Handheld systems leveraging Raman spectroscopy have been developed, but are expensive, making it unfeasible for most law enforcement agencies to afford multiple units. Accordingly, color tests are used for on-site, presumptive drug detection.² They are used as well for the rapid screening of illicit drugs in crime labs. Conventional color tests are highly subjective due to their dependence on the ability of the analyst accurately to match the color of the product of a reaction between the color test reagent and the analyte with that corresponding to a specific drug on a color chart. One source of misidentification is that the color produced

under the test may fail to distinguish a target compound (e.g., cocaine with Scott reagent) from one that is not of forensic interest (e.g., Benadryl® with Scott reagent).³ Another problem conventional drug detection methods are ill-equipped to confront is the constant introduction of new synthetic drugs and designer drugs each year. Given the variety of previously unidentified compounds being continually introduced into the underground drug market, chemical color tests would not be advantageous because there is no familiarity to the resulting reactions with each chemical reagent. Most commercial color test reagents are analyte-specific, therefore developing a new test for every novel drug is not viable due to the time and effort it would take. With hundreds of known drugs, chances are high for more than one drug to yield indistinguishable results when using a given color test reagent. Confirmatory tests would be the only option for identification. Color tests also destroy the sample. This is a significant disadvantage in the case that a trace amount of substance is being tested and still needs to be sent to the crime lab for confirmation on the identity. There are also safety concerns in regard to these field color test kits, in which many of the reagents are hazardous chemicals, such as concentrated acids. Police personnel may be poorly trained in handling these chemicals with care, which may lead to injuries on the job.

A promising avenue to explore for developing a more reliable and adaptable method for detecting illicit drugs is afforded by photoluminescent d^{10} metal cluster compounds, specifically those formed with copper(I) halides. One of the most commonly studied structures of these kinds of clusters is the tetranuclear cubane form $M_4X_4L_4$, in which M is a d^{10} metal, X is a counterion anion, and L is an organic ligand - an amine or

phosphine, each of which coordinates to one of the metal atoms via its nitrogen or phosphorous atoms.⁴⁻⁸ This coordination forms new charge-transfer excited states between the MX cluster and the ligands. Photoluminescence results from the interactions among the states generated between M and L, X and L, M and M, and M and X.^{6, 9-13} In addition to this cubane cluster, different kinds of coordination can occur to form mononuclear¹⁴⁻¹⁶, dinuclear¹⁶⁻¹⁷, octahedral tetranuclear^{16, 18-19}, hexanuclear²⁰⁻²², or heptanuclear²³ clusters, infinite polymers of the formula (MLX)_∞^{17, 19}, and even structures of 2-dimensional²⁴ and 3-dimensional²⁵ coordination networks. The coordination is dependent on the reaction stoichiometric ratio between the metal halide and organic ligand. For higher metal nuclearity, the ratio of MX to ligand must be greater than or equal to 1, and for lower nuclearity, less than 1. Some d¹⁰ metals are less promising for the formation of photoluminescent clusters than others. Although silver(I),²⁶⁻²⁸ gold(I),²⁶⁻²⁷ zinc(II),^{26-27, 29} cadmium(II),^{26-27, 29} and mercury(II)²⁶ all can form complexes with amines, the resulting complexes with monodentate amines do not photo emit in the visible range. Complexes formed between copper(I) halides and derivatives of pyridine, however, have been shown to photoemit across a much broader range that includes the visible spectrum.^{5-6, 26-27, 30-34} Copper(I) iodide (CuI) in particular, as we shall see, shows promise in the detection of common substances of abuse and illicit drugs. The fact d¹⁰ metals can form photoluminescent compounds with amines provides a way to detect alkaloids and synthetic amine drugs on the basis of their emission spectra. A reference database of spectral profiles of such clusters would be highly useful for presumptively identifying illicit drugs.

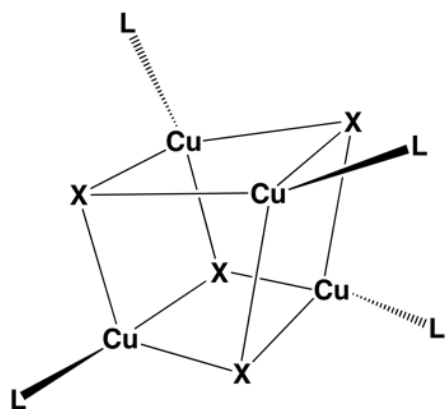


Figure 30. Structure of the cubane form of $\text{Cu}_4\text{X}_4\text{L}_4$ cluster.

Current chemical color tests cannot distinguish between cocaine and phenylcyclidine (PCP). Worse yet, they can confuse Benadryl® with cocaine.³ Additionally, benzyloperazine (BZP) is an illicit drug that cannot be detected by conventional color tests. The method we have developed has been shown to yield distinguishable presumptive results between PCP and cocaine, and further, detect the presence of BZP. Other cyclic amine compounds, including common illicit substances of abuse and many that contain structural building blocks of many recreational drugs, such as piperidine, piperazines, and opiates were also tested and yielded distinct spectral profiles for each. The ability to identify piperidine-based compounds and opiates would provide a potential route for presumptively identifying fentanyl and heroin, in a time the U.S. is facing an ongoing opiate epidemic that has led to the deaths of over 28,000 people in 2014.³⁵ It is reasonable to expect that CuI cluster compounds formed with different heterocyclic nitrogen-containing ligands will exhibit individualized spectral profiles, providing a means to build a reference database of luminescence emission spectra for

illicit and commonly-abused drugs. This reference database would allow for rapid presumptive testing in the crime lab and, potentially, the field. In this work, we present our findings on the photoluminescent spectra of clusters formed between CuI and various heterocyclic amines of forensic interest and suggest the practicality of using this data for their positive presumptive identification.

3.2 Experimental

3.2.1 Materials and Methods

The following chemicals were reagent grade: Copper(I) iodide, acetonitrile, absolute ethanol, methanol, methylene chloride, piperidine, piperazine, 1-(3-trifluoromethylphenyl)piperazine, 1-(4-trifluoromethylphenyl)piperazine, 1-(4-methylbenzyl)piperazine, 1-(4-*tert*-butylbenzyl)piperazine, 1-benzylpiperazine (1 mg/ml analytical standard solution), dextromethorphan HCl, caffeine, quinine sulfate dihydrate, DABCO, hexamine, xanthine, theophylline, theobromine, cinnarizine, indole, 1-methylindole, 3-methylindole, norephedrine.

All of the following illicit substances (except for BZP, in which a 1 mg/ml DEA-exempted solution was used) were tested at California State University-Los Angeles. Cocaine, PCP, morphine, N-phenethylpiperidinone, and 4-methoxybutyryl fentanyl.

3.2.2 Synthesis of Copper(I) Iodide Clusters

For each analyte, the following protocol was used. A saturated solution of CuI in acetonitrile was prepared by mixing 0.0302 g of CuI for every 1 ml of acetonitrile to make a 0.158 M solution. The solution was stirred for 10 minutes to dissolve the CuI. 2 mg/ml analyte solutions were prepared in acetonitrile. Dissolution was achieved by sonication of the solution for 1 minute. CuI-analyte samples were prepared in a 12 x 8 polypropylene round-bottom black microplate with 500 μ l wells. 150 μ l of the saturated CuI solution was added to a well, followed by 150 μ l of analyte solution. The solvent was allowed to evaporate overnight. All data for the CuI-analyte clusters represent the mixture of the saturated CuI solution and 2 mg/ml analyte solution unless otherwise specified (by another concentration or stoichiometric ratio).

CuI and amines are known to coordinate in several manners to yield different geometries depending on the reaction stoichiometry.¹⁴⁻²⁵ Much of the pioneering research on photoluminescent CuI clusters investigated the tetranuclear cubane structures produced by reacting 1:1 stoichiometric amounts of CuI to ligand. The photoluminescent properties of CuI clusters of different nuclearities have been scarcely studied, but the limited literature available shows that they may exhibit altered photoluminescent behavior.³⁶ Our CuI clusters were prepared using analyte solutions of 2 mg/ml, which when converted to molarity with respect to the analytes used, amount to a considerably smaller concentration than that of the saturated CuI solution (0.158 M). Therefore, when the CuI and analyte solutions are mixed together, the stoichiometric ratio is well below 1:1 for CuI to analyte. Because of this, it is possible for our method of CuI cluster synthesis

to form clusters of higher nuclearity and alternate photoluminescent properties. In order to provide a standard to compare the resulting photoluminescence data to, CuI-analyte mixtures of 4:1 stoichiometric ratios were prepared in solvent. A successful reaction was typically indicated by a rapid change in color of the solution, the formation of a precipitate, or both. Samples were prepared in a 12 x 8 polypropylene round-bottom black microplate with 500 μ l wells. The solutions were shaken to ensure their precipitate did not settle, then 250 μ l of the CuI-analyte mixtures were added to the wells. The solvent was allowed to evaporate overnight.

3.2.3 Limit of Detection (LOD) Studies

Analyte solutions with the concentration of 2 mg/ml, or 2000 ppm, were prepared by mixing 3 mg of analyte with 1.5 ml of acetonitrile. Dissolution was achieved through sonication of the solution for 1 minute. The 2000 ppm solution was serial diluted to obtain solutions of the concentrations 1000, 100, 10, and 1 ppm. A saturated CuI solution was prepared. CuI-analyte samples were prepared for LOD studies in a 12 x 8 polypropylene round-bottom black microplate with 500 μ l wells. 150 μ l of the saturated CuI solution was added to a well, followed by 150 μ l of analyte solution. The solvent was allowed to evaporate overnight. The limit of detection was determined by the presence of a photoemission signal comparable to that of the 4:1 stoichiometric CuI to analyte solution.

3.2.4 Testing Illicit Substances

Illicit substances were prepared and tested with Cul following the LOD studies method. Various stoichiometric ratio solutions were not prepared, due to the limited amount of illicit sample available.

3.2.5 Photoluminescence Analysis

Photoluminescence emission spectra for non-illicit substances were obtained using a TECAN Infinite® M200 PRO microplate reader with the following settings: excitation wavelength at 255 nm scanning for emission from 280 nm to 850 nm, mode: top, manual gain: 75, lag time: 0 μ s, integration time: 20 μ s, number of flashes: 5, settle time: 0 ms, step: 1 nm, z-position: 20000 μ m, and the temperature set at 27.0 degrees Celsius. The microplates used were 12 x 8 polypropylene black round-bottom with 500 μ l wells.

Photoluminescence emission spectra for illicit substances were obtained using a Molecular Devices Spectramax® i3x set up with the same parameters as the TECAN Infinite® M200 Pro.

Spectral profiles were established through Gaussian peak fitting, determining the Cul-analyte cluster peak location and full width-half max (FWHM).

3.3 Results and Discussion

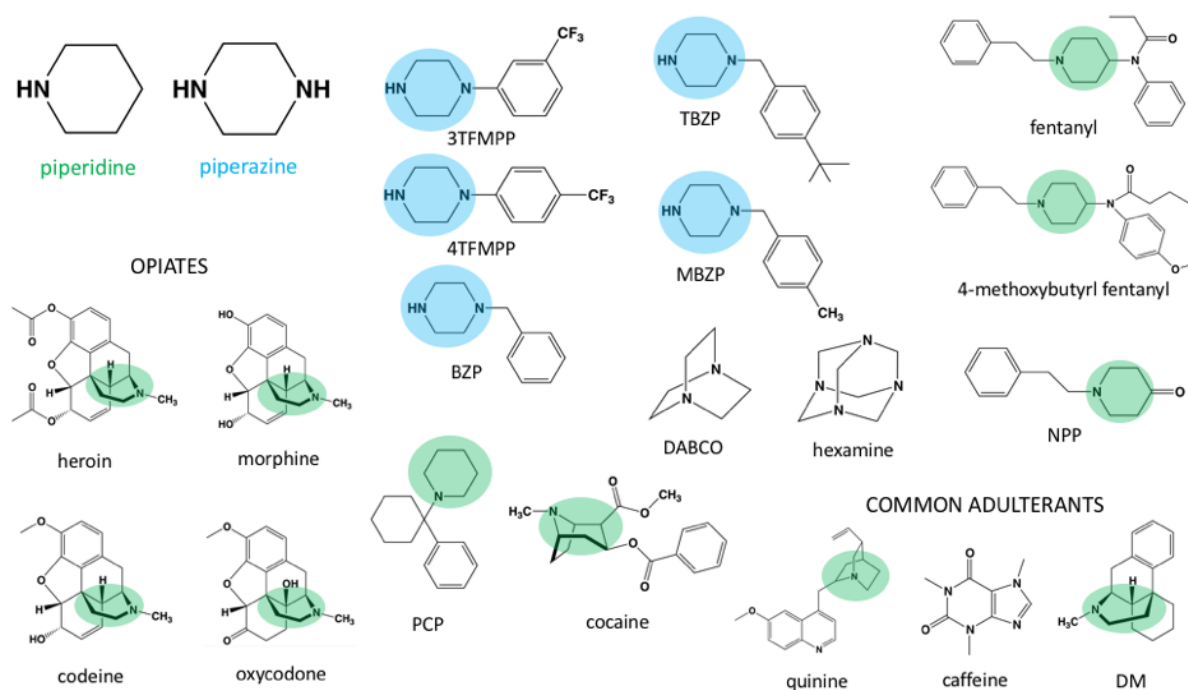


Figure 31. Chemical structures of various substances of forensic interest, as well as some of their analogues. Many of them contain a piperidine ring (green circle) or piperazine ring (blue circle) in their structure.

3.3.1 Copper(I) Iodide

Samples of CuI were prepared by adding saturated CuI solution to a well and allowing the solvent to evaporate overnight. The resulting CuI crystals normally exhibited one luminescence emission peak around 420 nm under UV radiation of 255 nm shown in Figure 32. An issue that was encountered was the consistency of peaks in the CuI PL spectrum. The recrystallization of CuI out of solution was not done in a controlled environment following our methods, which led to the inconsistent appearance of a red emission band in the PL spectra. These red emission bands have been investigated by

various research groups making CuI thin films or growing single crystals of CuI. We have observed the appearance of a broad band with peaks around 680 nm and 720 nm. The consensus explanation behind the cause of this low energy band is the oxidation of the iodide atoms and subsequent formation of iodide vacancies, giving rise to the peak at 680 nm, and further oxidation of the iodide vacancies to form trace amounts of Cu₂O on the surface of the CuI, giving rise to the peak seen at 720 nm.³⁷⁻⁴¹ Because this emission band may possibly overlap the PL emission peaks of the CuI-analyte clusters, it is necessary to explore ways to control and minimize the peaks that stem from the vacancy formation.

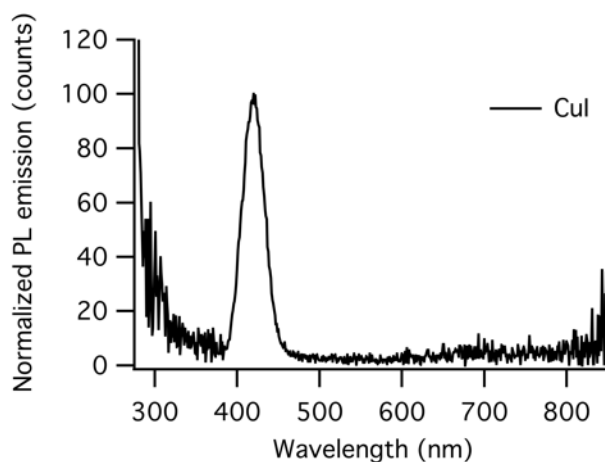


Figure 32. Normalized PL spectrum of CuI at 255 nm excitation, after recrystallization from a saturated acetonitrile solution.

3.3.2 Piperidine, Piperazine, and Piperazine Analogues

Piperidine is a six-membered heterocyclic ring with one nitrogen. The ring is found in the chemical structure of illicit drugs such as fentanyl, opiates, cocaine, and PCP. In

recent times, fentanyl has contributed to an epidemic of overdoses throughout the US due to its high potency as a pain killer and its use as a common adulterant in heroin. Piperazine is a heterocyclic amine with two nitrogens at the 1 and 4 positions in a six-membered ring. It is a structure that is prevalent in many pharmaceutical drugs. It is also found in an illicit substance that is used recreationally called benzylpiperazine. Until 2013, there was no existing presumptive method to detect BZP. The method that was discovered by Philp, *et al.*, uses sodium 1,2-naphthoquinone-4-sulphonate (NQS).⁴² Although practical for detecting the presence of piperazine-based compounds, it yields subjective results between similarly structured piperazine analogues and the reagent is not highly shelf-stable.⁴²

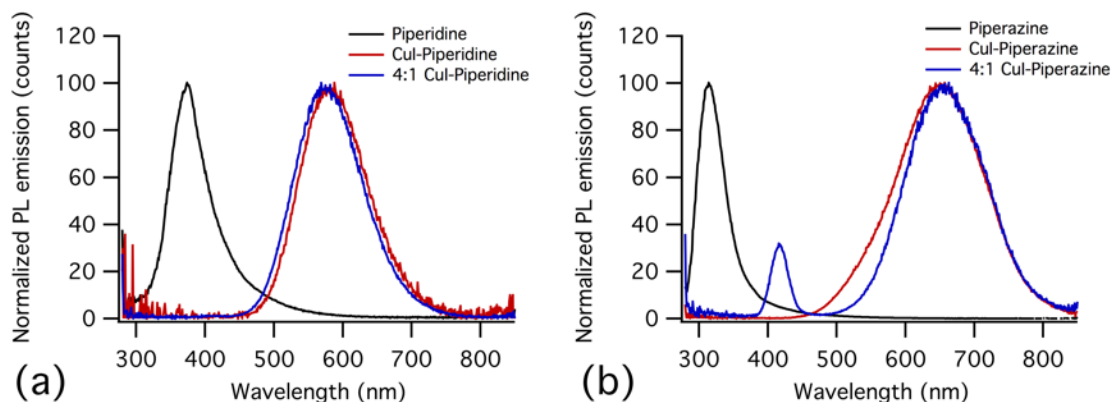


Figure 33. Normalized PL spectra of a) piperidine, Cul-piperidine cluster, and 4:1 Cul-piperidine cluster (the 4:1 Cul cluster spectra were used as a reference for comparison with the Cul-piperidine) and b) Piperazine, Cul-Piperazine cluster, and 4:1 Cul-piperazine cluster.

The piperazine analogues tested were 1-(4-*tert*-butylbenzyl)piperazine (TBZP), 1-(4-methylbenzyl)piperazine (MBZP), 1-(3-trifluoromethylphenyl)piperazine (3TFMPP),

and 1-(4-trifluoromethylphenyl)piperazine (4TFMPP). The latter two derivatives are isomers of each other that differ in the position of a trifluoromethyl group on the phenyl ring. 1-(3-trifluoromethylphenyl)piperazine, commonly used as an adulterant in ecstasy mixtures, was a controlled substance in the US until 2004.

The normalized PL emission spectra for piperidine and CuI-piperidine clusters is shown in Figure 33a. Piperidine exhibited an emission peak around 385 nm. The spectrum of the CuI-Piperidine cluster, (clusters formed from the mixture of 150 μ l of saturated CuI solution and 150 μ l of a 2 mg/ml piperidine solution) consisted of one peak at 587 nm, which closely concurred with the spectrum of the 4:1 CuI-Piperidine (clusters formed from a 4:1 stoichiometric mixture of CuI and piperidine in solution). Figure 33b shows the spectra for piperazine and CuI-piperazine clusters. Piperazine photoemits around 320 nm and CuI-Piperazine spectra consist of a major peak at about 650 nm. Some discrepancies are observed between CuI-Piperazine and 4:1 CuI-Piperazine. The spectrum of CuI-Piperazine exhibited a second peak around 420 nm, which is attributed to the presence of unreacted CuI. The major peak of 4:1 CuI-piperazine deviated from the Gaussian curve seen in CuI-Piperazine, exhibiting an obscure smaller peak around 580 nm. The peak correlates with the broad peak observed in the PL spectrum of the clusters formed from a 1:1 stoichiometric mixture of CuI and piperazine. The presence of this peak in 4:1 CuI-Piperazine may be evident of the unintended formation of various kinds of CuI clusters with distinct PL characteristics.

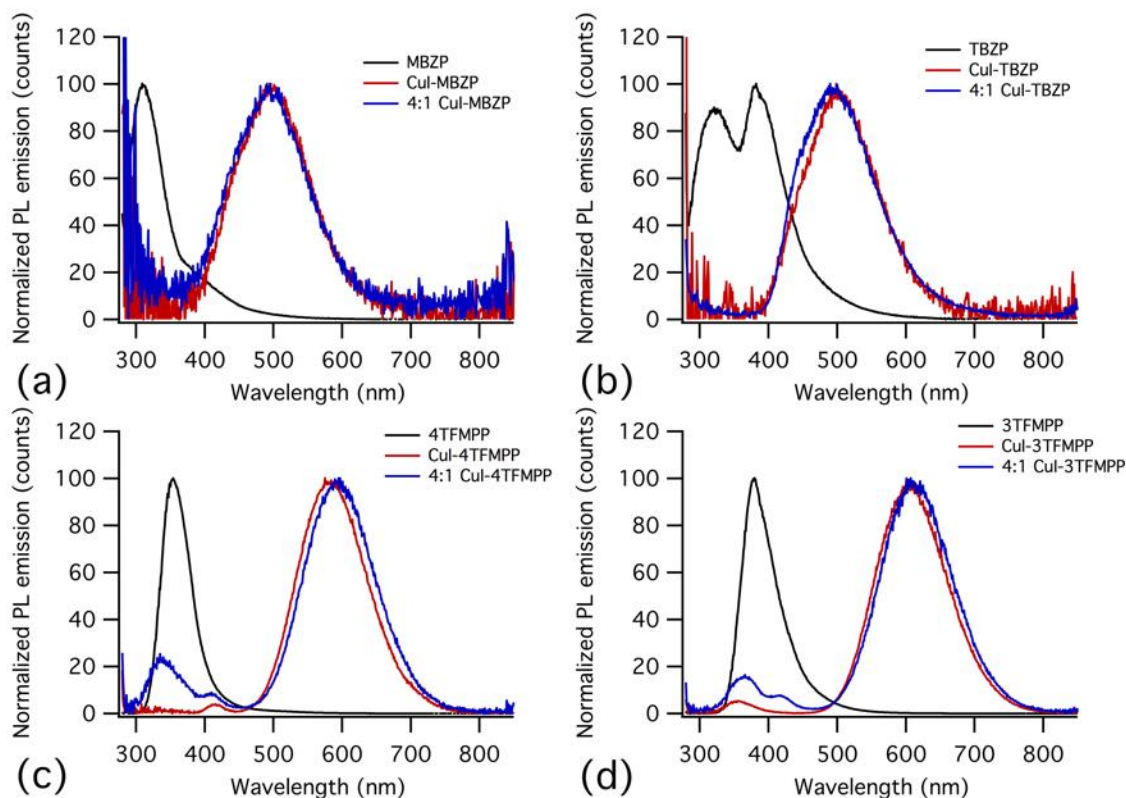


Figure 34. Normalized PL spectra of a) MBZP, CuI-MBZP cluster, and 4:1 CuI-MBZP cluster, b) TBZP, CuI-TBZP cluster, and 4:1 CuI-TBZP cluster, c) 4TFMPP, CuI-4TFMPP cluster, and 4:1 CuI-4TFMPP cluster, and d) 3TFMPP, CuI-3TFMPP cluster, and 4:1 CuI-3TFMPP cluster.

The spectral peaks of the piperazine analogues tested with CuI closely compare to their 4:1 counterparts. The CuI clusters with MBZP, TBZP, 4TFMPP, and 3TFMPP yielded PL peaks at approximately 498 nm, 505 nm, 586 nm, and 609 nm, respectively (Figure 34). The results between CuI-4TFMPP and CuI-3TFMPP show that two compounds with a structural difference as small as the position of a common functional group between them, can be distinguished spectroscopically by their respective CuI clusters. This capability would be significant in the presumptive identification of new designer drugs that are introduced into the illegal drug market.

3.3.3 DABCO and Hexamine

DABCO (1,4-diazabicyclo[2.2.2]octane) and hexamine (1,3,5,7-tetraazatricyclo[3.3.1.1^{3,7}]decane) are polycyclic compounds with six-membered rings containing nitrogen atoms. There is no known forensic interest for DABCO, but hexamine is a precursor to RDX, an explosive. Both compounds were chosen to observe the interaction of CuI with other heterocyclic amines and its resulting PL behaviour. The CuI clusters with DABCO and hexamine photoemitted around 614 nm and 600 nm, respectively (Figure 35).

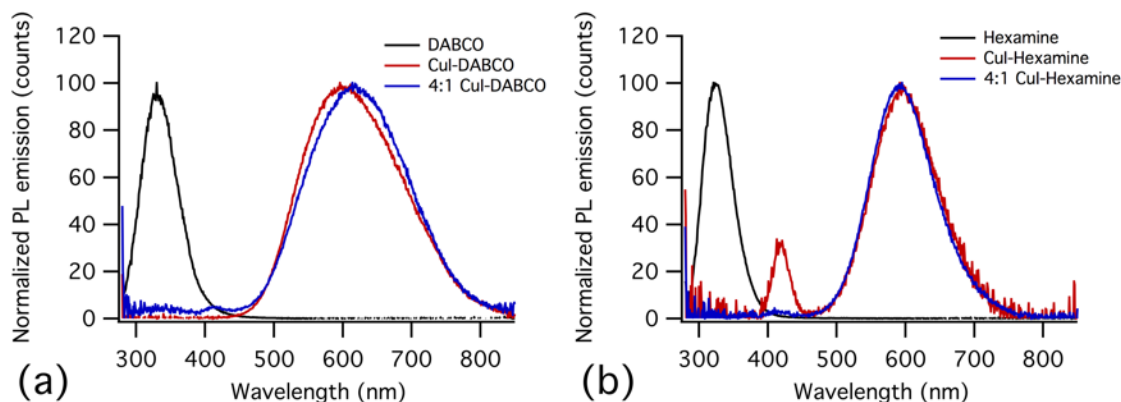


Figure 35. Normalized PL spectra of a) DABCO, CuI-DABCO cluster, and 4:1 CuI-DABCO cluster and b) hexamine, CuI-hexamine cluster, and 4:1 CuI-hexamine cluster.

3.3.4 Substances of Forensic Interest

Caffeine, quinine, and dextromethorphan (DM) are adulterants commonly found in street samples of illicit drugs. Caffeine and quinine are cutting agents for heroin, caffeine

is also found in cocaine, while dextromethorphan is used to cut ecstasy.⁴³ All three substances can be purchased over-the-counter. The CuI clusters with quinine sulfate dihydrate, caffeine, and dextromethorphan HCl resulted in major PL peaks around 605 nm, 688 nm, and 563 nm, respectively (Figure 36).

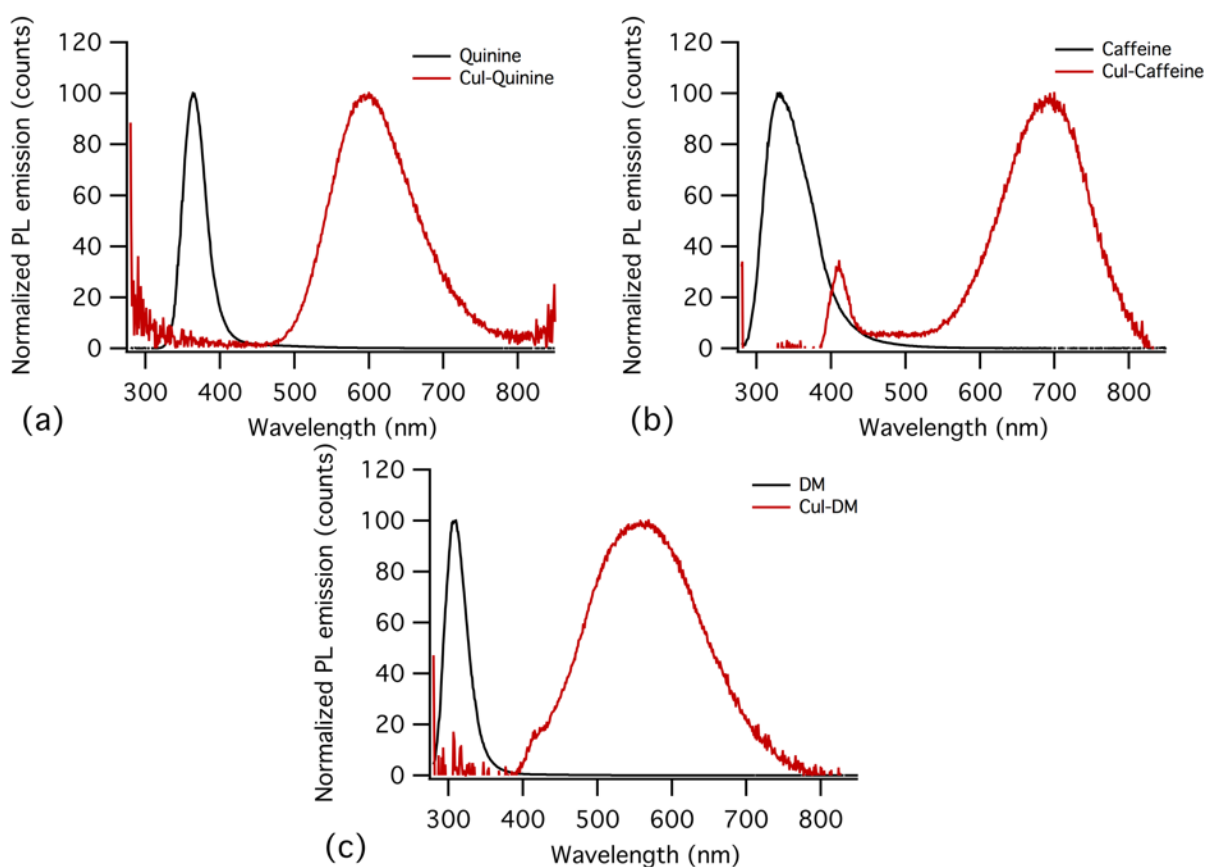


Figure 36. Normalized PL spectra of a) quinine and CuI-quinine cluster, b) caffeine and CuI-caffeine cluster, and c) DM and CuI-DM cluster.

As previously mentioned, 1-benzylpiperazine (BZP) is an illicit piperazine compound with no feasible presumptive test for identification. A 1 mg/ml (1000 ppm) solution was tested with CuI and it resulted in a cluster with a PL peak around 609 nm

(Figure 37). Although this peak location was very close to that of Cul-3TFMPP, the spectral peaks can be distinguished by their full width-half max (FWHM) measurements. Cul-BZP peak resulted in a FWHM of 128.01 nm while the FWHM of Cul-3TFPP peak was 120.24 nm, a large enough difference to distinguish the two by eye.

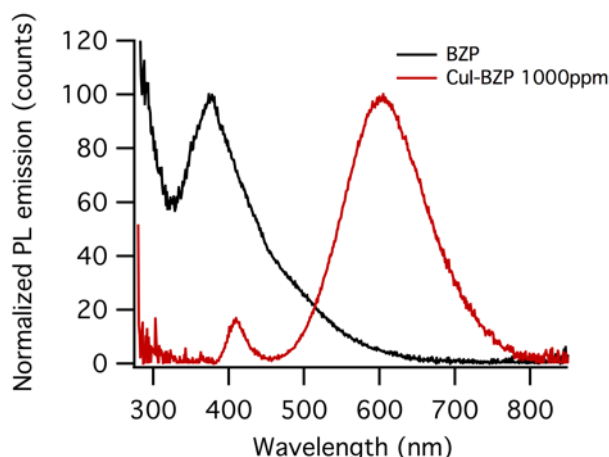


Figure 37. Normalized PL spectra of BZP and Cul-BZP.

Traditional color tests yield indistinguishable results when testing for cocaine and PCP. When tested with Cul, each illicit substance yields distinguishable spectral profiles (Figure 38). Note that the for the following illicit substances tested, the peak location and FWHM were not obtained due to the excessive noise in spectral data. The data is presented to show the general peaks of the of the resulting Cul clusters, while further experiments must be conducted to overcome the issue of noise in the data (which may be due to a poor detector in the instrument). Also, all of the following illicit substances tested were samples once seized by local (Los Angeles-area) law enforcement agencies, not reagent grade standards. The purity of each sample was not known, so adulterant

interference may be a possibility during the data collection. All spectra were obtained of illicit substances tested at a 2000 ppm concentration in acetonitrile.

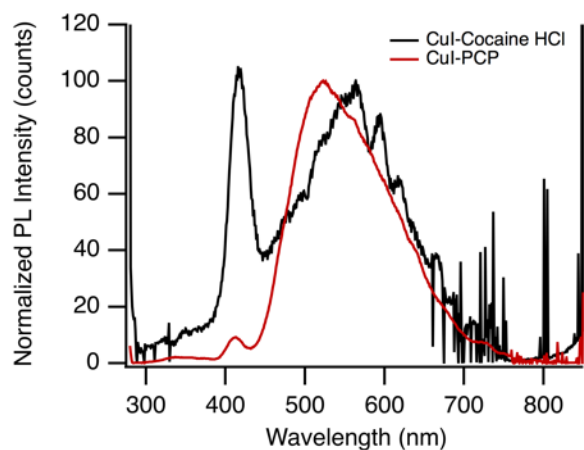


Figure 38. Normalized PL spectra for CuI clusters with cocaine-HCl (black) and PCP (red).

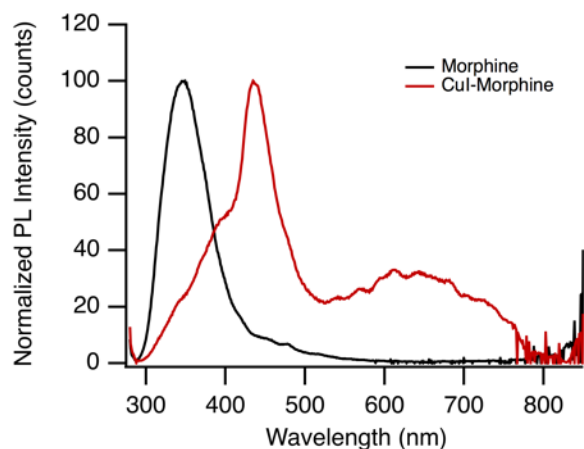


Figure 39. Normalized PL spectra of morphine and CuI-morphine.

Morphine was tested to determine if opioids would form photoluminescent clusters with CuI. Figure 39 shows that the CuI-morphine cluster exhibits a broad PL in the visible

range. The results of Cul-morphine and the Cul-DM are promising in the development of presumptive identification methods for other morphinan-based substances, which include popular recreational opioids like heroin, oxycodone, hydrocodone, and codeine.

Fentanyl is a synthetic opiate that is commonly available commercially in painkiller medications and illegally, as it is synthesized in clandestine labs for illegal distribution, especially as an additive to heroin. N-phenethylpiperidinone (NPP), a fentanyl precursor, and 4-methoxybutyryl fentanyl (4MB-fentanyl), a popular fentanyl analogue, are commonly encountered by law enforcement in the field. Each were tested with Cul, resulting in clusters yielding distinguishable spectral signals compared to the respective analytes by themselves (Figure 40). These results show promise in the ability for Cul to be capable of also detecting and identifying fentanyl and its analogues.

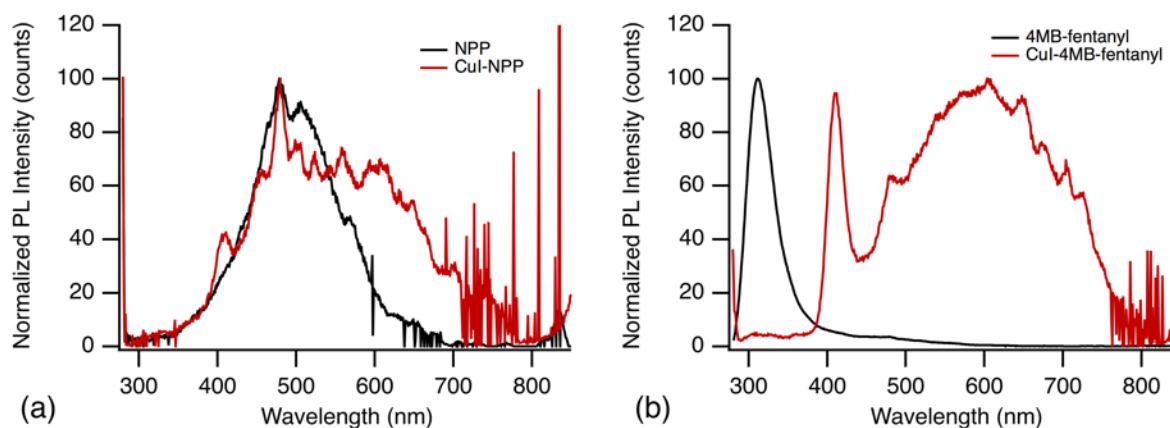


Figure 40. Normalized PL spectra of (a) NPP and Cul-NPP and (b) 4MB-fentanyl and Cul-4MB-fentanyl.

3.3.5 Other substances (Indoles, xanthines, amphetamines, and sterically-hindered amines)

To the best of our knowledge, literature only shows the formation of the luminescent $\text{Cu}_4\text{I}_4\text{L}_4$ cluster to occur between CuI and heterocyclic amines as the ligands. In addition to our work, some acyclic amines were tested but did not result in photoluminescent clusters with CuI. Also, heterocyclic aromatic amines were used, yielding mixed results.

Indole rings are found in the chemical structures of many synthetic cannabinoids, especially JWH cannabinoids, as well as the popular psychedelic drugs LSD and dimethyltryptophan (DMT). Basic indole analogues failed to form PL clusters with CuI, using our method. Indole, 1-methylindole, and 3-methylindole were all tested.

Caffeine, part of the xanthine family of compounds, formed a cloudy white precipitate that photoemits in the visible range under UV irradiation. Its interaction with CuI is physically evident. When the product is dried, it has a cotton fiber-like appearance. When xanthine, theophylline, and theobromine are mixed with CuI, there is no physical indication of cluster formation. Photoluminescence measurements indicate the presence of starting material and no apparent peak for a CuI-amine cluster in the visible range. Xanthines have low solubility in the common organic solvents we employed, which may be a reason why CuI-xanthine clusters were difficult to produce, if possible. Further experiments of the different xanthines with CuI refluxed in 1:1 volume solutions of acetonitrile-methanol, acetonitrile-ethanol, acetonitrile-water, acetonitrile-methylene chloride, and acetonitrile-acetone failed to yield photoluminescent products, with the

exception of caffeine. Further investigations are essential for the determination of the factors that favor CuI cluster formation with only caffeine, and none of the other xanthine compounds.

Amines in which the nitrogen is not part of a cyclic ring were tested and did not form photoluminescent products with CuI. Triethylamine, ethylenediamine, aniline, dodecylamine, di-n-decylamine, diphenylamine, and dicyclohexylamine were among the amines of non-forensic interest tested. Additionally, norephedrine was selected for its amphetamine structure and did not result in the formation of photoluminescent products. Based on these results, we predict CuI, as-is, is not capable of detecting commonly abused amphetamines such as methamphetamine and ecstasy.

Cinnarizine was expected to form a cluster with CuI, based on the presence of a piperazine ring in its structure. Instead, it did not react with CuI. Steric and inductive effects from the functionalities on each nitrogen of the piperazine ring may be factors that prevent the adduct formation between the nitrogen atoms and iodide atoms.

3.3.6 Limit of detection (LOD)

A vital figure of merit for any presumptive drug testing method is the limit of detection. In many cases, law enforcement and crime scene investigators may encounter trace amounts of substances that may lead to inconclusive results using conventional presumptive test kits. Situations in which remnants of the drug sample is on the surface of a syringe needle or other drug paraphernalia require a test that is capable of accurately

detecting drugs at a low concentration. Table 5 shows the LOD for several of the substances tested.

3.3.7 Spectral Peak Analysis

Gaussian peaks were fitted for notable photoemission peaks from spectral data of the samples to obtain their full width-half max (FWHM), in addition to their peak location (Table 5). With the spectral information, spectral profiles can be assigned to the analyte clusters formed with CuI, allowing for the potential use as reference data in a library database for substances of forensic interest.

Table 5. Major spectral peak location and FWHM of CuI clusters with various amines tested obtained by Gaussian peak fitting and the limit of detection (LOD), showing the ability for the method to detect various amines at low concentrations.

Sample	Peak	FWHM	LOD (ppm)
CuI	419.9	31.1	
CuI-TBZP	504.8	125.3	1000
CuI-MBZP	498.4	123.9	2000
CuI-Piperidine	587.2	114.2	2000
CuI-Piperazine	649.6	155.2	100
CuI-3TFMPP	609.0	120.2	1
CuI-4TFMPP	586.2	115.5	1
CuI-Hexamine	599.8	112.9	10
CuI-DABCO	613.8	171.4	100
CuI-BZP	608.9	128.0	1000
CuI-DM	563.2	184.3	10
CuI-Quinine	604.8	122.8	2000
CuI-Caffeine	687.6	132.5	1

3.4 Conclusion

Our copper(I) iodide test is shown to serve as a promising tool for forensic applications, specifically the presumptive identification of some common substances of abuse. The future implementation of this method into crime labs can provide analysts with a process for high-throughput drug screening, which can cut down on the time spent on the analysis of drug evidence and allow them to potentially get through more cases. Microplate readers are affordable relative to the common instruments used in crime labs, such as GCMS, LCMS, Raman spectrometers, and infrared spectrometers, so the adoption is more feasible than innovative methods performed using NMR instrumentation. The use of this method as a field test would require the development of a portable luminescence spectrometer and mobile access to a library database. This would give law enforcement officers a much-needed rapid, accurate, and safe test to identify suspected drugs on-site. Current results show the promise of using CuI to identify illicit substances that contain piperidine rings in their chemical structure, as well as piperazine-based drugs. Further experiments must be carried out on various illicit compounds to show that this method can presumptively identify substances law enforcement personnel and crime lab analysts encounter on a regular basis. This method, as-is, has not been able to detect acyclic amines (i.e. amphetamines and MDMA), indole-based compounds, xanthines, and sterically-hindered amines. Theoretical calculations have provided an explanation for the resulting photoluminescence emission due to the interaction between the surfaces of CuI and BZP.⁴⁴ More investigations via DFT can point to why the non-detectable substances do not yield photoluminescent products using this method and could

potentially provide an alternative route for successful presumptive identification. The ability for this method to analyze drug mixtures also requires further investigation, for most street samples are typically adulterated.

3.5 References

1. Peat, M. A., Analytical and Technical Aspects of testing for Drug Abuse: Confirmatory Procedures. *Clin. Chem.* **1988**, 34 (3), 471-473.
2. O'Neal, C. L.; Crouch, D. J.; Fatah, A. A., Detection of twelve chemical spot tests for the detection of drugs of abuse. *Forensic Science International* **2000**, 109, 189-201.
3. Tsumura, Y.; Mitome, T.; Kimoto, S., False positives and false negatives with a cocaine-specific field test and modification of test proptocol to reduce false decision. *Forensic Science International* **2005**, 155, 158-164.
4. Schramm, V., Crystal and Molecular Structure of Tetrameric Copper(I) Iodide-Piperadine, a Complex with a Tetrahedral Cu₄I₄ Core. *Inorganic Chemistry* **1978**, 17 (3), 714-718.
5. Gan, X.; Fu, W.-F.; Lin, Y.-Y.; Yuan, M.; Che, C.-M.; Chi, S.-M.; Li, H.-F. J.; Chen, J.-H.; Chen, Y.; Zhou, Z.-Y., Synthesis, structures and photophysical properties of polynuclear copper(I) iodide complexes containing phosphine and 4,4'-bipyridine ligands. *Polyhedron* **2008**, 27, 2202-2208.
6. Ryu, C. K.; Vitale, M.; Ford, P. C., Photoluminescence Properties of the Structurally Analogous Tetranuclear Copper(I) Clusters Cu₄X₄(dpmp)₄ (X = I, Br, Cl; dpmp = 2-(Diphenylmethyl)pyridine). *Inorganic Chemistry* **1993**, 32, 869-874.
7. Vogler, A.; Kunkely, H., Photoluminescence of Tetrameric Copper(I) Iodide Complexes in Solution. *J. Am. Chem. Soc.* **1986**, 108, 7211-7212.
8. Perruchas, S.; Tard, C.; Le Goff, X. F.; Fargues, A.; Garcia, A.; Kahlal, S.; Saillard, J.-Y.; Gacoin, T.; Boilot, J.-P., Thermochromic Lumiscence of Copper Iodide Clusters: The Case of Phosphine Ligands. *Inorganic Chemistry* **2011**, 50, 10682-10692.
9. De Angelis, F.; Fantacci, S.; Sgamellotti, A.; Cariati, E.; Ugo, R.; Ford, P. C., Electronic Transitions Involved in the Absorption Spectrum and Dual

- Luminescence of Tetranuclear Cubane [Cu₄I₄(pyridine)₄] Cluster: a Density Functional Theory/Time-Dependent Density Functional Theory Investigation. *Inorganic Chemistry* **2006**, *45*, 10576-10584.
10. Yam, V. W.-W.; Lo, K. K.-W., Luminescent polynuclear d10 metal complexes. *Chem. Soc. Rev.* **1999**, *28*, 323-334.
 11. Rath, N. P.; Holt, E. M.; Tanimura, K., Fluorescent Copper(I) Complexes: Structural and Spectroscopic Characterization of Bis(p-toluidine)bis(acetonitrile)tetraiodotetracopper and Bis[(p-chloroaniline)(acetonitrile)diiododicopper] Tetrameric Complexes of Mixed-Ligand Character. *Inorganic Chemistry* **1985**, *24*, 3934-3938.
 12. Vitale, M.; Ryu, C. K.; Palke, W. E.; Ford, P. C., Ab Initio Studies of the Copper(I) Tetramers Cu₄X₄L₄ (X= I, Br, Cl). Effects of the Cluster Structure and of Halide on Photophysical Properties. *Inorganic Chemistry* **1994**, *33*, 561-566.
 13. Vitale, M.; Palke, W. E.; Ford, P. C., Origins of the Double Emission of the Tetranuclear Copper(I) Cluster Cu₄I₄(pyridine)₄: An ab Initio Study. *J. Phys. Chem.* **1992**, *96*, 8329-8336.
 14. Ohara, H.; Kobayashi, A.; Kato, M., Simple Manual Grinding Synthesis of Highly Luminescent Mononuclear Cu(I)-Iodide Complexes. *Chem. Lett.* **2014**, *43*, 1324-1326.
 15. Simon, J. A.; Palke, W. E.; Ford, P. C., Photophysical and ab Initio Studies of Mononuclear Copper(I) Complexes. *Inorganic Chemistry* **1996**, *35*, 6413-6421.
 16. Maini, L.; Mazzeo, P. P.; Farinella, F.; Fattori, V.; Braga, D., Mechanochemical preparation of Copper Iodide clusters of interest for luminescent devices. *Faraday Discussions* **2014**.
 17. Rath, N. P.; Maxwell, J. L.; Holt, E. M., Fluorescent Copper(I) Complexes: an X-Ray Diffraction Study of Complexes of Copper(I) Iodide and Pyridine Derivatives of Rhombic, [Cu₂I₂(3Me-py)₄], and Polymeric Structure, [{CuI(2Me-py)}] and [{CuI(2,4Me₂-py)}]. *J. Chem. Soc. Dalton Trans.* **1986**, 2449-2453.
 18. Yam, V. W.-W.; Lo, K. K.-W.; Wang, C.-R.; Cheung, K.-K., Synthesis, Photophysics, and Transient Absorption Spectroscopic Studies of Luminescent Copper(I) Chalcogenide Complexes. Crystal Structure of [Cu₄(u-dtpm)₄(u₄-S)](PF₆)₂ {dtpm = Bis[bis(4-methylphenyl)phosphino]methane}. *101* **1997**, 4666-4672.

19. Liu, Z.; Djurovich, P. I.; Whited, M. T.; Thompson, M. E., Cu₄I₄ Clusters Supported by P^N-type Ligands: New Structures with Tunable Emission Colors. *Inorganic Chemistry* **2012**, *51*, 230-236.
20. Hesse, R.; Aava, U., The Crystal and Molecular Structure of the Copper(I) Dipropylthiocarbamate Hexamer. *Acta Chemica Scandinavica* **1970**, *24*, 1355-1366.
21. Lobana, T. S.; Ritu, S.; Bermejo, E.; Castineiras, A., Construction of a Novel Copper(I) Chain Polymer of Hexanuclear Cu₆(2-SC₅H₄NH)₆I₆ Cores with A New (u³-S) Mode of Bonding of Pyridine-2-thione and of an Unusual Triangular Cu₃I₃(dppe)₃(2-SC₅H₄NH) Cluster. *Inorganic Chemistry* **2003**, *42* (42), 7728-7730.
22. Xie, H.; Kinoshita, I.; Karasawa, T.; Kimura, K.; Nishioka, T.; Akai, I.; Kanemoto, K., Structure Study and Luminescence Thermochromism in Hexanuclear 6-Methyl-2-Pyridinethiolato Copper(I) Crystals. *J. Phys. Chem.* **2005**, *109*, 9339-9345.
23. Cheon, S.; Kim, T. H.; Jeon, Y.; Kim, J.; Park, K.-M., Novel heptanuclear copper(I) iodide cluster with a pinwheel shape. *CrystalEngComm* **2013**, *15*, 451-454.
24. Ohi, H.; Tachi, Y.; Kunimoto, T.; Itoh, S., Structure and photoluminescence property of two-dimensional coordination polymer complexes involving CuI₆X₆ (X=Cl, Br, I) hexagon prism cluster supported by a tripodal tripyridine ligand with 1,3,5-triethylbenzene spacer. *Dalton Trans.* **2005**, 3146-3147.
25. Zhang, Y.; He, X.; Zhang, J.; Feng, P., CuI Cluster-Based Organic Frameworks with Unusual 4- and 5-Connected Topologies. *Crystal Growth & Design* **2011**, *11* (1), 29-32.
26. Ford, P. C.; Vogler, A., Photochemical and Photophysical Properties of Tetranuclear and Hexanuclear Clusters of Metals with d¹⁰ and s² Electronic Configurations. *Acc. Chem. Res.* **1993**, *26* (4), 220-226.
27. Barbieri, A.; Accorsi, G.; Armaroli, N., Luminescent complexes beyond the platinum group: the d¹⁰ avenue. *Chem. Commun*, **2008**, 2185-2193.
28. Yang, J.-H.; Zheng, S.-L.; Yu, X.-L.; Chen, X.-M., Syntheses, Structures, and Photoluminescent Properties of Three Silver(I) Cluster-Based Coordination Polymers with Heteroaryldicarboxylate. *Crystal Growth & Design* **2004**, *4* (4), 831-836.
29. Zheng, S.-L.; Chen, X.-M., Recent Advances in Luminescent Monomeric, Multinuclear, and Polymeric Zn(II) and Cd(II) Coordination Complexes. *Aust. J. Chem.* **2004**, *57*, 703-712.

30. Ryu, C. K.; Kyle, K. R.; Ford, P. C., Photoluminescence Properties of the Copper(I) Chloride Clusters $\text{Cu}_4\text{Cl}_4\text{L}_4$ (L= Pyridine, Substituted Pyridine, or Saturated Amine). *Inorganic Chemistry* **1991**, 30 (21), 3982-3986.
31. Perruchas, S.; Le Goff, X. F.; Maron, S.; Maurin, I.; Guillen, F.; Garcia, A.; Gacoin, T.; Boilot, J.-P., Mechanochromic and Thermochemic Luminescence of a Copper Iodide Cluster. *J. Am. Chem. Soc.* **2010**, 132, 10967-10969.
32. Parmeggiani, F.; Sacchetti, A., Preparation and Luminescence Thermochemism of Tetranuclear Copper(I)-Pyridine-Iodide Clusters. *Journal of Chemical Education* **2012**, 89, 946-949.
33. Kyle, K. R.; Ryu, C. K.; DiBenedetto, J. A.; Ford, P. C., Photophysical Studies in Solution of the tetranuclear Copper(I) Clusters $\text{Cu}_4\text{I}_4\text{L}_4$ (L = Pyridine or Substituted Pyridine). *J. Am. Chem. Soc.* **1991**, 113, 2954-2965.
34. Tran, D.; Bourassa, J. L.; Ford, P. C., Pressure-Induced Luminescence Rigidochromism in the Photophysics of the Cuprous Iodide Cluster $\text{Cu}_4\text{I}_4\text{py}_4$. *Inorganic Chemistry* **1997**, 36, 439-442.
35. Rudd, R. A.; Seth, P.; David, F.; Scholl, L. *Increases in Drug and Opioid-Involved Overdose Deaths - United States, 2010-2015*; Center for Disease Control: Dec. 30, 2016, 2016; pp 1445-1452.
36. Wallesch, M.; Volz, D.; Zink, D. M.; Schepers, U.; Nieger, M.; Baumann, T.; Bräse, S., Bright Coppertunities: Multinuclear Cu^{I} Complexes with N-P Ligands and Their Application. *Chem. Eur. J.* **2014**, 20, 2-15.
37. Gao, P.; Gu, M.; Liu, X.; Zheng, Y.-Q.; Shi, E.-w., Crystal growth and luminescence properties of CuI single crystals. *Optik* **2014**, 125, 1007-1010.
38. Sirimanne, P. M.; Rusop, M.; Shirata, T.; Soga, T.; Jimbo, T., Characterization of CuI thin films prepared by different techniques. *Materials Chemistry and Physics* **2003**, 80, 461-465.
39. Sirimanne, P. M.; Rusop, M.; Shirata, T.; Soga, T.; Jimbo, T., Characterization of transparent conducting CuI thin films prepared by pulse laser deposition technique. *Chemical Physics Letters* **2002**, 366, 485-489.
40. Gao, P.; Gu, M.; Zheng, Y.-Q.; Shi, E.-w., Photoluminescence study of annealing effects on CuI crystals grown by evaporation method. *Cryst. Res. Technol.* **2012**, 47 (7), 707-712.

41. Lin, G.; Zhao, F.; Zhao, Y.; Zhang, D.; Yang, L.; Xue, X.; Wang, X.; Qu, C.; Li, Q.; Zhang, L., Luminescence Properties and Mechanisms of CuI Thin Films Fabricated by Vapor Iodization of Copper Films. *Materials* **2016**, 9, 990-997.
42. Philp, M.; Shimmon, R.; Stojanovska, N.; Tahtouh, M.; Fu, S., Development and validation of a presumptive colour spot test method for the detection of piperazine analogues in seized illicit materials. *Anal. Methods* **2013**.
43. Cole, C.; Jones, L.; McVeigh, J.; Kicman, A.; Syed, Q.; Bellis, M. A. *CUT: A Guide to Adulterants, Bulking Agents, and Contaminants Found in Illicit Drugs*; Liverpool John Moores University: 2010.
44. Rawal, T. B.; Turkowski, V.; Rahman, T. S., Complementary roles of benzylpiperazine and iodine 'vapor' in the strong enhancement of orange photoluminescence from CuI(111) thin film. *J. Phys.: Condens. Matter* **2014**, 26.

CHAPTER 4: INTEGRATING BASIC RESEARCH WITH APP-BASED ANALYSIS

4.1 Project Scope

The scope of this project focuses on the development of an alternative drug testing method for crime lab and law enforcement use. This method consists of a three-component system: a drug-indicating test strip, a handheld fluorescence spectrometer, and a mobile app that contains a reference spectral database for substances of forensic interest. This solution is intended to provide a simple, accurate, precise, rapid, and affordable drug testing method to the criminalistics and law enforcement communities.

To understand the necessity for a new drug testing system, the current state of drug testing must be explained. From a legal perspective, methods of drug testing can be classified into two types. Presumptive methods, one of the types, are normally used by law enforcement personnel in the field to provide probable cause to arrest a person in possession of an illicit substance. The most common method used is the color test. In using color tests, the suspected substance is added to a pouch that contains a specific color test reagent. For example, Scott test for cocaine detection is a mixture of cobalt(II) thiocyanate in hydrochloric acid. Once the suspected substance and color test reagent are mixed, a specific color change will indicate the presence of an illicit substance. The resulting color is subject to human interpretation and matched against a color chart to presumptively identify the suspected substance. The subjectivity of the results is a source of false positives. Literature has also shown the possibility of false positives due to non-

illicit samples, such as salt, sugar, and nutmeg, yielding similar results as illicit substances when using certain color tests. The validity of color tests is an issue that has the potential to widely affect the ecosystem between citizens and the law enforcement entities. If an officer relies on a false positive result, an innocent citizen will get arrested causing the officer to spend man hours doing paperwork on the wrongful arrest. The suspected drug sample will eventually be sent to the crime lab, in which the crime lab analysts spend more time to correctly identify the substance since they were initially misled to believe it was a different substance. The wrongfully arrested citizen can also litigate against the law enforcement agency, which can lead to public attorneys spending unnecessary man hours on the case and possibly settling with the plaintiff. The countless man hours spent between the arresting officer, the crime lab analyst, and perchance the attorneys, along with the possibility of a monetary settlement to the wrongfully arrested, ultimately wastes the money of the tax-paying citizens. A better alternative for field drug testing will not only help law enforcement officers in the realm of accurate drug identification, but may also increase the work efficiency of the different parties involved and prove itself cost-efficient.¹

The second type, known as confirmatory methods, typically follows the use of presumptive methods. After an arresting police officer seizes a suspected drug sample, that sample will be sent to the crime lab for further analysis. The objective of confirmatory methods is to positively determine the chemical identity of the suspected sample. Since the presumptive color tests cannot positively identify the sample, the crime lab analysts are responsible for either confirming or disproving the initial presumptive test results through various analytical techniques. Most crime labs follow testing criteria for the

determination of a positive identification set by SWGDRUG.² This requires the crime lab analyst to obtain a positive identification of an illicit substance in the suspected sample via a combination of techniques. These techniques are categorized as A, B, and C (see Table 6). A positive identification is realized by a minimum of one of the following:

- Positive detection or identification of a drug by two category A techniques
- Positive detection or identification of a drug by one category A technique and one category B technique
- Positive detection or identification of a drug by one category A technique and one category C technique
- Positive detection or identification of a drug by three category B techniques
- Positive detection or identification of a drug by two category B techniques and one category C technique

Table 6. Categories of recommended analytical techniques used for drug analysis.²

Category A	Category B	Category C
Infrared spectroscopy	Capillary electrophoresis	Color tests
Mass spectrometry	Gas chromatography	Fluorescence spectroscopy
NMR spectroscopy	Ion mobility spectrometry	Immunoassay
Raman spectroscopy	Liquid chromatography	Melting point
X-ray diffractometry	Microcrystalline tests	Ultraviolet spectroscopy
	Pharmaceutical identifiers	
	Thin layer chromatography	
	For cannabis only: Macroscopic and microscopic examination	

For all categories, it is required that the sample must be tested along with a standard to assure validity of substance identification. Category A methods provide information

specific to the chemical structure of the sample, and are therefore deemed the most reliable of the three categories. In contrast to category A methods, results for category B and category C methods are more dependent on method conditions (i.e. solvent used, chromatography parameters, irradiation wavelength for spectroscopic techniques, etc.) and can vary in degree of subjectivity. In crime labs, color tests are also used and the results are ultimately leveraged as evidence in a court case. Note that the initial color test conducted by the police officers are considered “presumptive” while the crime lab analysts use the same test as one of the many techniques to confirm the identity of the suspected sample. This is because in crime labs highly trained and experienced analysts conduct the tests following strict testing criteria, thus providing more reliable results.

Overall, efficiency can be increased with the adoption of new testing methods that can provide rapid, accurate results. Law enforcement officers can benefit from a presumptive test that is easy to use and yield non-subjective results. In other words, a test that eliminates the requirement of human interpretation of results would be valuable. With accurate results from the initial presumptive test, the confirmation of sample identity by the crime lab personnel will be more straightforward due the decrease in initial misidentifications by the law enforcement officers and subsequent time-consuming corrective measures taken by the crime lab analysts.

This project proposes the development of a new drug identification method based on UV photoluminescence spectroscopy. For field use, a three-component drug identification system consisting of a handheld UV fluorescence spectrometer, drug-indicating test strip, and mobile app that leverages a reference database will be

developed. The handheld drug identification system would provide law enforcement officers the capability to more easily and accurately identify suspected drugs on-site compared to conventional presumptive methods. This method would yield definitive results, using electronic software to interpret the data instead of requiring the user to do it. Crime lab analysts can use this method as a rapid screening test, preceding any other analytical technique used to identify the sample.

The objective of this project is to integrate prior research on novel drug identification techniques based on photoluminescence spectroscopy into a mobile app designed to assist in the process of drug identification by law enforcement and crime lab personnel. Although the contributions to forensic science research, specifically in drug analysis, has seen a great deal of effort from academia, the criminalistics community has not widely adopted many new techniques into common crime lab practices. The reluctance to implement new techniques may be due to the lack of feasibility in using certain methods. For example, there are methods of drug identification that involve using NMR. NMR requires an expensive instrument and highly-skilled users to provide chemical structure information, while techniques such as IR spectroscopy, Raman spectroscopy, and XRD, which are easier for a user to operate, can provide data just as vital for drug identification. Thus, with the development of a novel drug identification technique, it is necessary to research and validate the market to ensure market adoption.

4.2 Customer Discovery and Market Validation

4.2.1 Market Research

The U.S. is facing a decades-long fight against controlled substance abuse, spending substantial amounts of public capital and resources at the federal, state and local levels, at a time when public spending budgets are under extreme pressure. So far, the results are discouraging. According to the Centers for Disease Control, there were over 47,000 drug-induced overdose deaths in 2014, roughly a third greater than deaths resulting from motor vehicle accidents or firearms, making it the leading cause of injury death in the U.S.³ Overdose deaths have surpassed these other causes in every year since 2008, and the trend has continued to increase while that for the other two causes has been roughly stagnant. In 2014, prescription opioid painkillers and heroin accounted for over 28,000 drug poisoning deaths in the U.S., accounting for roughly 61 percent of the total drug poisoning deaths as they continue to increase in usage over other substances of abuse. For these reasons, the DEA has ranked opioids the number one drug threat to the U.S.³⁻⁴ The Drug Enforcement Agency (DEA) estimates that there are 1.4 million active street, prison, and outlaw motorcycle gang members in the U.S. who derive the majority of their illegal revenue through street-level drug trafficking and distribution.³ To continue to fight the catastrophic situation, the U.S. 2017 budget requested \$9.7 billion in federal spending for domestic law enforcement to combat illegal drugs.⁵ Given that the DEA only accounts for approximately 2.2% of all law enforcement drug arrests, spending by state and local governments on drug enforcement is estimated

to be much greater than federal spending. The majority of spending goes toward funding law enforcement, prosecutions, and corrections, with the intent of equipping each entity with the necessary manpower and tools to effectively serve their roles against illegal drug abuse. Public funds for illegal drug law enforcement must be spent efficiently, for the legal action which is grounded on illegitimate presumptive evidence due to false positive results from the flawed color tests wastes not only the time, effort, and resources of law enforcement and crime lab personnel, but that of the judicial process as well.

One route to help the enforcement of illegal drugs is to provide law enforcement officers with better resources for field drug testing. They are first in line in the chain of custody once a suspected drug sample is seized. The time and effort expended on proceeding activities can be highly dependent on the presumptive test results conducted by the arresting officer. Following the officer along the chain of custody of the evidence is a crime lab analyst. Many crime labs are backlogged as it is⁶, and thus could use resources that could increase their case efficiency. An accurate presumptive test result can make the tasks of the crime lab analysts and prosecutors more easily and quickly attainable. Additionally, it would be profoundly impactful on the lives and families of innocent individuals caught up in this process.

4.2.2 Customer Discovery and Validation through NSF I-Corps™

Customer discovery was conducted through the NSF I-Corps™ program in order to validate the existence of a sustainable market for the proposed technology. Between a regional I-Corps™ cohort at the University of Central Florida in 2015 and a National I-

Corps™ cohort in San Francisco in 2016, over 200 potential customers and key partners were interviewed. The concept of the drug testing system was originally developed with the intent to commercialize it and market it to the law enforcement and crime lab customer segments, and as expected, these two segments proved to be the most promising of the various markets surveyed.

In 2008, there were roughly 765,000 badged and sworn full-time personnel in state and local law enforcement across nearly 18,000 agencies. Non-badged full-time personnel accounted for another roughly 369,000, and another 120,000 full time federal personnel were authorized to make arrests.⁷ According to the National Narcotics Officers' Associations' Coalition, an estimated 55,000 of the sworn personnel are narcotics officers and agents.⁸ In 2015, law enforcement in the U.S. made close to 1.5 million drug-related arrests.⁹ Many jurisdiction require probable cause provided by a positive presumptive drug identification for law enforcement officers to make an arrest. Research resulting from interviews with state and local law enforcement conducted during regional and National NSF I-Corps™ cohorts concluded that both badged and non-badged personnel are known to use field drug test kits. Further deduction from interviews indicates that narcotics officers and agents, who encounter illegal drugs on a regular basis, are the most frequent users of field drug tests. Additionally, there are over 400 publicly funded crime labs in the U.S. that received upward of 3.8 million total cases in 2014, in which close to a third of the case load were drug cases.⁶ The heavy reliance on inconsistent presumptive testing methods by a large law enforcement customer segment, on the local, state, and federal levels, would suggest that there is an untapped commercial market for a field drug testing

solution. With support from the criminalistics community, the necessity for a better field drug testing method for law enforcement can be realized, allowing for the potential commercial exploitation of the market.

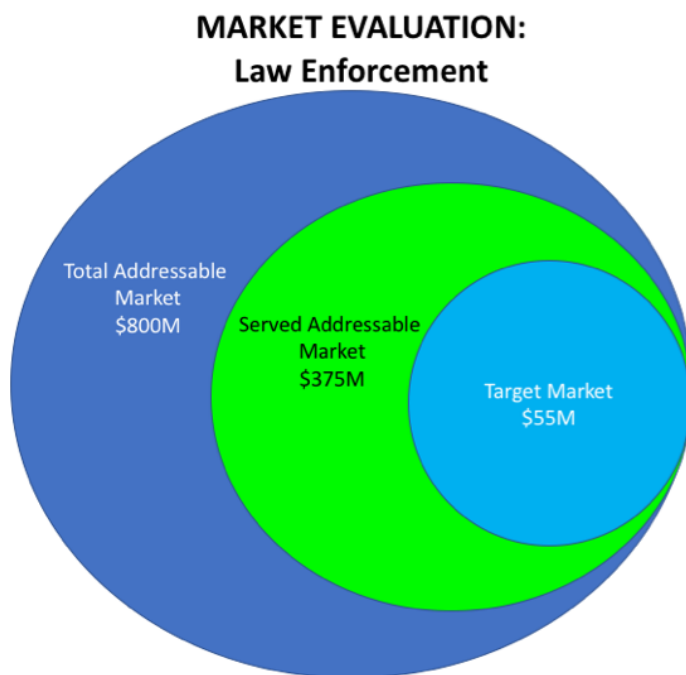


Figure 41. An initial market evaluation of the law enforcement customer segments.

Overall, customer discovery with potential customers within the law enforcement and crime lab segments revealed the following needs associated with field drug testing by law enforcement: simplicity, rapid response, accuracy, definitive, safe, and affordable. This revelation insinuates that many within law enforcement understand that conventional methods are inadequate in countering the current illegal drug problem in the U.S.

4.2.3 Competing Technology in Commercial Market

4.2.3.1 Color Tests

Law enforcement is generally dependent on unreliable field drug tests and that have hardly changed in decades. State laws commonly require an arrest to be supported by probable cause, and color tests are typically employed to establish probable cause when illegal substances are involved. Because of the nature, complexity, and unreliability of the color tests, law enforcement reported via customer interviews that this technology is complex, slow, unreliable, subject to human variability, and potentially hazardous. The kits are commercially available for around \$1 to \$2 each, are non-reusable, and the method may require multiple test kits to be used before a positive result can be obtained for a suspected sample. The two most common brands of color tests are NARK II® kits and NIK® kits, manufactured by Sirchie® and Safariland®, respectively.

Through customer discovery during the NSF National I-Corps program, we learned that the more experienced a law enforcement officer is in using these color tests, the more likely it is for the officer to have a negative opinion toward these test kits. Specifically, narcotics officers and agents do not like the conventional color tests and believe that there is a need for a better method of identifying drugs in the field. One of the common criticisms by the more experienced users interviewed was that they would often accidentally cut themselves when breaking the reagent-containing glass vials inside the plastic pouches of the color test kits. A bigger safety problem is that many police officers were not properly trained to use the color tests. So aside from determining whether the test results are valid

or not, many officers did not know that the test kits may contain hazardous chemicals such as corrosive acids, increasing the probability for nuisance injuries that law enforcement agencies must subsequently deal with.



Figure 42. A 2-step NARK II® color test kit to test for synthetic cannabinoids. The test pouch on the right has been opened, showing a glass capsule filled with the test chemical reagent.

4.2.3.2 Handheld Raman Systems

A more technologically advanced alternative for presumptive drug identification in the field is the handheld device based on Raman spectrometers. The most popular of the bunch commercially available is the TruNarc™, supplied by Thermo Fisher Scientific. With the help of its reference database, this device is advertised to have the ability to identify over 30 thousand chemical compounds, including most of the common illegal drugs law enforcement regularly encounters. The sample preparation and testing is

typically simple for the user and can obtain a positive identification of the suspected drug sample in less than a minute. The device does the analysis and provides the user with the name of the identified substance on a LCD screen, eliminating the need for human interpretation and thus, decreasing the subjectivity of test results. Although this technology possesses superior capabilities compared to color tests, according to the law enforcement personnel responsible for deciding which drug testing method their agency uses, the biggest issue with this method is the price of the device. They are available for around \$30,000 per unit. This price is not affordable for most law enforcement agencies, whose annual budgets for drug testing kits are less than the price of one device. Affordability must be emphasized in the development and commercialization of a new drug testing method in order to achieve widespread market adoption.



Figure 43. The Thermo Fisher Scientific TruNarc™ being used to identify a rock of crack cocaine in a plastic bag.

4.2.4 Business Model Canvas: Product-Market Fit

A product-market fit is how well a product and its features, and thus its value propositions, satisfy the needs of a specific customer segment.

4.2.4.1 Customer Segments

The most promising market to initially target would be the law enforcement market. Law enforcement officers currently rely on a flawed drug testing method that has not seen much improvement in decades. This market can be broken down into three separate customer segments: Upper-level and mid-level management within law enforcement agencies, narcotics officers and agents, and the patrol officers.

Upper-level and mid-level management within an agency consists of personnel in supervising roles, such as sheriffs, chiefs, commissioners, and unit commanders. Those that hold these positions have a certain degree of authority to make decisions, depending on the position. An important decision the commercialization of this technology is dependent on is which method of drug identification the agency's officers and agents are using in field. During customer interviews, those in management spoke on the issues with using color tests. The ones that were most vocal about the issues were the supervisors and commanders of narcotics units, which is expected since their workers use the color tests on a regular basis and they have vast experience in using the flawed method as well. The narcotics unit supervisors and commanders may either have the authority to decide whether the agency uses an alternative drug identification method that is better or

they may have a strong influence on that decision-making process, so it is vital to the commercialization of the technology to have the support of management within the law enforcement agencies.

Another very important market to garner support from is the customer segment consisting of the narcotics officers and agents. Of all the sworn-in and badged officers or agents within an agency, they have the most expertise and experience on illegal drugs and their methods of identification. They have the most concerns about the use of color tests and understand that a better method is necessary for them to do their jobs more effectively. They have a very strong influence on their superior's decision for the agency to use an alternative method, making them major end users. Another reason to have their support is to get their input on what requirements they need in a drug identification method, which would be collected through a beta testing phase.

Patrol officers and deputies represent the customer segment that is least aware of the necessity for a better field drug identification method. This segment covers a wide range of different experience levels regarding the color tests. Through the customer interviews, it was concluded that the more experienced the officer was in using the color test the more complaints they had about the method, and vice-versa. The less experienced officers typically felt that color tests were sufficient in field drug identification. Although they represent the largest market of potential end users of the three law enforcement customer segments, the opinions of patrol officers and deputies are a lower priority than the other two. They do not have organizational power and usually do not have strong influence on the decisions of management regarding the use of alternative

drug identification methods. Focusing on gaining the support of narcotics officers and agents and management for the technology would be the best approach to eventually achieve widespread market adoption.

4.2.4.2 Value Propositions

The value propositions are the features of the product that would meet the needs of the end users. This information would help determine the requirements for the development of the minimum viable product (MVP). In the case of the drug identification technology, there were five value propositions that were conveyed from potential customer interviews:

- A method that provides accurate results
- A method that is easy to use
- A method that is safer to use
- A method that can adapt to the ever-changing illegal drug environment
- A method that is affordable relative to other electronic-based devices

Accurate drug identification test results are vital to the operation of illegal drug law enforcement. The job of a police officer requires attention to detail and awareness of their surroundings at all times for their own safety, due to the dangers they potentially face in their line of work. When testing a suspected drug sample, they have the task of simultaneously monitoring the suspect or suspects. An inaccurate drug test result can

bring about multiple trials when testing the suspected sample, taking up more time and effort in testing the drug. Accurate and precise tests can make the process more efficient in regards to the number of trials and time spent to determine the identity of the suspected sample, allowing for a rapid decision to be made to either arrest the suspect (or suspects) or let them go. The more time spent on the process, the less time the officer is spending on other duties, such as patrolling. For color tests, the source of false positives could be from several issues. First, the test requires the user to determine the color of a result, which makes the test highly subjective since different people may perceive colors differently.¹⁰ Another issue is that users are not always trained properly to use the color tests, which can lead to human error-caused false positives. Lastly, color tests are not specific for their target compound. Non-illicit substances (tea, salt, spearmint, olive oil, etc.) are known to yield false positives.¹¹⁻¹³ There are no established statistics on the rate of false positives for color tests, but even just one such result can ultimately become costly for the wrongfully arrested person, law enforcement agency, crime lab, and judicial entities, so the minimization of false positive results must be emphasized.

A drug testing method with easy directions for use would have benefits like that of an accurate drug testing method. As previously mentioned, the lack of law enforcement training in using color tests may be a source of false positives. With no consistent standard operating procedure used by all law enforcement agencies, police officers may be skipping important steps for the test. A method with an easy standard operating procedure will require less user training and allow the user to confidently test a sample. The color test method can become complicated when testing for certain drugs. Some

drugs require a series of multiple tests just to presumptively detect their presence. For a law enforcement officer that is not sufficiently trained, the process could be confusing. A simple process would cut down the testing time and rate of false positives.

Safety is a key issue that law enforcement officers deal with when using color tests. There are three common hazards they may encounter during the process of testing samples. Users, especially those without sufficient training, may not know that the chemical reagents in the plastic pouches of the color test kits frequently consists of a corrosive acid solution. Because of this, injuries have occurred, in which users would conduct the test without the proper personal protection equipment (PPE) or do the test over their laps and spill some of the reagent on themselves. Another safety issue lies in the packaging of the test kits. Common color test kits are available as a plastic pouch encasing small glass capsules of the reagents. The procedure requires the user to break these capsules through the plastic pouch by hand, to release and mix the reagent with the sample. This step has led to users injuring themselves when the broken glass capsules cut through the plastic pouch and into their hands. To avoid this, some users use pens, instead of their hands, to push down on and break the capsules. A third safety issue is the improper handling of certain drugs. Fentanyl has been a significant contributor to the recent opiate epidemic. It is a synthetic painkiller that is 80 times more potent than morphine and is a common additive found in heroin.¹⁴⁻¹⁵ If a law enforcement officer is testing heroin and handles a sample without PPE, it is possible that some of the sample can get on their skin. Heroin samples are dangerous if they contain fentanyl, because fentanyl will readily absorb through the skin. Doses of even milligram amounts are said

to be fatal. The minimization, or ideally the elimination, of any of these safety hazards would be key value propositions that would be attractive to the law enforcement customer segments.

The illegal drug market is always changing. Some common drugs have remained prevalent over the decades, such as cocaine and heroin, while others seem to phase out of popularity over a few years, but there are always new formulations of different drugs being introduced to the illegal drug market. In the 1980s, crack cocaine became a popular form of cocaine made from free basing cocaine HCl salt. It contributed to a devastating drug epidemic wherein its residual effects remain.¹⁶⁻¹⁸ The drug epidemic of current times involves the well-known family of opioids. Opioids are naturally or synthetically derived from opium. Many opioids have strong analgesic effects and have been leveraged by pharmaceutical companies for successful commercial sales.¹⁹ Painkillers such as codeine, hydrocodone, oxycodone, and morphine have been used in medicine for decades. These drugs are known to be highly addictive, in which prolonged medical use may lead to recreational use.²⁰ These opioid-class pharmaceutical drugs are legal to possess with a prescription. Heroin, a DEA schedule I drug, is a recreational opioid with a “high potential for abuse” and “no medical use”. Heroin has always been a problem for law enforcement, but of late, it has been at the center of the opiate epidemic. Even worse, it is commonly found to be laced with fentanyl, an extremely potent synthetic opiate itself. Fentanyl is one of the strongest painkiller narcotics of medical use¹⁵ and due to its popularity, clandestine labs have managed ways to synthesize for illegal use. The combination of the two, in addition to the other opiate drugs, have led to over 28,000 fatal

overdoses in 2014.⁴ Police officers have stated that the color test methods have difficulties in testing black tar heroin. Also with the available color tests, there is no easy way to presumptively detect the presence of fentanyl. Sirchie® has developed a method, but a positive presumptive identification requires a series of multiple NARK II™ color tests. Even handheld Raman systems have trouble identifying the black tar heroin due to the mixture of impurities in the drug.²¹ Additionally, another class of drugs known as “designer drugs” have run rampant worldwide. Designer drugs, many used recreationally and commonly as “party drugs”, are structural analogues of controlled substances. New drugs with ecstasy-like or other psychoactive effects are synthesized to circumvent legal constraints, flooding the illegal drug market with many substances that are difficult, or even impossible, to enforce. A controlled substance typically has a known chemical structure, as well as both presumptive and confirmatory methods to identify them. When a new compound is encountered in the field, law enforcement officers are not readily-equipped with a presumptive test to positively identify whatever the substance is, making it difficult to provide probable cause for an arrest. If relying on color tests, the development of a new presumptive test could take years to develop, due to the lack of research efforts for new presumptive drug tests. Handheld Raman systems are capable of simple method development for designer drugs, wherein the identification of drugs is reliant on the support of a library database. Once a new drug is encountered, crime lab analysts can use confirmatory techniques to determine its chemical identity, and obtain its Raman spectral profile. That spectral profile could be quickly implemented into the handheld systems, giving law enforcement officers the ability to presumptively identify that drug in

the field. This ability to adapt to the constant introduction of new dangerous drugs is very valuable for law enforcement in their task to enforce illegal drug laws.

Superior methods of field drug identification exist in handheld Raman systems, but they are too expensive for most law enforcement agencies to afford and effectively equip their officers. Price points for these devices range from \$10,000 to \$35,000 depending on the brand. This leaves most law enforcement agencies and their officers with no other choice but to use color test kits in the field. Color tests are only \$1 to \$2, a justification for law enforcement agencies choosing to periodically purchase multiple kits at low prices over paying a large sum for the cost of the handheld Raman systems. Providing them with a superior alternative that is also affordable would be commercially attractive to this market.

Considering these five value propositions in the development of new drug testing technology will be the best approach in attaining a product-market fit. Law enforcement users currently deal with many issues regarding field drug testing that they have expressed, and a solution that eliminates those issues would make a case for commercial viability.

4.3 Background on Drug Identification Technology Based on Photoluminescent Drug Indicators

The technology is based on fluorescence spectroscopy, with the development of a handheld fluorescence spectrometer that works with a mobile app database and photoluminescent drug indicators. The drug indicators are test strips containing a

substance that interacts with narcotic compounds to yield a photoluminescence signal. The fluorescence spectrometer will be built using relatively inexpensive parts, to keep the cost under \$200 per unit. The main components, a UV excitation source to irradiate the test strip, a dispersive element to separate the colors of the light emission, and mirrors to direct the resulting colors to be projected onto a surface, will be encased in a 3D-printed plastic housing. A mobile app would be used to capture an image of the resulting colors emitted and ultimately determine the identity of the tested sample by matching the spectral profile with that of a standard in the library database.



Figure 44. A prototype version of the handheld fluorescence spectrometer.

4.4 Mobile App Development

A major obstacle to overcome to achieve success with the drug identification system will be the development of a properly functioning software in the mobile app. The software component will be responsible for the data analysis of the samples that are

tested. The following will be a description of the first version of the mobile app, developed in 2016 to serve as a prototype to be used with the spectrometer component.

4.4.1 Application Maps

An application map was designed for the mobile app, to determine what screens were necessary and how the user would navigate through the app. It was established that two different modes of the app would be required for two kinds of users, a “Street Mode” and a “Lab Mode”. The user will be able to select the desired mode at the *Login* screen.



Figure 45. The *Home* screen of the mobile app.

“Street Mode” (seen in Figure 47) is anticipated for use by law enforcement personnel in field. Once the user logs in and gets to the *Home* screen (Figure 45), they will be able to select from the following: *Settings*, *Browse*, *Help*, or *Logout* with a footer consisting of three buttons for *Home*, *Capture & Identify*, and *Archive*. For sample testing purposes,

Capture & Identify directs the user to a photo capturing screen, which allows them to capture an image of the resulting photoemission of the test strip from the fluorescence spectrometer. Once the image is captured, the user can accept the photo for it to be subsequently converted into spectral data and matched to a reference data set in the cloud database. If there is no match, the user will be notified. If there is a match, the user will be directed to a *Results* screen containing the test results. From here, the user can access the *Information* screen (seen in Figure 46), which provides the common pseudonyms of the substance or substances present in the sample and key information about them (i.e. legal status, appearance, what they are commonly mixed with, etc.). Each accepted image is archived by date and time to allow the user to refer to it, by pressing the *Archive* button in the footer, for evidence booking or reporting purposes.

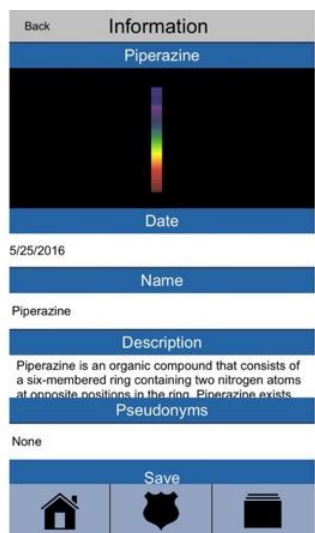


Figure 46. The *Information* screen after a positive match.

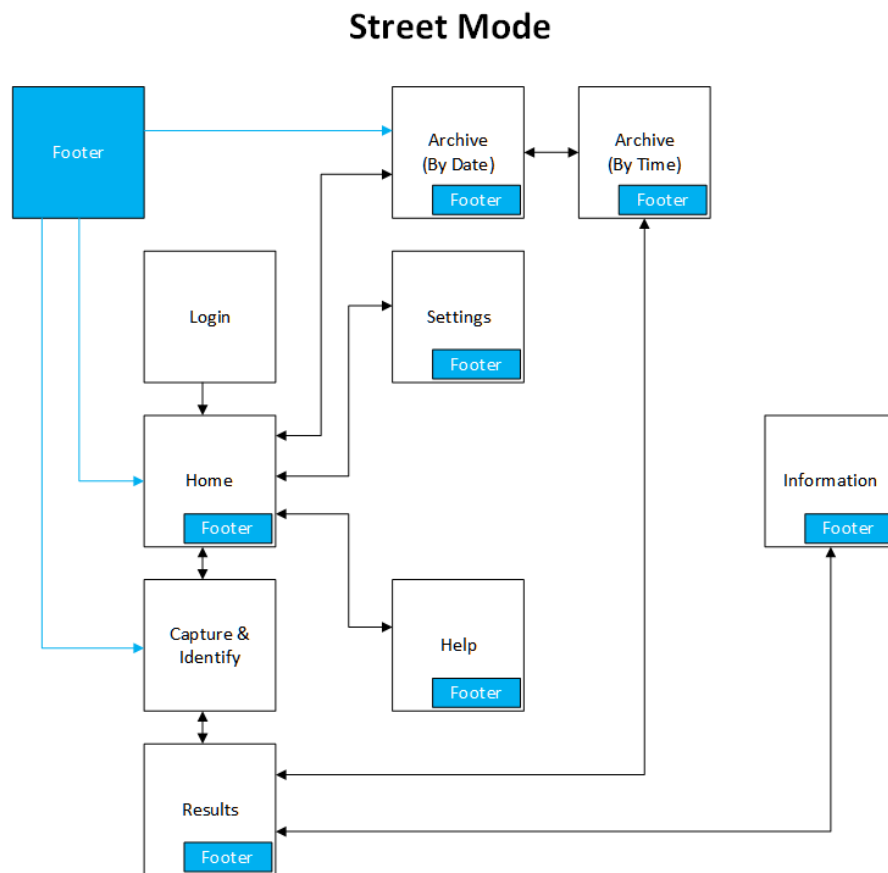


Figure 47. Application app for “Street mode”.

“Lab Mode” (seen in Figure 48) is intended for crime lab personnel use. It will contain all the features and capabilities available in “Street Mode”, as well as the addition of a few advanced ones. The main difference between the two is that the user will have the ability to add new data sets to the reference database after the *Capture & Identify* process through the *New Substance* screen. This is vital to the development and the anticipated constant update of the library database. Only allowed personnel, crime lab analysts, will be able to access “lab mode” and utilize this option. With the need to adapt to the ever-changing illegal drug environment, this will allow crime labs to quickly acquire

data on new drugs and implement them into the reference database so that law enforcement in the field have the ability to identify and enforce laws on the possession of new drugs. Another difference from “Street Mode” is that the user can view the spectral data once the image is processed. The importance that was considered in planning the two modes was to assure that law enforcement users were provided the features that were necessary to help them in the field, excluding all of the extra features provided in “Lab Mode”. “Street Mode” is a simplified mode of the app which is intended to be operated as conveniently as possible, even to a poorly trained user.

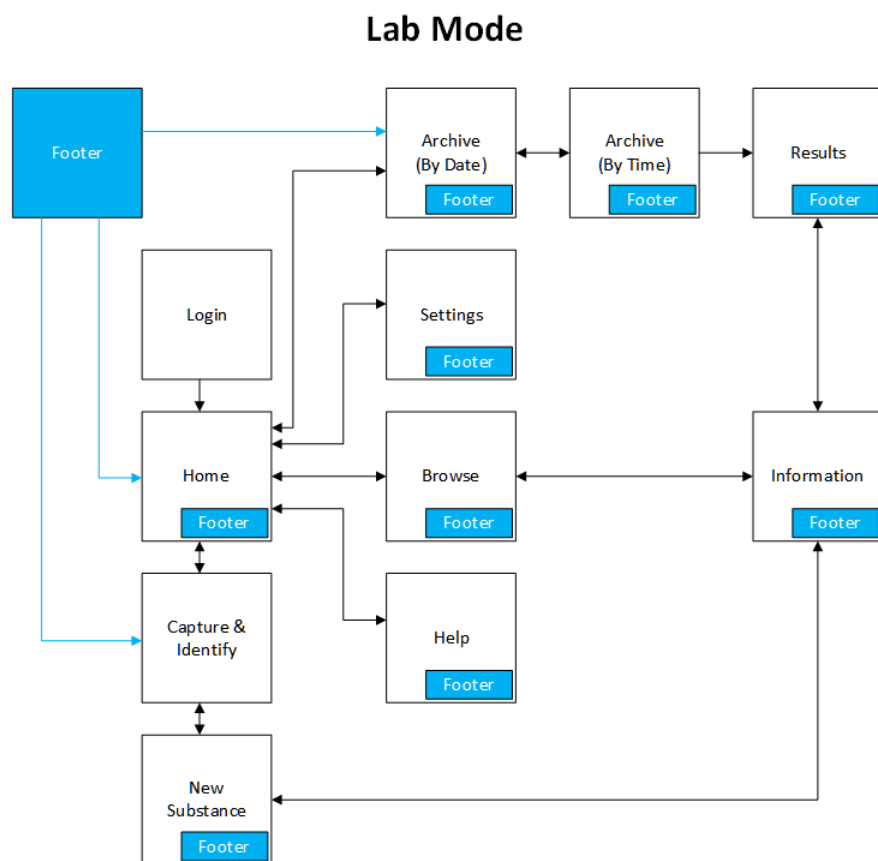


Figure 48. Application map for “Lab Mode”.

The keys to the mobile app will be its algorithms for converting the image to spectral data and then matching it to references in the database. Eliminating human interpretation of the results will provide consistent results in the practice of drug identification.

4.5 References

1. Izenman, A. J., Statistical and Legal Aspects of the Forensic Study of Illicit Drugs. *Statistical Science* **2001**, 16 (1), 35-57.
2. SWGDRUG, Scientific Working Group for the Analysis of Seized Drugs (SWGDRUG) Recommendations. In *Methods of Analysis/Drug Identification*, 2016.
3. DEA 2016 National Drug Threat Assessment Summary; U.S. Department of Justice Drug Enforcement Administration: 2016.
4. Rudd, R. A.; Seth, P.; David, F.; Scholl, L. *Increases in Drug and Opioid-Involved Overdose Deaths - United States, 2010-2015*; Center for Disease Control: Dec. 30, 2016, 2016; pp 1445-1452.
5. U.S., E. O. o. t. P. o. t. *FY 2016 Budget and Performance Summary*; Executive Office of the President of the U.S. : 2015.
6. Durose, M. R.; Burch, A. M. *Publicly Funded Forensic Crime Laboratories: Resources and Services, 2014*; Bureau of Justice Statistics: 2016.
7. Reaves, B. A. *Census of State and Local Law Enforcement Agencies, 2008*; Bureau of Justice Statistics: 2011.
8. NNOAC About the NNOAC. <http://www.natlnarc.org/about-the-nnoac/>.
9. FBI *Crime in the United States, 2015*; Federal Bureau of Investigation: 2016.
10. Cornsweet, T. M., *Visual Perception*. Academic Press: New York, 1970.
11. O'Neal, C. L.; Crouch, D. J.; Fatah, A. A., Detection of twelve chemical spot tests for the detection of drugs of abuse. *Forensic Science International* **2000**, 109, 189-201.

12. Tsumura, Y.; Mitome, T.; Kimoto, S., False positives and false negatives with a cocaine-specific field test and modification of test protocol to reduce false decision. *Forensic Science International* **2005**, 155, 158-164.
13. Kelly, J. F.; Addanki, K.; Bagasra, O., The Non-Specificity of the Duquenois-Levine Field Test for Marijuana. *The Open Forensic Science Journal* **2012**, 5, 4-8.
14. Marinetti, L. J.; Ehlers, B. J., A Series of Forensic Toxicology and Drug Seizure Cases Involving Illicit Fentanyl Alone and in Combination with Heroin, Cocaine or Heroin and Cocaine. *Journal of Analytical Toxicology* **2014**, 38, 592-598.
15. Trescot, A. M., *Opioid Pharmacology and Pharmacokinetics*. Springer International Publishing: Switzerland, 2016.
16. Cornish, J. W.; O'Brien, C. P., Crack Cocain Abuse: An Epidemic with Many Public Health Consequences. *Annu. Rev. Public Health* **1996**, 17, 259-273.
17. Cook, P. J.; Laub, J. H., After the Epidemic: Recent Trends in Youth Violence in the United States. *Crime and Justice* **2002**, 29, 1-37.
18. Reinarmann, C.; Harry, G. L., *Crack in America: Demon Drugs and Social Justice*. University of California Press: 1997.
19. Katari, R., The role of industry in the modern opioid crisis. *Toxicol Forensic Med Open J* **2016**, 1 (1), 21-23.
20. Kolodny, A.; Courtwright, D. T.; Hwang, C. S.; Kreiner, P.; Eadie, J. L.; Clark, T. W.; Alexander, G. C., The Prescription Opioid and Heroin Crisis: A Public Health Approach to an Epidemic of Addiction. *Annu. Rev. Public Health* **2015**, 36, 559-574.
21. Vítek, P.; Ali, E. M. A.; Edwards, H. G. M.; Jehlička, J.; Cox, R.; Page, K., Evaluation of portable Raman spectrometer with 1064 nm excitation for geological and forensic applications. *Spectrochimica Acta Part A* **2012**, 86, 320-327.